Tools and Techniques for Flow Characterization in the Development of Load Leveling Valves for Heavy Truck Application

Yashvardhan Gupta

Thesis submitted to the faculty of the Virginia Polytechnic Institute and State University
in partial fulfillment of the requirements for the degree of

Master of Science
In
Mechanical Engineering

Mehdi Ahmadian - Chair
Clinton L. Dancey
Steve C. Southward

April 23, 2018
Blacksburg, Virginia

Keywords: Pneumatic Suspension, Load Leveling Valve, Flow Rates, CFD

Tools and Techniques for Flow Characterization in the Development of Load Leveling Valves for Heavy Truck Application

Yashvardhan Gupta

Abstract

This research examines different techniques and proposes a Computational Fluid Dynamics (CFD) model as a robust tool for flow characterization of load leveling valves. The load leveling valve is a critical component of an air suspension system since it manages air spring pressure, a key function that directly impacts vehicle dynamic performance in addition to maintaining a static ride height. Efficiency of operation of a load leveling valve is established by its flow characteristics, a metric useful in determining suitability of the valve for application in a truck-suspension configuration and for comparison among similar products. The disk-slot type load leveling valve was chosen as the subject of this study due to its popularity in the heavy truck industry. Three distinct methods are presented to model and evaluate flow characteristics of a disk-slot valve. First is a theoretical formulation based on gas dynamic behavior through an orifice; second is an experimental technique in which a full pneumatic apparatus is used to collect instantaneous pressure data to estimate air discharge; and third is a CFD approach. Significant discrepancies observed between theoretically estimated results and experimental data suggest that the theoretical model is incapable of accurately capturing losses that occur during air flow. These variations diminish as the magnitude of discharge coefficient is altered.

A detailed CFD model is submitted as an effective tool for load leveling valve flow characterization/analysis. This model overcomes the deficiencies of the theoretical model and improves the accuracy of simulations. A 2-D axisymmetric approximation of the real fluid domain is analyzed for flow characteristics using a Realizable k-ϵ turbulence model, scalable wall functions, and a pressure-based coupled algorithm with a second order discretization function. The CFD-generated results were observed to be in agreement with the experimental findings. CFD is found to be advantageous in the evaluation of flow characteristics as it furnishes precise data without the need to experimentally evaluate a physical model/prototype of the valve, thereby benefitting suspension engineers involved in the development and testing of load leveling valve designs. This document concludes with a sample case study which uses CFD to characterize flow in a modified disk-slot load leveling valve, and discusses the results in light of application on a heavy truck.

Tools and Techniques for Flow Characterization in the Development of Load Leveling Valves for Heavy Truck Application

Yashvardhan Gupta

General Audience Abstract

A majority of heavy trucks in North America equipped with air suspensions use a device known as a load leveling valve. This is a mechanical control system which manages pressure in air springs to maintain a preset/constant static ride height irrespective of the payload, doing so by sensing the distance between the truck frame and the axle. The rate of airflow to/from air springs in response to a road disturbance or load shift is critical to the stability of the truck when on the road. This rate of airflow for a given set of conditions constitutes flow characteristics of a load leveling valve. Accurate measurement of flow characteristics is necessary to understand the actual effect of the use of a particular valve on a truck-suspension configuration. This research addresses that requirement by presenting three distinct methods to model and evaluate flow characteristics of a load leveling valve, conducted on the disk-slot valve for its popularity in the heavy truck industry. First is a theoretical formulation based on flow of gas through an orifice; second is an experimental technique in which a full pneumatic apparatus is used to collect instantaneous pressure data to estimate air discharge; and third is a Computational Fluid Dynamics (CFD) approach. Significant discrepancies observed between theoretically estimated results and experimental data suggest that the theoretical model is incapable of accurately capturing losses that occur during air flow. The disparities also justify the adoption of CFD as an alternate method.

A comprehensive CFD model is proposed as a capable tool for load leveling valve flow analysis/characterization. This model overcomes the deficiencies of the theoretical model and improves the accuracy of simulations. CFD-generated results are found to be in agreement with the experimental findings, highlighting its effectiveness at flow characterization. The ability of a CFD model to furnish precise data without the need to experimentally evaluate a physical model/prototype of the valve promises to benefit suspension engineers involved in the development and testing of load leveling valve designs. This document concludes with a sample case study which uses CFD to characterize flow in a modified disk-slot valve, and discusses the results in light of application on a heavy truck.

To my father..

Acknowledgements

I would like to take this opportunity to express my sincere gratitude and respect for my advisor, Dr. Mehdi Ahmadian, who took me under his tutelage and opened up a wide horizon for my growth and learning. I am indebted to him for his constant guidance and encouragement throughout the course of my stay at Virginia Tech, and I'll keep his teachings close to my heart for what lies ahead. Working in the CVESS lab has truly been an enriching experience, both academically and on a personal front. I have had the good fortune to find a friend in each one of my colleagues and staff members. Working with them has further broadened the spectrum of my knowledge and made me a better person. I am certain that my association with them will only grow stronger from here on.

I am sincerely grateful to my committee members, Dr. Clinton L. Dancey and Dr. Steve C. Southward, for their support and assistance for my research endeavors. Your suggestions and input along the way have given me great perspective.

I will fondly remember my time with each and every person I have interacted with at Virginia Tech. It has been a memorable experience that I will cherish for the rest of my life.

Special thanks to my father and my sister, who have always encouraged me to put my best foot forward and push my boundaries. Without their belief, support and trust in me, I wouldn't be where I am today.

Table of Contents

List of Figures

List of Tables

1. Introduction

1.1 Overview

Heavy trucks are indispensable to the transportation and logistics industry. In the United States alone, freight in excess of 10.4 billion tons were moved by trucks in 2015, generating a revenue of 719.3 billion dollars [1]. One breakthrough technology that revolutionized trucking was the air suspension system. So profound were its advantages that most trailers and Class-8 trucks are equipped with air suspensions on their rear tandem axles.

A component of the air suspension system vital to its function is the load leveling valve. This is a mechanical control system that maintains a set ride height of the truck, and is comprised of a valve mounted onto the truck frame connected to the axle by a linkage mechanism. Departures from the design ride height of the truck are sensed by the valve through the linkage and are corrected by supplying or purging air from the air springs. A truck may use a single load leveling valve supplying the left and right side air springs, or two valves with one for each side. As such, these load leveling valves present the following benefits if developed correctly [2]:

- Diminished driveline vibration.
- Diminished suspension air consumption, which translates to improved compressor life and reduced fuel consumption.
- Easier coupling and uncoupling with trailers due to a precise 5^{th} wheel height.
- Enhanced ride quality.
- Improved roll stability for a two leveling valve system.

Considering the importance of load leveling valves and the unavailability of comprehensive product attributes for proprietary reasons, the need for tools that aid in the development and testing of these valves was appreciated. This study addresses the matter by presenting three techniques to test load leveling valves for flow characteristics, of which the Computational Fluid Dynamics (CFD) modeling technique will be especially useful in the development stage of load leveling valves, thereby saving time and resources.

1.2 Motivation

Currently there are multiple air spring and load leveling valve designs available in the market. Most of these designs have unique characteristics, the intricate details of which are undisclosed by most manufacturers for proprietary reasons. The practice of installing the two components without knowing their properties may lead to a truck with substandard performance, when the goal is to attain a best fit among the valve-air spring-truck combination. Since truck and air spring characteristics cannot be altered without capital investments, suspension performance may be adjusted to a great degree by modifying flow characteristics of the leveling valve. Chen modeled the balanced (two load leveling valve) pneumatic suspension and combined it with a multi-degree of freedom model of a heavy truck to study dynamic performance under various driving conditions [3]. Models such as those developed by Chen can be used to predict flow characteristics that provide the desired/optimal truck performance. The recommended flow characteristics can be used as a target for a new valve design, which can then be evaluated using the proposed CFD modeling technique to predict actual performance, leading to a parametric study using CAD and CFD. Therefore, it would be redundant for the designer/engineer to manufacture prototypes for experimental testing for flow characterization, thereby saving time and resources. Hence, the outcome of this work indirectly contributes to improve suspension performance in air suspension and leveling valve equipped trucks.

1.3 Objectives

This project aims to develop and propose a CFD modeling technique that can assess flow characteristics of a load leveling valve with improved accuracy and worth over theoretical and experimental evaluation, respectively.

The principal goal was achieved by fulfilling the following objectives:

- Research and evaluate flow characteristics of the leveling valve through theoretical formulations.
- Test flow characteristics of the leveling valve by experiment to create a benchmark against which theoretical and CFD results will be validated.

- Develop a CFD modeling technique to accurately determine flow characteristics of the leveling valve.
- Validate theoretical and CFD modeling against experiment and justify those results.

1.4 Approach

A commercially available load leveling valve of the disk-slot type is selected as the subject for this study. This valve has been chosen over similar products due to its popularity, simplicity and cost, hence broadening the impact of the work presented.

Following are the steps adopted to realize the set objectives:

- Mechanically analyze the valve structure and its operation. Establish conditions (level of actuation and pressures) to test that are representative of flow characteristics of the valve and can differentiate performance of valve designs.
- Develop a theoretical model predicting mass flow rates for the established conditions, based on the structure controlling air flow and using knowledge of gas dynamics. Note the results.
- Test the leveling valve for actual flow rates through experiment.
- Validate the theoretical model against the experiment. In case of disagreement, note the difference and interpret possible sources for the differences.
- With a background knowledge of internal flow fluid dynamics, understand the analysis schemes involved in CFD simulation. Choose the appropriate analysis settings.
- Perform CFD simulations for the same established conditions. Note the results.
- Validate CFD-generated results against experiment. Note the differences and interpret possible sources for the difference.

1.5 Outline

Chapter 1 opens the study and apprises the reader of the relevance, objectives, and approach of the work reported in this document.

Chapter 2 delivers background information on air suspensions and the working principle of general and disk-slot type load leveling valves. Challenges in working with leveling valves are discussed along with past attempts to address the deficiency. Lastly, concepts of fluid dynamics relevant to CFD analysis in Chapter 5 are presented.

Chapter 3 demonstrates an attempt to accurately estimate flow characteristics of a disk-slot valve using theoretical and empirical formulations for its advantage of easy coupling with other models for co-simulation.

Chapter 4 furnishes details on experimental testing for flow characteristics of a disk-slot valve using a full pneumatic apparatus, the outcome of which is used as a benchmark to validate theoretical results from Chapter 3, and CFD-generated results in Chapter 5.

Chapter 5 initially presents CFD modeling and analysis schemes available for simulating flow through a disk-slot valve. Steps taken and options selected in the process of developing the model are logically explained, after which the validity and usefulness of CFD modeling is discussed.

Chapter 6 presents a sample case study in which the disk-slot valve design is modified and analyzed using the developed CFD model, followed by the strategy to practically implement the resulting changes in flow characteristics on the truck.

Chapter 7 summarizes this study with recommendations for future work.

2. Background on Air Suspensions and Fluid Dynamics

This chapter presents knowledge fundamental to suspension systems and fluid dynamics. The air suspension system is detailed, with special focus on the load leveling valve for its functional importance as the 'brain' of the suspension system. Shortcomings related to available flow characteristics' data, critical for accurate and optimal modeling of air suspensions, are featured in light of the literature review. Nomenclature and concepts consistent with accurate CFD analysis of the load leveling valve are also presented.

2.1 General Suspension Systems

Suspensions are one of the most important sub-systems of a vehicle. At the least, they consist of springs, along with dampers braced by mechanical elements between the axle and the chassis. They serve the purpose of:

- Carrying vehicle load.
- Chassis isolation from road conditions through wheel vertical compliance.
- Retaining appropriate steering geometry.
- Resisting and transmitting forces generated during driving, cornering etc.
- Maintaining tire to road contact.
- Resisting chassis roll.

Over the years, these functions have been implemented on heavy trucks through the following two major suspension types (Figure 2.1):

- Leaf Spring Suspensions
- Air/Pneumatic Suspensions

Figure 2.1: Leaf suspension in application [4] (left); Air suspension in application (right)

Leaf spring suspensions have been around as early as the 18th century [5] and are popular even today due to their simplicity. They rely on material properties of spring steel and the flexural property of beams of rectangular cross-section to provide a springing action. They typically consist of multiple beams (of progressively reducing length), stacked together and clipped.

Although proposed in 1847, pneumatic suspensions were not popular until the mid-20th century when reinforced rubber components to enable pneumatic suspensions were developed [6]. In pneumatic suspensions, pressurized air in flexible air springs supports a load equal to the product of the air pressure and effective cross-sectional area of the air-spring.

Pneumatic suspensions have the following advantages over leaf suspensions:

- Adjustable spring stiffness compared to constant stiffness on leaf springs, enabling a near constant natural frequency with varying load.
- Lower air spring stiffness improving ride quality.
- Adjustable ride height using valves and air supply.
- Lighter mechanical components and reduced structural noise.

The aforementioned benefits brought about a replacement of conventional leaf spring suspensions with air spring suspensions on heavy trucks during the latter half of the 1990's and early 2000's [7]. The trend was so profound that heavy trucks operating air suspensions increased from 36% in 1996 to about 75% in the present [8].

2.2 Pneumatic Suspension System and Components

Modern pneumatic suspensions at their simplest consist of air springs, a load leveling valve (also known as a height control valve), piping and plumbing elements, pressure protection valves, and an air reservoir.

2.2.1 Air Springs

Air springs are located between the chassis and the axle. They are essentially variable volume air reservoirs supporting vehicle static and dynamic loads. Early air springs were double convolutes which were substituted by a rolling lobe/diaphragm structure for increased design height and desired stroke (Figure 2.2). Improved suspension systems for heavy trucks were designed with adjustable air spring pressure and self-leveling systems [9].

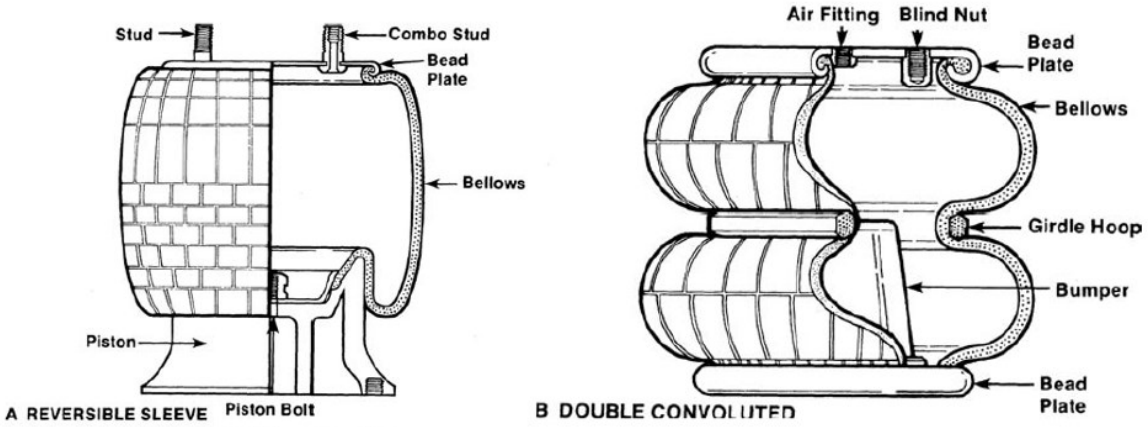

Figure 2.2: The rolling lobe (left) and double convoluted (right) air spring [10]

2.2.2 Load Leveling Valves

The load leveling valve is a device that maintains a set ride height of the truck irrespective of payload weight. It does so by 'sensing' the distance between the sprung mass and unsprung mass, and accordingly supplying or dumping air from the air springs to maintain the design ride height of the truck. Once installed, it functions independently without the need for any intervention until it fails. Such a function qualifies this device to be considered the 'brain' of the air suspension

system. The above function can be achieved by mechanical or electronic means. Mechanical load leveling valves are more commonly used due to their low cost and reliability.

A mechanical load leveling valve is typically comprised of a valve body with an attached lever arm and a control rod link. The valve body is mounted onto the truck frame (sprung mass), with one end of the control rod attached to the lever arm and the other end attached to the axle (unsprung mass) to form a linkage arrangement as shown in Figure 2.3 and Figure 2.4.

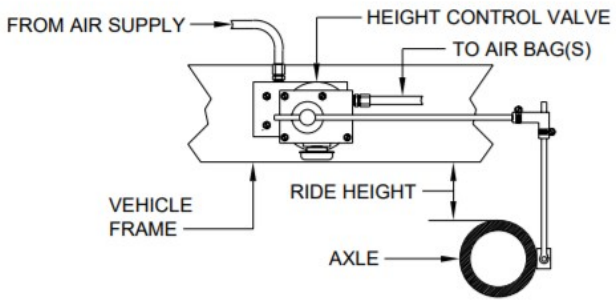

Figure 2.3: Installation schematic of a load leveling valve [11]

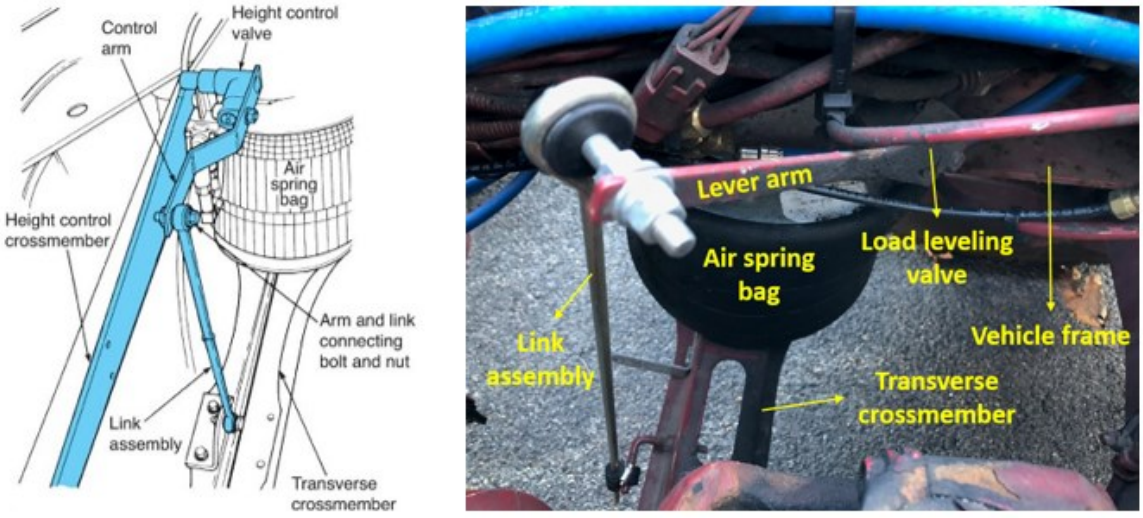

Figure 2.4: Load leveling valve on a truck – schematic [10] (left); actual (right)

From a pneumatic context, mechanical load leveling valves are virtually three position and three port type valves, as seen in Figure 2.5. Air springs are connected to port A (air spring port), the air

tank/reservoir is connected to port S (supply), and port D (dump/purge) is left open to the atmosphere. Thus, the valve either charges air into the air springs (port A and S connected), isolates all three ports (dead-band/level position), or discharges the air springs (port A and D connected). The dead band, typically 2 degrees to -2 degrees of lever arm rotation/actuation about the level position, restricts any airflow to compensate for chattering due to high frequency road excitations, thereby reducing total air consumption. In reality, these valves are designed to have infinite angular positions (degrees of lever arm rotation in the working range) within supply and dump operations to allow varied quantities of airflow for a given set of pressure conditions. Flow rate data at varied lever arm actuations, as well as supply and dump pressures constitute the flow characteristics of a load leveling valve.

Operation-wise, load added to the truck causes the frame to dip (reducing the distance between the frame and the axle), which, due to the constant length control rod linkage, causes the lever arm to rotate upwards (counterclockwise, typically up to 45 degrees). This results in an airflow into the air springs, increasing pressure in them until the frame rises, and the lever arm rotates clockwise and is level again. In a similar fashion, when load is removed from the truck, the frame rises, causing the lever arm to rotate downwards (clockwise, typically up to -45 degrees), resulting in airflow out of the air springs, and reducing pressure until the frame drops and the lever arm is level again (Figure 2.5).

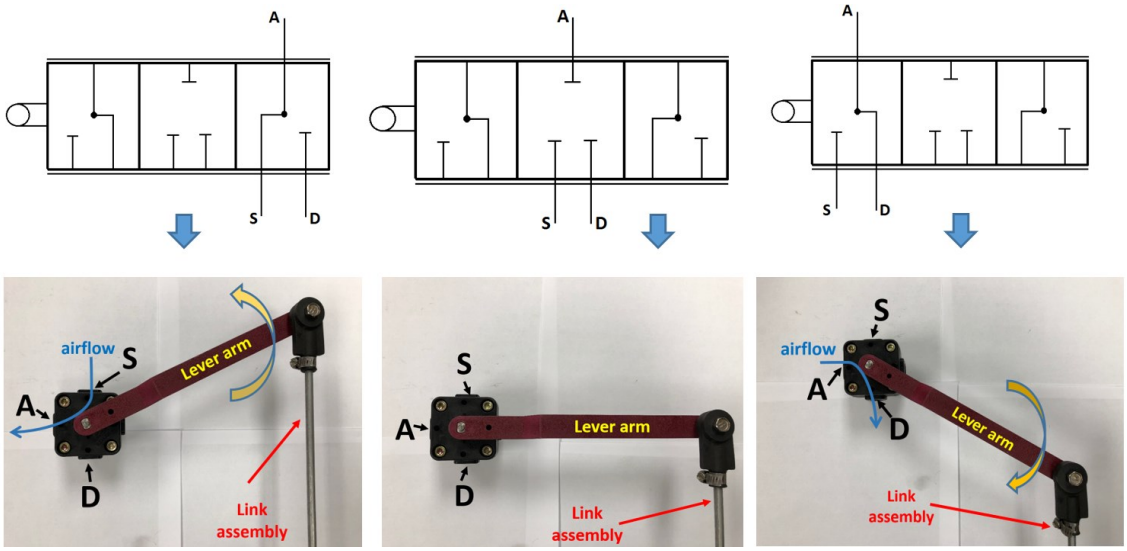

(a) Air springs being charged *(b) Valve closed* *(c) Air springs being discharged*

Figure 2.5: Load leveling valve (disk-slot valve) modes of operation

It is noticeable that by geometry, the arc traced by the point of connection of the lever arm to the control rod linkage is a measure of the rise/drop of the truck frame (suspension travel). Thus, for a given length of control rod linkage and flow characteristics with respect to lever arm rotation, valve response analogous to suspension travel can be adjusted by varying the length of the lever arm. This is due to the fact that for a constant arc length, included angle is larger for smaller radii than it is for larger radii by simple geometry (arc length = angle $_{(in\ radian)}$ *radius $_{(of\ arc)}$).

2.2.3 Suspension Pneumatic Layouts

The load leveling valve is placed between the air reservoir and the air springs. One or two load leveling valves may be used with plumbing configurations, as seen in Figure 2.6 and Figure 2.8. While the one-valve system can only control CG height of the truck, the two-valve system in addition to CG height control can provide roll stability by suppling air to the air spring in jounce and dumping air from the air springs in rebound. This feature is better appreciated and visualized by representing the suspension system as a control system block diagram (Figure 2.7 and Figure 2.9). The block diagram chiefly highlights the importance of flow characteristics of a load leveling valve towards maintaining a stable ride and an effective service.

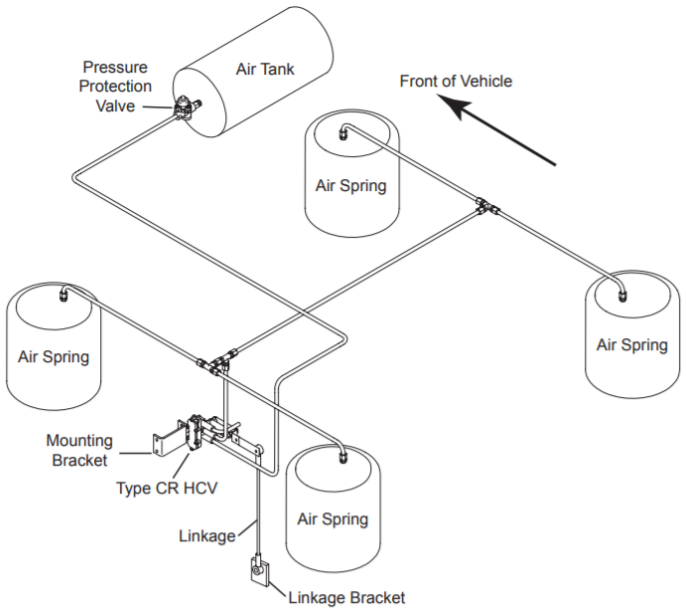

Figure 2.6: Plumbing schematic of a one leveling valve pneumatic suspension [12]

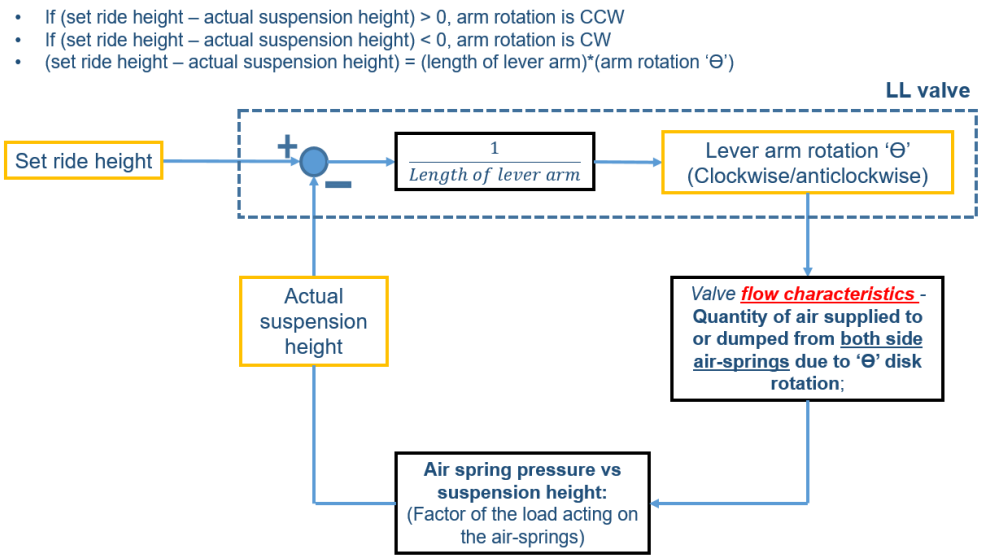

Figure 2.7: Block diagram of a one load leveling valve pneumatic suspension

The difference between actual and set ride height is sensed by the load leveling valve, which then supplies/dumps a certain quantity of air (depending on its flow characteristics) to/from the air springs to equalize actual and set ride heights. For a given vehicle configuration and air spring characteristics, response of the closed loop system for both the one and two leveling valve suspension configurations, is controlled by flow characteristics of the load leveling valve only.

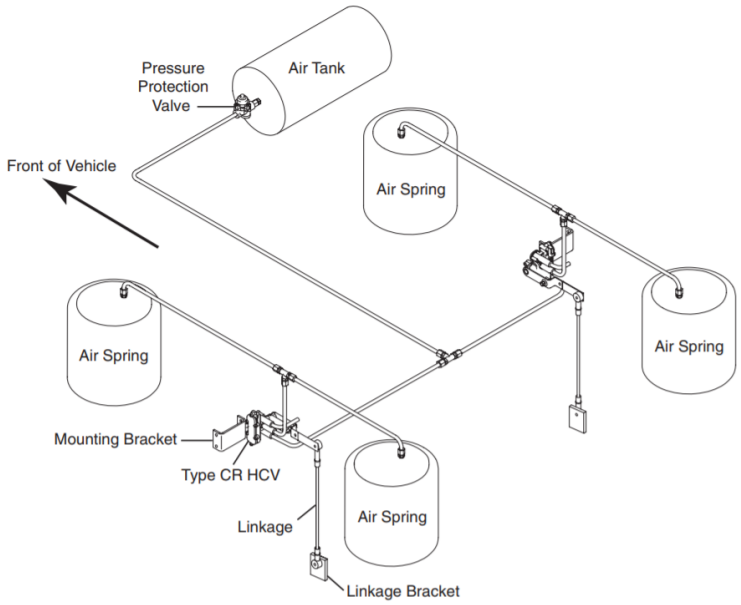

Figure 2.8: Plumbing schematic of a two load leveling valve pneumatic suspension [13]

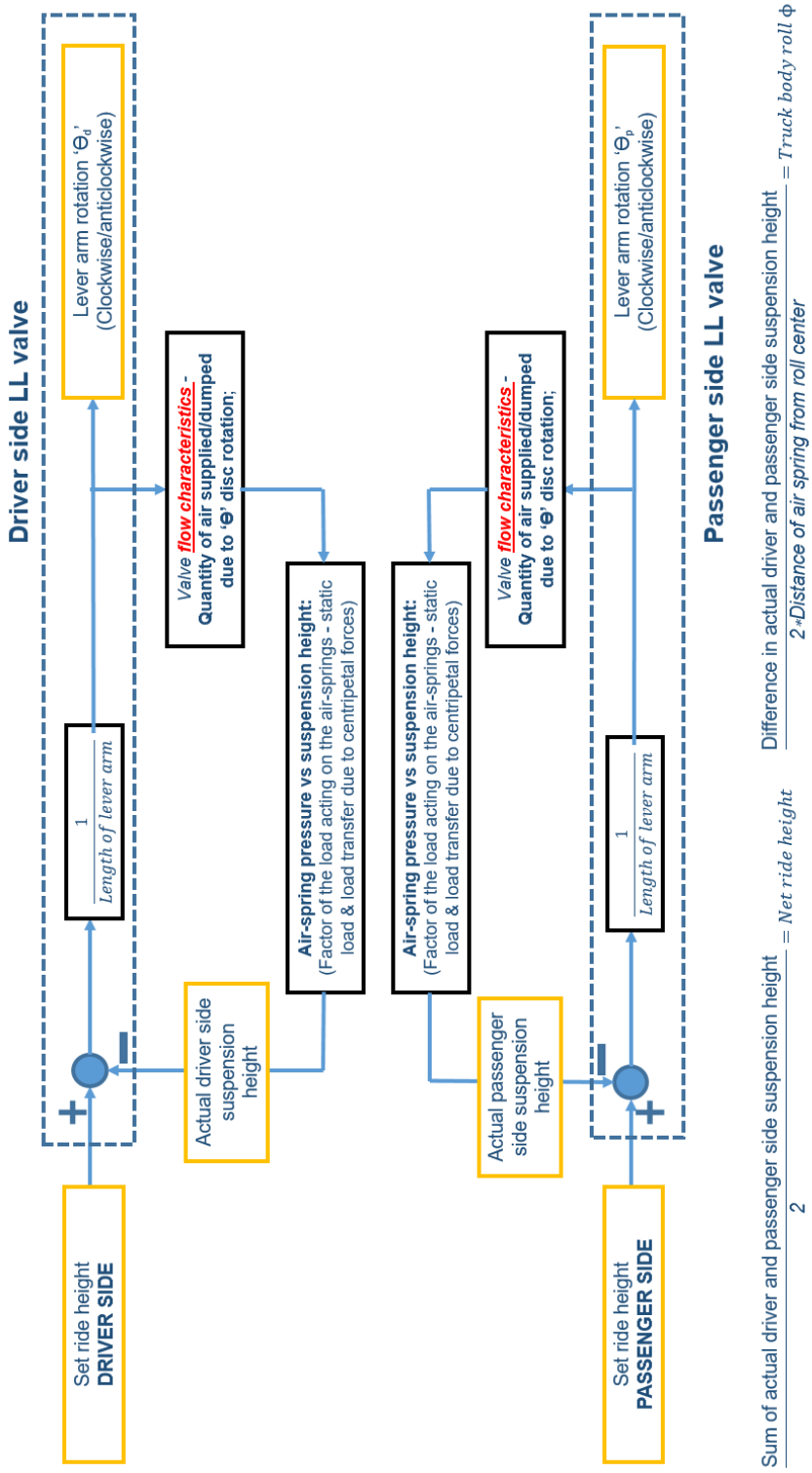

Figure 2.9: Block diagram of a two leveling valve pneumatic suspension

2.2.4 Types of Load Leveling Valves

Multiple types of load leveling valves are available in the market, and are differentiated from one another by virtue of flow rates and the internal workings in supply/dump operations. Some of the popular types are:

- Chambered Valves
- Disk-Slot Valves
- Piston Valves
- Lever Paddle Valves

The chambered and disk-slot load leveling valves are the most popular among heavy truck users.

Chambered Valve

This valve is assembled out of multiple components, as seen in Figure 2.10. Supply and dump operations are achieved by a rubber head covering and uncovering specific cutouts in a plastic seat. The rubber head is maneuvered by a hollow stem with a flared tip connected to the lever arm of the valve. The chambered valve also features a piston-based hydraulic damper system to make the valve invulnerable to high frequency fluctuations experienced during on-road application. Although high flow rates are an advantage to this valve, there are certain disadvantages, such as the valve size (at least two times larger than the disk-slot valve), cost (up to three times the cost of the disk-slot valve) and the number of parts used in the construction (increased sensitivity to failure).

Figure 2.10: The chambered load leveling valve – assembled (left); components [14] (right)

Disk-Slot Valve

The disk-slot load leveling valve is the most commonly used valve in the heavy truck industry. An estimated 70% of all heavy tractor-trailer air suspension systems in North America use this type of valve [15]. It is a simple design employing a slotted disk overlapping two drilled (to create orifice), vertically movable cylinders (one each for supply and dump) pressed against the disk by a spring. Disk and orifice surfaces are mirror finished and lubricated to prevent any leaks. The lever arm is connected to the disk by a common shaft, so that as the arm rotates from the level position (orifice completely covered), it slowly uncovers the orifice, increasing the aperture size until it is fully uncovered, thus regulating airflow. Designed dead band is ±2 degrees and working range is ±75 degrees for supply or dump operation. Figure 2.11 illustrates the parts of a disk-slot valve. This valve has a proven record for reliability, with nineteen class 8 trucks using this valve reporting zero failures after 500,000 road miles, as well as positive results for 100 million cycles of testing [15]. It is also constructed out of common engineering materials such as anodized aluminum, stainless steel, engineering plastic, and Buna-S sealing rings [16]. The fore mentioned traits of the valve make it ideal for this study, i.e. its simplicity will not overcomplicate the CFD analysis, while any future/recommended adjustments to flow characteristics can be implemented easily without a significant increase in cost. It must be noted that the disk-slot valve has two air spring ports in the body, of which one is blocked in most applications.

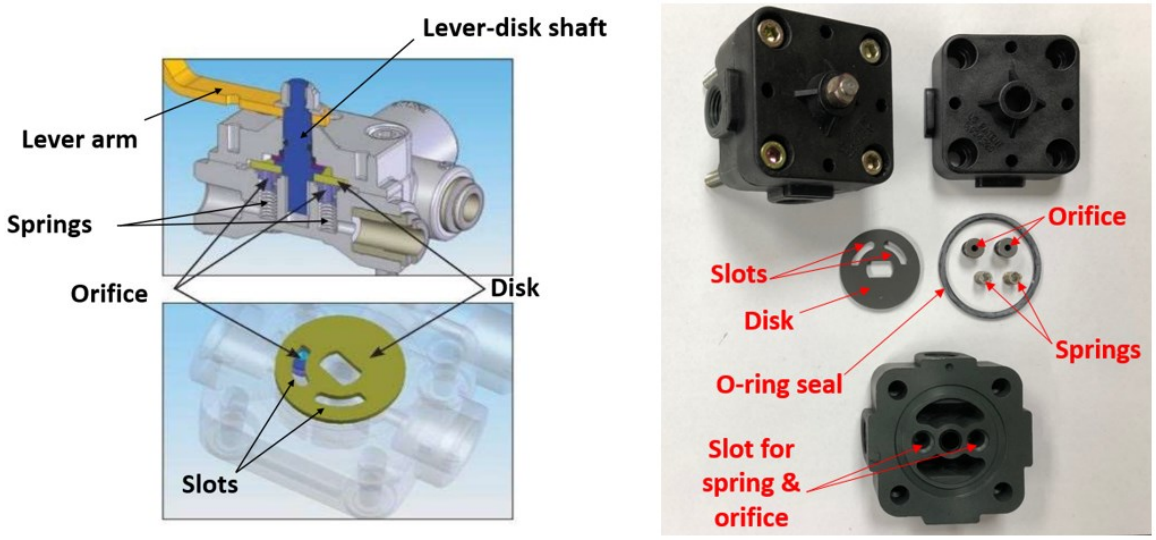

Figure 2.11: Mechanical components of the disk-slot valve [17]

2.2.5 Available Flow Characteristic Data of Load Leveling Valves

Commercial load leveling valves come with a datasheet in which the flow characteristic data is not comprehensive. Figure 2.12 is an example of flow characteristic data provided by a manufacturer of a disk-slot valve. Professionals designing air suspension systems would need more information than the given 'standard' and 'low flow' characteristics during application to ensure the best fit between the valve-air spring-truck combination. A consequence of ineffective flow characteristics leads to an oscillatory overshoot/undershoot behavior of ride height or a non-responsive system during operation. Numerous researchers have published work on modeling pneumatic suspensions in an attempt to better design them, with some bypassing details on the load leveling valve. Nakajima et al. used leveling valve flow characteristics as a function of pressures and lever arm displacement without mentioning details of how the flow rates were obtained [18]. Robinson et al. in the absence of manufacturer-provided flow rate data, applied compressible flow equations through an orifice in order to formulate flow characteristics and used a correction factor to adjust theoretical results with conducted experiments [19]. Researchers such as Lee, Hao et al., and Nieto et al. concentrated on the development of the air spring, plumbing, and tank model with scant or no mention of leveling valves [20-22]. Kim et al. researched the height and leveling control of automotive suspensions using a solenoid valve modeled by a static area-normalized mass flow equation [23]. Sreedhar et al. published work on an air suspension model coupled with multibody dynamics simulation of the vehicle with little mention of how leveling valve characteristics were determined [24].

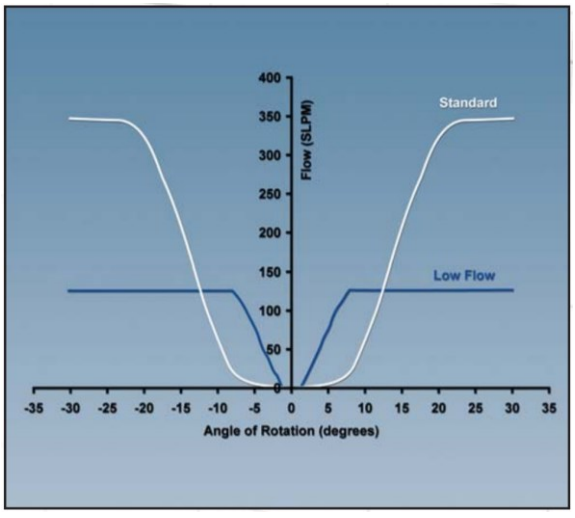

Figure 2.12: Manufacturer specified flow rates for the disk-slot valve [16]

The literature reviews also highlighted advancement in air suspension modeling techniques, in which an increasing number of complex components and their non-linearities are accounted for in formulations. For example, Chen predicted truck performance under various conditions by coupling load leveling valve characteristics with a truck-suspension dynamics model [3]. Using results from that model, recommendations may be made for leveling valve flow characteristics which yield an optimal truck performance. This is especially true when implementing a two load leveling valve plumbing configuration to introduce an additional anti-roll effect using the air springs. It would help suspension designers to have a tool to test their new/improved valve designs for flow characteristics, a feature addressed by this study.

2.3 Basics of Fluid Dynamics

This subsection reviews and highlights the concepts of airflow critical to understanding fluid behavior and conducting Computational Fluid Dynamics analysis of the valve.

Internal and External Flow - Flow completely enclosed by a solid boundary/wall/surface such as in a pipe or duct is called internal flow, while flow over a solid object such as a plate or sphere placed in a flow field is called external flow.

One, Two and Three Dimensional Flows - These flows are identified by the major velocity component. If the fluid flow has significant velocity in only one primary direction, the flow is one dimensional. Significant velocity in two and three primary directions constitutes two- and three-dimensional flow respectively.

Compressible and Incompressible Flow - Extent of density variation at the time of flow is the differentiating factor here. If there is a large variation during flow, it is said to be compressible. Incompressible flow, on the other hand, is an approximation for fluids that maintain a fairly constant density. By nature, liquids are incompressible fluids, while gases are highly compressible. A simplification for analysis of gas flows widely accepts flow as incompressible if the density change is below 5 percent, which corresponds to a flow of less than a Mach number of 0.3. Mach number is the ratio of speed of flow to the speed of sound. Speed of sound in air is $=\sqrt{\gamma RT}$, where γ is the isentropic index of air, R is the gas constant, and T is the temperature.

Steady and Unsteady Flow - Steady flow is characterized by fluid properties that are constant at a point over time but vary from point to point within a domain. Unsteady flow occurs when properties at a point change with time, i.e. they are transient.

Viscous and Inviscid Flow - Viscous fluids have a property (called viscosity) in which fluid layers moving relative to one another during flow develop a frictional force between them. This results in the slower layer trying to slow down the faster layer. Thus, flows with a dominant friction effect are called viscous flows. On the other hand, a fluid with absent viscous effects is called superfluid. Practically, inviscid flow is an approximation where the friction effects are neglected, usually away from walls. They are brought in to simplify calculations.

Laminar and Turbulent Flows - The motion of fluid particles differentiates laminar and turbulent flow. Distinct, smooth and strikingly ordered motion of the fluid, such that individual fluid molecules travel at a consistent axial velocity in the direction of streamline, is a characteristic of laminar flow. Turbulent flow, on the other hand, has fluid motion that is rather chaotic and disordered, distinguished by velocity fluctuations and swirls (called eddies). These eddies result in excessive blending of the fluid, thereby increasing momentum and energy transfer between fluid particles, whilst also adding to losses.

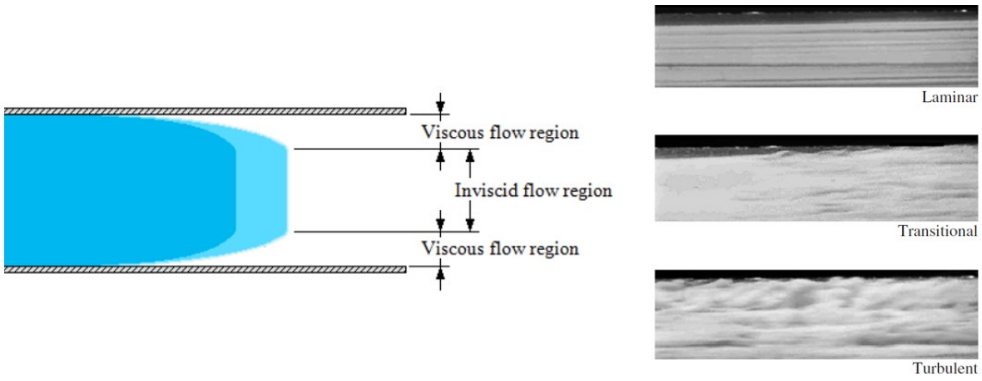

Figure 2.13: Viscous and inviscid flow [25] (left); Laminar and turbulent flow [26] (right)

Reynolds Number - Reynolds Number (Re) is the ratio of inertial forces to viscous forces. It is perhaps the most important dimensionless constant in fluid mechanics prescribing whether the flow is laminar, transitional (between laminar and turbulent), or turbulent.

$$\mathrm{Re} = \frac{\text{Inertial forces}}{\text{Viscous forces}}$$

Re < ~2300	Laminar Flow	
~2300 < Re < ~4000	Transitional Flow	(Circular Pipe)
~4000 < Re	Turbulent Flow	

The above values for Reynolds number are generally accepted to distinguish between flow regimes, although the actual Re value for the onset of transition and turbulence may be higher or lower depending on the type of fluid, external disturbances, surface temperature and roughness, geometry, etc.

2.3.1 Flow in Pipes

It is understood that bounded fluid flow can be internal or external. In either of the flow instances, the fluid will interact with the wall/boundary to give rise to a boundary layer. As air moves through the pipe, air molecules adjacent to the boundary stick to the surface due to adhesive forces and/or wall roughness. Flowing molecules that collide with the molecules stuck at the surface are slowed down, which in turn also slows the molecules flowing above them. A thin layer of liquid is thus created, having a velocity equal to zero at the boundary surface and equal to the free stream value away from it. This layer is known as the boundary layer. The Reynolds number affects the thickness of the boundary layer in an inverse relationship.

Boundary layers may be either laminar (layered) or turbulent (disordered), their velocity profiles are seen in Figure 2.14.

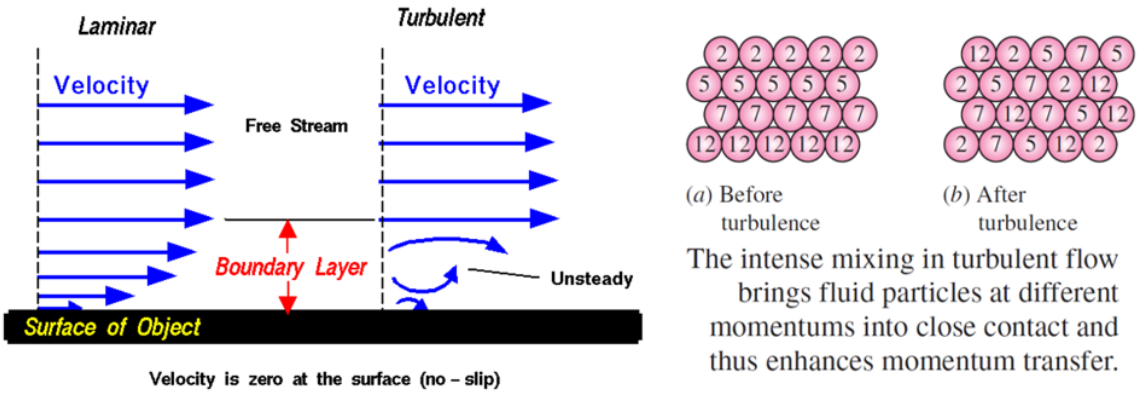

Figure 2.14: Laminar and turbulent boundary layers [26,27]

Now let us examine air as it enters a circular pipe at a consistent velocity. A boundary layer will be created as described previously, but radially over the circular perimeter of the pipe. A velocity gradient will also develop along the pipe as the midsection fluid velocity surges to maintain a constant mass flow rate. Figure 2.15 (a) helps visualize the fluid as it enters a pipe.

The flow profile thus formed can be divided into the boundary layer region, where viscous effects are dominant and cause a velocity change in the radial direction, and the core/irrotational flow region, where viscous effects are negligible as is exhibited by the constant fluid velocity in the radial direction [26], separated by a hypothetical boundary surface. The boundary layer increases in thickness in the direction of flow until it reaches the pipe axis to fill up completely. The corresponding length of pipe from inlet to the point of coincidence of the pipe centerline and the boundary layer is called the hydrodynamic entrance region/length. Beyond this exists the hydrodynamically fully developed region where no velocity profile change takes place. Similarly, turbulent flow develops initially along the length of the pipe with a velocity profile different from laminar flows.

A velocity profile that is parabolic in nature is characteristic of laminar flow, unlike turbulent flows in which velocity profiles are fuller, with a steep decline immediate of the pipe wall as a consequence of effective momentum transfer due to rapid mixing. Hence a turbulent velocity profile has unique characteristics radially inwards from the pipe walls. This is better understood by dividing the profile into four zones, namely [26]:

- Viscous sublayer – Dominated by viscous effects (immediate to the wall)
- Buffer layer – Turbulent effects noticeable (between viscous sublayer and inertial sublayer)
- Overlap/Transition layer or Inertial sublayer – Significant but not dominant turbulent effects
- Turbulent layer – Outermost layer, furthest away from the wall. Viscous effects dominated by turbulence.

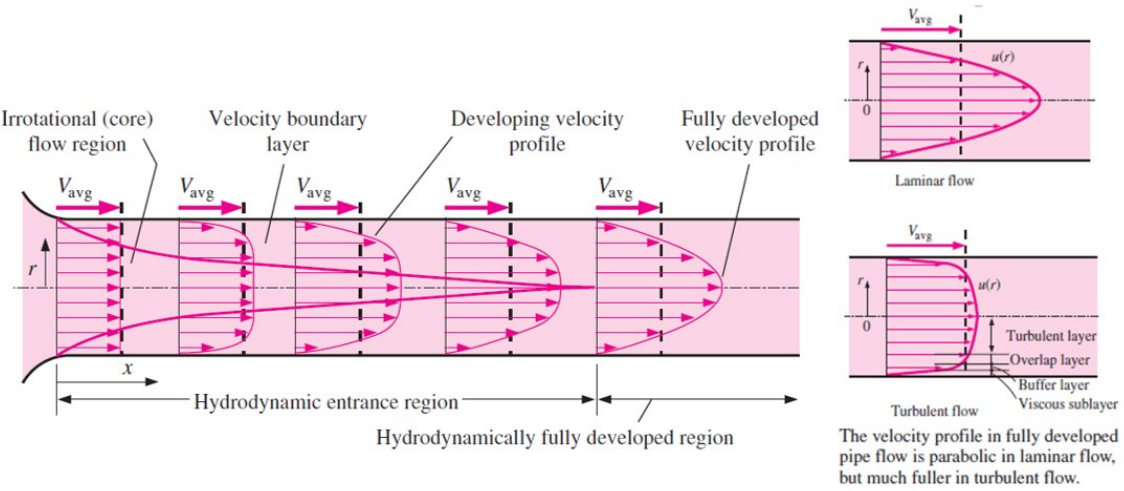

(a) *(b)*

Figure 2.15: Velocity profile for viscous fluid flow in pipes [26]

2.3.2 Concept of Law of the Wall

In an attempt to better understand turbulence and the corresponding velocity profile, researchers applied dimensional analysis to flow near a solid boundary, in a concept known as law of the wall. It is derived assuming that the turbulence near that boundary is a function only of the flow conditions pertaining to that wall, and is independent of the flow conditions further away, while constants are determined through experiments [26]**.** It must be noted that the viscous sublayer is very thin (usually a great deal lower than 1/100th of pipe diameter) [26]. Although thin, this layer dominates flow characteristics since it involves large velocity gradients. Eddy motion, if any, is damped by the wall, basically leading to laminar flow and shear stress that is really laminar shear stress proportional to fluid viscosity. There is a sharp increase in velocity across this thin viscous sublayer (Figure 2.15 (b)), which favors the approximation that velocity profile is linear here, a fact confirmed by experiments [26].

If μ is the dynamic viscosity of the fluid, u is the local velocity, and y is distance of point of interest from the wall ($y = R - r$ for a circular pipe), then [26]:

$$\text{Wall shear stress } \tau_w = \mu\frac{u}{y} = \rho\nu\frac{u}{y} \tag{2.1}$$

Or,

$$\frac{\tau_w}{\rho} = \frac{\nu u}{y} \tag{2.2}$$

Where ν is the kinematic viscosity of the fluid.

Analyzing the dimensions of $\frac{\tau_w}{\rho}$ tells us that its square root gives us the dimension of velocity. It is thus handy to consider it as an imaginary velocity called friction velocity 'u_*' where,

$$u_* = \sqrt{\frac{\tau_w}{\rho}} \tag{2.3}$$

Reviewing Equation 2.2,

$$\frac{\tau_w}{\rho} = \sqrt{\frac{\tau_w}{\rho}}\sqrt{\frac{\tau_w}{\rho}} = u_* u_* = \frac{\nu u}{y}$$

Rearranging,

$$\frac{y u_*}{\nu} = \frac{u}{u_*} \tag{2.4}$$

For $0 \leq \frac{y u_*}{\nu} \leq 5$, Equation 2.4 (i.e. the law of the wall) is quite comparable to experimental data for smooth surfaces. Viscous sublayer thickness can thus be approximated as [26]:

$$viscous\ sublayer\ thickness\ = y = \frac{5\nu}{u_\tau} = \frac{25\nu}{u_{boundary\ layer\ edge}} \tag{2.5}$$

Where $u_{boundary\ layer\ edge} \simeq u_{average\ flow\ velocity}$

This relation reveals that the viscous sublayer thickness is directly proportional to viscosity and inversely proportional to average flow velocity. It is physically manifested by thin viscous sublayers for high velocity (hence, high Reynolds number) flows, a consequence of which is that the velocity profile gets flatter and the velocity distribution becomes more uniform.

Dimensional analysis also showed that $\frac{\nu}{u_*}$ has a dimension of length. This quantity is known as the viscous length, and it is applied on 'y' (distance from the surface) to nondimentionalize it since boundary layer analysis is simpler when working with non-dimensional variables.

Thus,

Non-dimensional distance from the surface/wall= $y^+ = \frac{y u_*}{\nu}$ (2.6)

y^+ may also be defined as the ratio of turbulent to laminar influence.

Non-dimensional velocity= $u^+ = \frac{u}{u_*}$ (2.7)

Or, $y^+ = u^+$ (Normalized law of the wall) (2.8)

Practical application of y^+ will be seen in Chapter 5 dealing with CFD analysis, where it dictates the applied meshing strategy.

Connecting experimental data with velocity yielded the following relation [26]:

$\frac{u}{u_*} = \frac{1}{\kappa}\ln\frac{yu_*}{\nu} + B$ (The logarithmic law) (2.9)

Where $\kappa \cong 0.4$ and $B \cong 5$ are experimentally determined constants. Hence,

$\frac{u}{u_*} = 2.5\ln\frac{yu_*}{\nu} + 5$ (2.10)

$u^+ = 2.5\ln y^+ + 5$ (2.11)

It so happens that the logarithmic law (Equation 2.9 or Equation 2.10) sufficiently correlates with experimental data everywhere, but falls short in the wall adjacent region and near the pipe center, as seen in Figure 2.16. It is thus accepted as the 'universal velocity profile' for surface bounded turbulent flows.

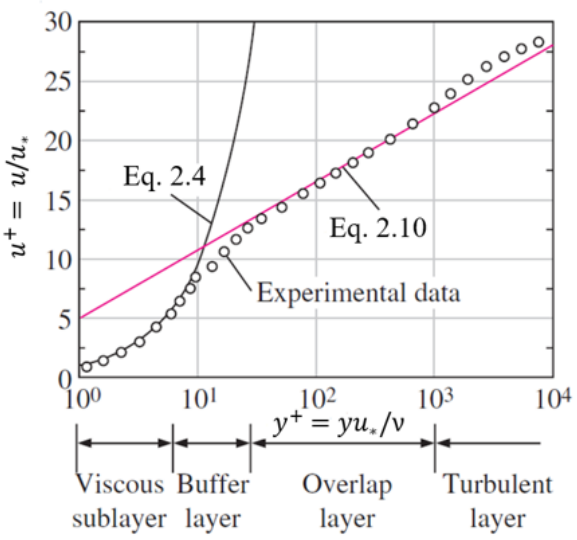

Figure 2.16: Developed turbulent boundary layer profile [26]

Figure 2.16 shows that neither Equation 2.4 nor Equation 2.10 is accurate in the buffer layer ($5 < y^+ < 30$). It is also seen that for the y^+ value, the sublayers are approximately:

- Viscous sublayer ($y^+<5$)
- Buffer layer ($5< y^+<30$)
- Turbulent/log-law region ($30<y^+<60$)

2.3.3 Concept of Turbulent Shear Stress

Laminar flows are relatively simple to model with confidence as compared to turbulent flow. Specific concepts and hypotheses are applied to model turbulent flows, each with their own strengths and weaknesses. One such hypothesis is the existence of turbulent shear stress, widely used in CFD to model turbulence.

We know that turbulent flows are characterized by eddies and fluctuations in properties as the fluid flows. The same may occur in spite of a steady average flow. Velocity fluctuations in a steady turbulent flow are shown in Figure 2.17, where it is evident that the average value is constant while instantaneous values fluctuate. This characteristic permits velocity to be split into an average part '$\bar{u}$' and a fluctuating part $\acute{u}$ such that fluid velocity,

$$u = \bar{u} + \acute{u}$$

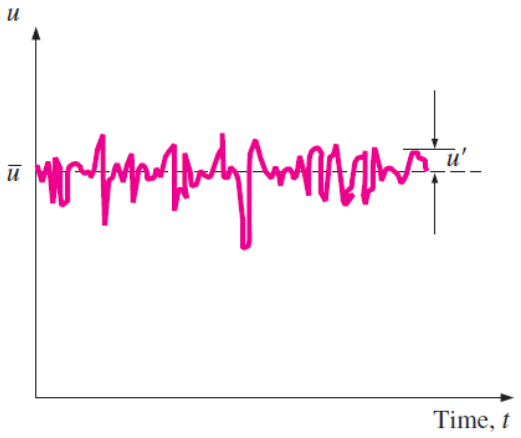

Figure 2.17: Local velocity in turbulent flow [26]

The same logic is extended to other quantities: $v = \bar{v} + \acute{v}$ (Kinematic viscosity), $P = \bar{P} + \acute{P}$ (Pressure) and $T = \bar{T} + \acute{T}$ (Temperature).

These properties are time averaged over a large interval to obtain the average value of the property at a location. Hence, the average of fluctuating components (for example, $\bar{\acute{u}}$) will be equal to zero. The absolute value of $\acute{u}$ is generally a small fraction of $\bar{u}$, however, its constituent high frequency eddies make them excessively potent at transporting mass, momentum and energy [26].

Shear stress for laminar flow is known and established as $\tau = -\mu\frac{d\bar{u}}{dr}$. Attempts were made to try to correlate shear stress for laminar flow with shear stress for turbulent flow, but to no headway since experiments showed larger shear stress for turbulent flows due to turbulent fluctuations. It was thus accepted that turbulent shear stress would consist of two components. First, the laminar shear stress component due to friction between fluid layers in the direction of flow ($\tau = -\mu\frac{d\bar{u}}{dr}$), and second, the turbulent shear stress component due to friction between the fluctuating fluid particles and the fluid body (Figure 2.18).

Hence, total shear stress for turbulent flows may be conveyed as:

$$\tau_{total} = \tau_{laminar} + \tau_{turbulent}.$$

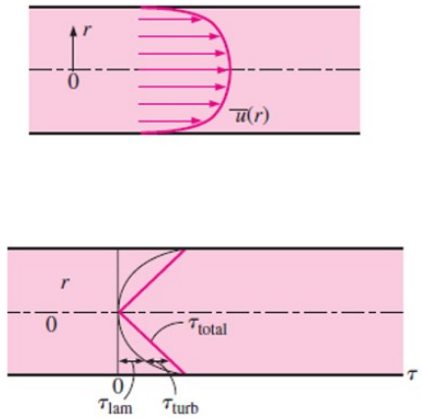

The velocity profile and the variation of shear stress with radial distance for turbulent flow in a pipe.

Figure 2.18: Turbulent velocity profile and total shear stress [26]

Let us examine a horizontal pipe with turbulent flow (Figure 2.19) [26]:

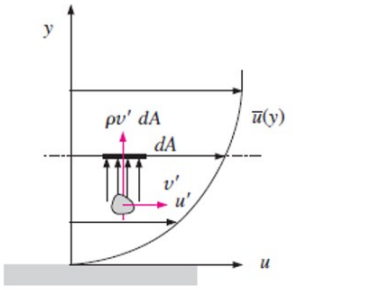

Fluid particle moving upward through a differential area dA as a result of the velocity fluctuation v'.

Figure 2.19: Movement of fluid particle in turbulent flow [26]

Fluid particles in a layer of low velocity move by means of an upward eddy motion, through a differential area dA, to an adjoining layer of higher velocity as a consequence of velocity fluctuation $\acute{v}$. Fluid particles will move through differential area dA with a mass flow rate of $\rho\acute{v}dA$. Momentum transfer will result in the fluid particles under consideration to speed up by $\acute{u}$ at the cost of slowing down the faster moving fluid above dA. The rate of momentum exchange is thus equal to $\acute{u}(\rho\acute{v}dA)$. By Newton's second law, horizontal force experienced by the fluid element above dA as a reaction to the fluid particles passing through dA is equal to $\delta F = (-\acute{u})\rho\acute{v}dA$. It can be concluded that eddy motion of the fluid particles have caused a shear stress (shear force per unit area dA) equivalent to:

$$\frac{\delta F}{dA} = \frac{(-\acute{u})\rho\acute{v}dA}{dA} = -\acute{u}\rho\acute{v} = -\rho\acute{u}\acute{v} \tag{2.12}$$

Expression for turbulent shear stress thus becomes: $\tau_{turbulent} = -\rho\overline{\acute{u}\acute{v}}$ (2.13)

Time-averaging the product of fluctuating velocity components $\acute{u}$ and $\acute{v}$ results in $\overline{\acute{u}\acute{v}}$ such that $\overline{\acute{u}\acute{v}} \neq 0$, although it so might happen that $\overline{\acute{u}} = 0$ and $\overline{\acute{v}} = 0$.

Notably, $-\rho\overline{\acute{u}^2}$ like $-\rho\overline{\acute{u}\acute{v}}$ has a dimension of stress. Such terms are known as Reynolds stresses, in addition to being known as turbulent stresses. Reynolds stresses are modeled in terms of average velocity gradients in numerous semi-empirical formulations so as to implement mathematical closure to the equations of motion [26]. The aforementioned models, known as turbulence models, are extensively used in Computational Fluid Dynamics, and the different types will be discussed in Chapter 5.

3. Flow Characterization of the Disk-Slot Valve by Theoretical Estimation

This chapter takes up theoretical characterization of flow in the disk-slot load leveling valve. Considering the internal structure of the valve, thermodynamic principles and gas laws are used to develop a formulation to calculate mass flow rates. A literature survey conducted to relate theoretical and experimental results is also presented. The chapter ends with the presentation of theoretically estimated flow characteristics of the disk-slot valve.

3.1 Flow Through Pneumatic Valves (Orifice)

Flow control is achieved by means of restricting fluid in a calculated manner. These restrictions are introduced by means of a controlled orifice opening. An orifice here would imply a geometric feature in the flow domain that forces the fluid to suddenly pass through a short, narrow passage, and then in most cases, allows it to return to the original passage size (Figure 3.1).

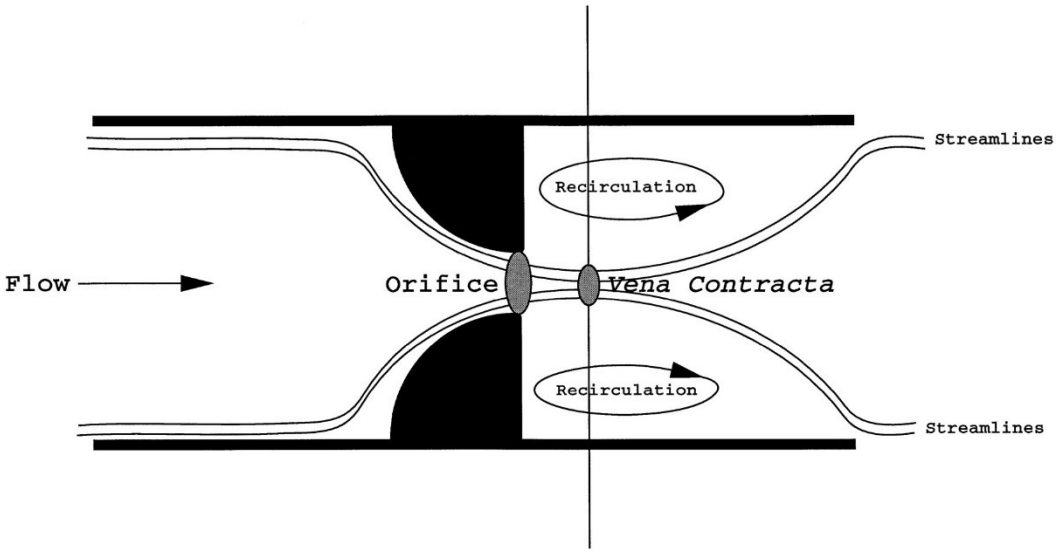

Figure 3.1: Fluid flow through an orifice [28]

Airflow control devices use orifice to meter the flow through them. Figure 3.2 shows a pneumatic solenoid valve with an orifice, which because of its fixed diameter/size, cannot alter the level of flow under a given set of conditions. Figure 3.3 shows the disk-slot and orifice of the disk-slot type load leveling valve. The orifice here can be differentially covered/uncovered (reducing/increasing aperture size) to alter flow rates at a given set of conditions.

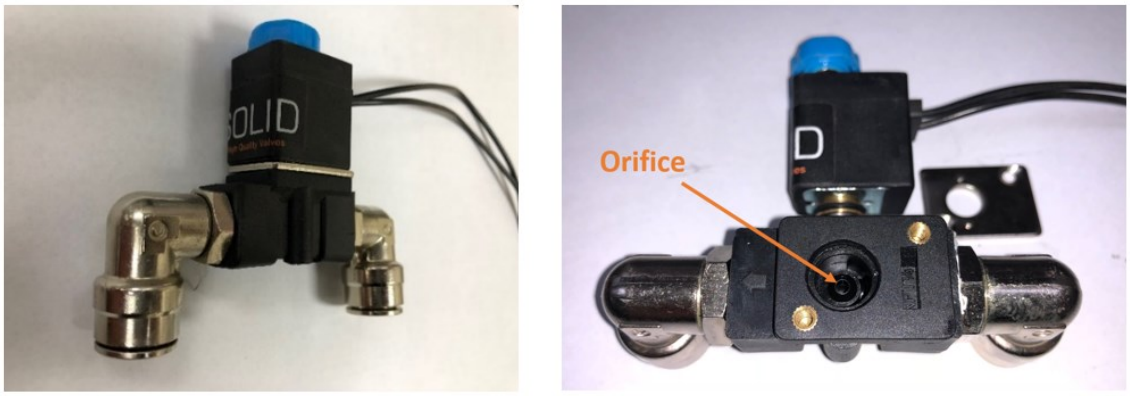

Figure 3.2: Solenoid valve and its orifice

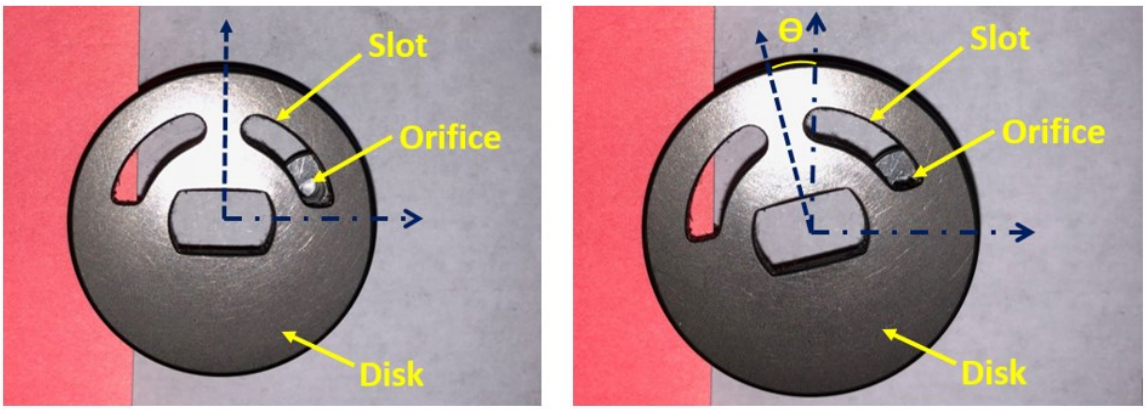

Figure 3.3: Fully uncovered (left) and partially covered (right) orifice of the disk-slot valve

3.2 Formulation of Flow Rate Equations

Let us consider an orifice placed in line between an air reservoir (inlet) and an outlet, as shown in in Figure 3.4.

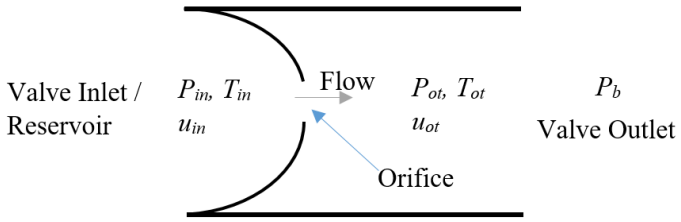

Figure 3.4: Air discharge through orifice (schematic)

P_{in} and T_{in} are inlet pressure and temperature, respectively (assumed constant). P_{ot} and T_{ot} are the outlet pressure and temperature, respectively. u_{in} and u_{ot} are the inlet and outlet velocities, respectively. Let A be the flow area of the orifice, and let P_b be the external downstream pressure. By assuming that the orifice model remains at constant equilibrium such that there is an airflow output once pressure is applied at the inlet at a given temperature, the energy balance equation for an open system is derived as [29]:

$$m_{in}h_{in} + \frac{1}{2} m_{in}u_{in}^2 + m_{in}gz_{in} + Q = m_{ot}h_{ot} + \frac{1}{2} m_{ot}u_{ot}^2 + m_{ot}gz_{ot} + W \quad (3.1)$$

Where,

$m_{in}h_{in}$ is the inflow air enthalpy

$\frac{1}{2} m_{in}u_{in}^2$ is the inflow air kinetic energy

$m_{in}gz_{in}$ is the inflow air potential energy

Q is the heat exchanged in the system

$m_{ot}h_{ot}$ is the outflow air enthalpy

$\frac{1}{2} m_{ot}u_{ot}^2$ is the outflow air kinetic energy

$m_{ot}gz_{ot}$ is the outflow air potential energy

W is the work done by the system

The potential energy term can be neglected since elevation difference between input and output is very small (negligible).

Mass inflow = Mass outflow (conservation of mass and no leakage in valve)

$Q = 0$, $W = 0$, since there is no heat exchange or work done by the system.

Hence,

$$h_{in} - h_{ot} + \frac{1}{2} u_{in}^2 + \frac{1}{2} u_{ot}^2 = 0 \tag{3.2}$$

We know that,

$$h = c_p T \text{ and } c_p = \frac{\gamma R}{\gamma - 1}$$

Thus,

$$\frac{\gamma R}{\gamma - 1} T_{in} - \frac{\gamma R}{\gamma - 1} T_{ot} - \frac{1}{2} u_{ot}^2 = 0 \qquad (u_{in} \approx 0 \text{ due to stagnation conditions}) \tag{3.3}$$

Substituting $T = \frac{P}{\rho R}$ for inlet and outlet, respectively, and solving for outlet velocity,

$$u_{ot} = \sqrt{\frac{2\gamma}{\gamma - 1}} \sqrt{\frac{P_{in}}{\rho_{in}} \left(1 - \frac{\rho_{in} P_{ot}}{\rho_{ot} P_{in}}\right)} \tag{3.4}$$

Assuming an isentropic flow, $\frac{P}{\rho^\gamma}$ = constant

$$u_{ot} = \sqrt{\frac{2\gamma}{\gamma - 1}} \sqrt{RT_{in} \left(1 - \left(\frac{P_{ot}}{P_{in}}\right)^{\frac{\gamma - 1}{\gamma}}\right)} \tag{3.5}$$

Mass flow rate = $\dot{m} = \rho_{ot} A u_{ot}$

$$\dot{m} = \rho_{ot} A u_{ot} = \rho_{ot} A \sqrt{\frac{2\gamma}{\gamma - 1}} \sqrt{RT_{in} \left(1 - \left(\frac{P_{ot}}{P_{in}}\right)^{\frac{\gamma - 1}{\gamma}}\right)} = \frac{\rho_{ot}}{\rho_{in}} \rho_{in} A \sqrt{\frac{2\gamma}{\gamma - 1}} \sqrt{RT_{in} \left(1 - \left(\frac{P_{ot}}{P_{in}}\right)^{\frac{\gamma - 1}{\gamma}}\right)} \tag{3.6}$$

$$\Rightarrow \dot{m} = P_{in} A \sqrt{\frac{2\gamma}{\gamma - 1}} \sqrt{\frac{1}{RT_{in}} \left[\left(\frac{P_{ot}}{P_{in}}\right)^{\frac{2}{\gamma}} - \left(\frac{P_{ot}}{P_{in}}\right)^{\frac{\gamma + 1}{\gamma}}\right]} \qquad \text{(the theoretical mass flow rate)} \tag{3.7}$$

The mass flow rate (Equation 3.7) is a function of $\frac{P_{ot}}{P_{in}}$ (ratio of outlet to inlet pressure). Maxima/minima of this function can be obtained on solving $\frac{d\dot{m}}{d(\frac{P_{ot}}{P_{in}})} = 0$.

Maxima was found at a pressure ratio given by the relation:

$$\frac{P_{ot}}{P_{in}} = (\frac{2}{\gamma+1})^{\frac{\gamma}{\gamma-1}} \tag{3.8}$$

Equation 3.8 is known as the critical pressure ratio (P_{cr}). It defines the magnitude of pressure ratio at and below which, flow at the orifice is sonic, a condition known as choked flow. Its significance is that for a given inlet pressure, flow rate does not increase with lowered the downstream pressure (hence, P_{cr}), since flow at the orifice is sonic.

For an isentropic index of 1.4 for dry air, critical pressure ratio $P_{cr} = \frac{P_{ot}}{P_{in}} = 0.528$.

The expression of mass flow rate thus becomes:

$$\dot{m} = P_{in}A\sqrt{\frac{2\gamma}{\gamma-1}}\sqrt{\frac{1}{RT_{in}}\left[(\frac{P_{ot}}{P_{in}})^{\frac{2}{\gamma}} - (\frac{P_{ot}}{P_{in}})^{\frac{\gamma+1}{\gamma}}\right]} \qquad \text{if } (\frac{P_{ot}}{P_{in}}) > P_{cr} \text{ (subsonic flow)} \tag{3.9}$$

$$\dot{m} = P_{in}A\sqrt{\frac{2\gamma}{\gamma+1}}\sqrt{\frac{1}{RT_{in}}}(\frac{2}{\gamma+1})^{\frac{\gamma}{\gamma-1}} \qquad \text{if } (\frac{P_{ot}}{P_{in}}) \leq P_{cr} \text{ (sonic flow)} \tag{3.10}$$

Actual mass flow rate through the orifice will have a dimensionless multiplication factor C_d to account for losses in actual fluid flow:

$$C_d = \frac{Actual\ mass\ flow\ rate}{Theoretical\ mass\ flow\ rate}$$

$$\dot{m}_{actual} = C_d\,\dot{m} \tag{3.11}$$

Where C_d is the coefficient of discharge ($0 < C_d < 1$).

3.3 Estimation of Coefficient of Discharge

The coefficient of discharge or discharge coefficient is a representation of the irrecoverable pressure loss that occurs at the orifice. In totality, losses due to friction and plumbing elements may

be accommodated in it to represent losses of the entire system. Although the discharge coefficient is calculated experimentally in most cases, there is literature that suggests an empirical calculation based on upstream pressure, downstream pressure, orifice thickness, and orifice and inlet pipe diameter. Later it will be found that this factor is the most significant shortcoming of the theoretical model.

Stanton mentioned that compressible fluid flow through the orifice has been long known to demonstrate an increase in the coefficient of discharge as the downstream to upstream pressure ratio is reduced [30]. This increment is sustained even after passing the critical pressure ratio when the flow is sonic because the subsonic mean velocity in the plane of the orifice is influenced by the downstream pressure, unless the discharge coefficient is already equal to one. Driskell, on the other hand, outlined choked flow as the case in which lowering downstream pressure does not increase the flow rate, adding that the vena contracta shifts towards the orifice and coincides with it at choked condition [31]. The fact that the vena contracts, coinciding with the orifice (as affirmed by Driskell) would imply a C_d equal to 1.0, a professed disagreement with the C_d values of well-formed nozzles being less than 1.0.

Crane indicated that a nearly constant discharge coefficient for sharp edge orifice at high Reynolds numbers ($>10^5$) depends only on the ratio of orifice to pipe diameter [32]. An expansion factor calculated by means of a function of pressure drop ratio and expansion coefficient would need to be used to adjust for gases and vapors. However, no minimum value as such is mentioned in the Crane method for square-edged orifices. Jobson proposed a method which related downstream to upstream pressure ratio to the discharge coefficient, assuming that on the orifice upstream side, the velocity pattern at the walls was independent of flow rate [33]. The assumption fails and supplies false results for discharge coefficients greater than 0.65 and at very low values of pressure ratio, on account of compressibility affecting the upstream velocity pattern. Bragg improved upon Jobson's discharge coefficient formulations but again, they were valid for high pressure ratios only [34]. Kayser et al. experimentally studied the subsonic and critical flow regions of compressible gas flow through knife-edged orifices, straight-bore orifices, rounded entry, and elliptical entry nozzles with diameters ranging from 0.9 to 1.9mm [35]. The study concluded that flows across knife-edge orifices are not as complex as that across straight bore orifices since the vena contracta is affected by the walls of the bore, thus supporting the case that the length to diameter ratio profoundly affects the discharge coefficient. Coefficient profile was also found to be roughly constant for subsonic

and sonic flow in the case of larger length to diameter ratios for the gases and temperatures studied, but high pressure effects needed further research. It was also deduced that minute differences in orifice construction/geometry can alter the discharge coefficients. Ward-Smith summarized that the ratio of orifice thickness (t) to the orifice diameter (d) is the major parameter affecting sonic discharge coefficient [36]. A claim was also made that once sonic velocity is attained, velocity through the vena contracta does not increase on lowering the downstream pressure but vena contracta size can increase for thin orifice plates. Ward-Smith provided the following C_d values:

Sharp edge, t/d = 0, $C_d = 1$
Thin plate (0<t/d<1), C_d = f (t/d) with 1< C_d <0.81
Thick plate (1<t/d<7), $C_d = 0.81$
Very thick plate, (t/d>7) C_d<0.81 (per Fanno friction)

The ASME standard MFC-3M-1989 offers C_d relations as a function of orifice to inner pipe diameters but there are limitations. It is applicable to pressure difference devices having turbulent and subsonic flow, specified pipe size, Reynolds number limits, diameter ratio (orifice to upstream pipe) between 0.2-0.7, and downstream to upstream pressure ratio more than or equal to 0.75. Most notable, pressure ratios greater than the critical pressure ratio and choked flow through orifice are not covered.

Perry's polynomia [37], used in the widely available software AMESim, suggested discharge coefficients for subsonic, sonic, and supersonic compressible fluids as a function of pressure ratios (Equation 3.12). It also exhibits a trend of C_d vs pressure ratios which is in agreement with the literature reviewed (pressure ratio decreases, C_d increases), as seen in Figure 3.5.

$$C_d = \left(\left(\left(\left(-1.6827\frac{P_{ot}}{P_{in}} + 4.6\right)\frac{P_{ot}}{P_{in}} - 3.9\right)\frac{P_{ot}}{P_{in}} + 0.8415\right)\frac{P_{ot}}{P_{in}} - 0.1\right)\frac{P_{ot}}{P_{in}} + 0.8414 \qquad (3.12)$$

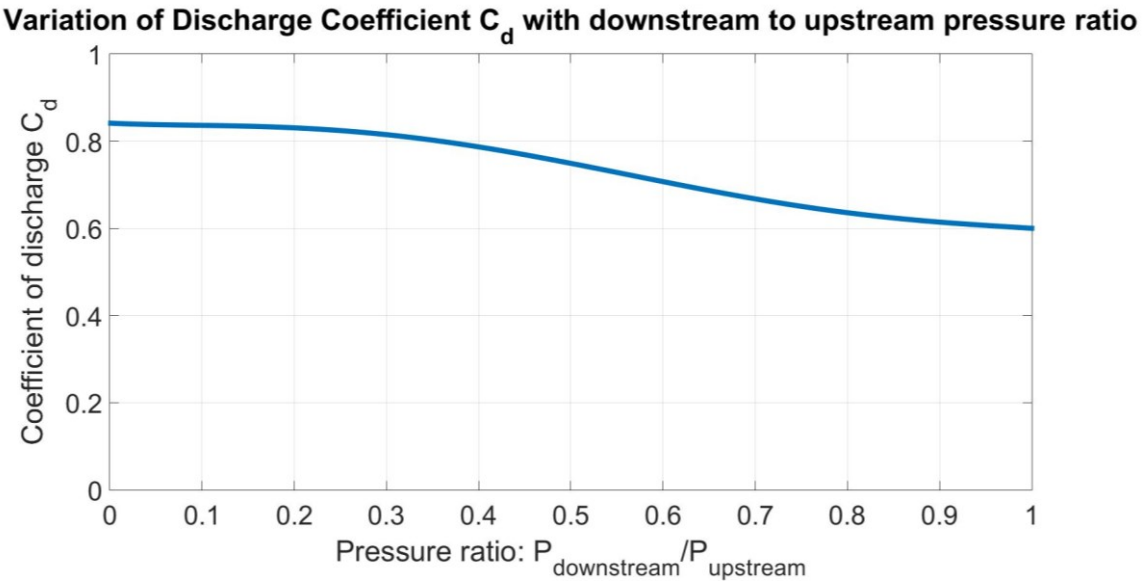

Figure 3.5: Trend of C_d using Perry's formula

The literature review has highlighted the absence of a well-defined and accurate method to calculate discharge coefficient in modeling subsonic and sonic flows while covering a wide range of pressure ratios for a variety of orifice geometries. Also, precise results may be achieved, but only for standard orifice geometries based on empirical relations which may not even represent the real valve orifice as in this study (Figure 3.6). Thus, this study, and specifically Chapter 5, aims to provide a physics-based Computational Fluid Dynamics (CFD) approach to accurately simulate fluid dynamics in any load leveling valve geometry, with minimum required user inputs and reduced model development time.

3.4 Estimated Flow Characteristics of the Disk-Slot Valve

Gauge pressures of 35psi, 50psi, and 65psi were selected as three independent cases of upstream pressure (P_{in}), and atmospheric pressure of 0psi (gauge) was selected as the downstream pressure (P_{ot}). The three cases apply to supply and purge operations in the actuation range (-45 degrees to +45 degrees lever arm/disk rotation) of the valve. The test parameters replicate actual conditions of air being supplied to empty air springs (supply operation) and discharged from pressurized air springs into the atmosphere (purge operation). Equation 3.8 suggested that choked flow conditions (sonic flow at the orifice) would prevail for the given upstream and downstream pressures. MATLAB is used to calculate flow rates using Equation 3.11. Equation 3.12 is applied to calculate the discharge coefficient since it was an empirical formulation as a function of pressure ratios, hence applicable to orifices of varied shapes and sizes. Area of cross-section of the orifice is calculated using a CAD model of the valve by measuring the aperture (uncovered part) area of the orifice (Figure 3.6).

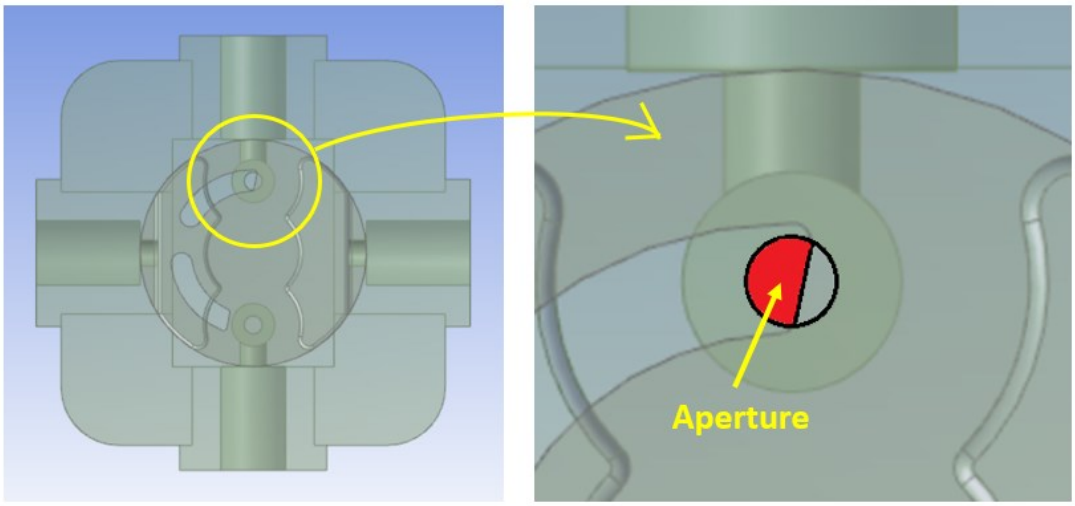

Figure 3.6: Area calculation of orifice aperture for disk-slot valve (12 deg. disk rotation)

Area of cross-section of the uncovered part (aperture) of the orifice was noted against lever arm/disk angle (Table 3.1) from fully covered (lever arm is level) to fully uncovered, for each of the supply (counterclockwise rotation of the disk/lever arm) and purge operations (clockwise

rotation of the disk/lever arm) when the supply port is oriented to face north as was shown in Figure 2.5. Actuation is quantified in terms of lever arm (or disk) angle since it is a valve design feature, a metric common to valves having lever arm of any length, as opposed to suspension travel, which is an application/installation feature dependent on the length of the lever arm.

Table 3.1: Orifice aperture areas for disk-slot valve

Disk-Slot Valve Orifice Aperture Calculation		
Action	**Angle of Disk (degrees)**	**Area of Opening (mm^2)**
Supply Operation - Port S to Port A (Counterclockwise rotation of disk)	18	4.909
	16	4.842
	14	4.33
	12	3.605
	10	2.776
	8	1.918
	6	1.098
	5	0.727
	4	0.401
	3	0.14
Dead band - No flow	2	0
	1	0
	0	0
	-1	0
	-2	0
Dump Operation - Port A to Port S (Clockwise rotation of disk)	-3	0.14
	-4	0.401
	-5	0.727
	-6	1.098
	-8	1.918
	-10	2.776
	-12	3.605
	-14	4.33
	-16	4.842
	-18	4.909

It must be noted that due to the size of the orifice and the length of the slot, the orifice remains fully uncovered after 18 degrees and -18 degrees of disk/lever arm rotation (seen in Figure 3.6).

Mass flow rate vs lever arm/disk angle from -45 degrees to +45 degrees at 35psi, 50psi and 65psi is plot to represent theoretically estimated flow characteristics of the disk-slot valve (Figure 3.7). The results are carried forward to Chapter 4 for verification against experimental results.

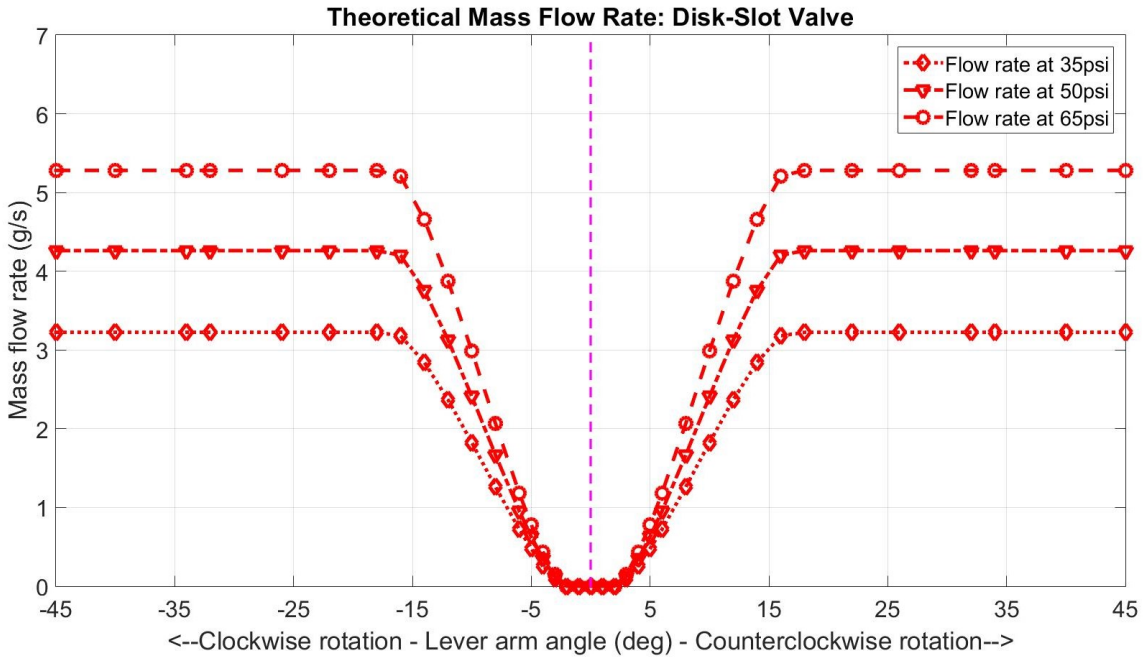

Figure 3.7: Theoretically determined flow characteristics of the disk-slot valve

It is seen from Figure 3.7 that the flow rates are 0 g/s for lever arm/disk angles from -2 to +2 degrees (the dead band region). Maximum flow rates are achieved at full opening ±18 degrees and beyond.

4. Flow Characterization of the Disk-Slot Valve by Experiment

This chapter reviews the purpose and presents a method for an experimental test to determine flow characteristics of the disk-slot valve. The theory behind the experiment and experimental procedure is explained. In addition, flow characteristics obtained by theoretical estimation is co-plotted with results from experimental testing to inspect for agreement in values. Experimental results are also carried forward to Chapter 5 to validate CFD-generated results.

4.1 Purpose and Available Techniques to Determine Actual Flow Rates

To evaluate the actual performance of any valve, it must be physically tested for flow rates. Flow rates may be measured in terms of volume at standard temperatures and pressures, or in terms of mass, as in this study. Experimental testing is undertaken to test for the validity of theoretical and CFD results. To test for flow characteristics of the valve, it was necessary to understand valve operation, and to design an experiment for an accurate measurement of parameters, which were identified as pressure, lever arm angle, and flow rate.

There are gauges available in the market that can measure pressures, angles, and flow rates. Pressure and angle gauges are simple to use and calibrate, hence their selection did not pose a problem, unlike instruments for flow rate measurement. Ideally, flowmeters would be the device of choice to determine flow rates, but there are drawbacks.

Let us consider the digital gas flowmeter (Figure 4.1), which measures flow rates employing heat transfer to gas flowing through an instrumented tube with two temperature sensors and a heating coil [38,39]. By measuring heat imparted to the flowing gas, molecular gas flow rates are computed. The requirements of such sensitive sensors in the construction of flowmeters drive up the cost. Larger the range of measurement and precision, the higher the cost. Full scale for the device suited for current applications would be 0 to 1000 standard liters per minute, the maximum offered by the manufacturer. Since the flowmeter would have no application following this study, its purchase was not justified.

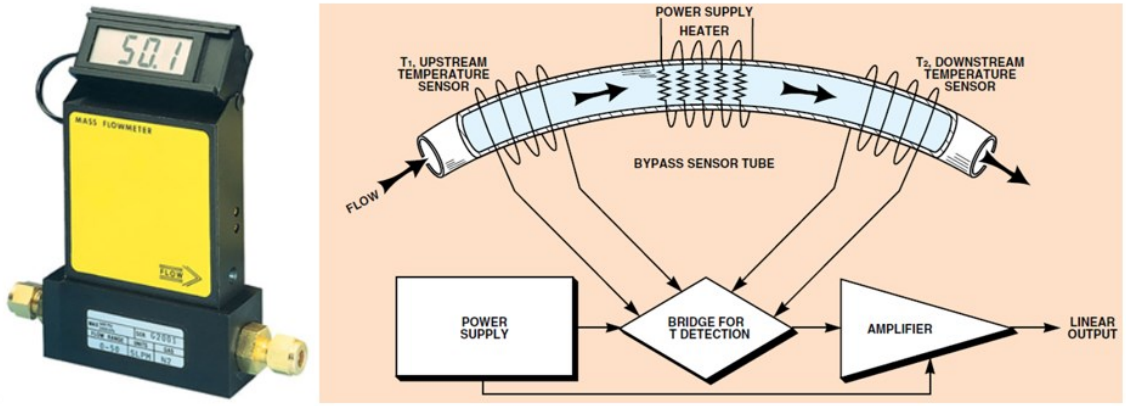

Figure 4.1: Digital flowmeter [38] (left); instrumented sensor tube of flowmeter [39] (right)

A significant shortcoming with the flowmeter is that it is calibrated to a particular inlet pressure, a feature discouraging comprehensive evaluation of flow rates of the load leveling valve using the device. Departures from the calibrated pressure cause erroneous readings. The flowmeter also introduces a back pressure in the line, which is undesirable. Considering all of the above, the use of flowmeters would not yield data worth its cost. Hence, an alternative setup was designed for measuring flow rates.

The alternate setup must measure flow rates in an economical manner with reasonable accuracy. The setup discussed in the next section takes advantage of gas laws and discharge of air from a pressure instrumented fixed volume air tank to measure flow rates, and angle sensors to measure lever arm angles. The presented setup will also be flexible to accommodate and calculate flow rates through any other valve at multiple pressures.

4.2 Formulation of a Flow Rate Relation for Experimental Testing

Air discharged from any fixed volume tank takes a finite amount of time to balance pressure with either another tank or the atmosphere. During this process, there is a gradual decrease of air pressure in the tank. This property can be utilized in an attempt to measure flow rate [40].

Mass of air 'm' at any given time:

$m = \rho V$ where ρ and V are the density and volume of air respectively (4.1)

Differentiating both sides with time:

$$\frac{dm}{dt} = \frac{d(\rho V)}{dt}$$

$$\Rightarrow \dot{m} = \dot{\rho} V + \rho \dot{V} \quad (4.2)$$

Now let us consider a tank with rigid walls (hence, fixed volume V_{to}) containing air of pressure P_{to} placed in an environment of temperature T_o. From the ideal gas equation with R as the universal gas constant, the density of air in the tank:

$$\rho_{to} = \frac{P_{to}}{RT_o} \quad (4.3)$$

Let P_t and ρ_t be the instantaneous pressure and density of air in the tank, respectively.

Discharge of air will cause a pressure drop, which in turn will cause the air density in the tank to change. Since the volume of the air tank is constant ($\dot{V} = 0$), the mass of air discharged:

$$\dot{m} = \dot{\rho}_t V_{to} \quad (4.4)$$

Assuming an isentropic expansion of air in the tank during discharge, we obtain:

$\frac{P_{to}}{\rho_{to}{}^{\gamma}} = \frac{P_t}{\rho_t{}^{\gamma}}$ where 'γ' is the isentropic index of air

$$\Rightarrow \rho_{to} = \rho_t \left(\frac{P_{to}}{P_t}\right)^{\frac{1}{\gamma}} \quad (4.5)$$

Substituting Equation 4.3 into Equation 4.5, we obtain:

$$\rho_t \left(\frac{P_{to}}{P_t}\right)^{\frac{1}{\gamma}} = \frac{P_{to}}{RT_o}$$

$$\Rightarrow \rho_t = \left(\frac{P_{to}}{RT_o}\right)\left(\frac{P_t}{P_{to}}\right)^{\frac{1}{\gamma}} \quad (4.6)$$

Now differentiating Equation 4.6 with time yields:

$$\dot{\rho}_t = \left(\frac{1}{\gamma RT_o}\right)\left(\frac{P_t}{P_{to}}\right)^{\frac{1-\gamma}{\gamma}} \dot{P}_t \quad (4.7)$$

Substituting Equation 4.7 into Equation 4.4, we obtain:

$$\dot{m} = \left(\frac{1}{\gamma R T_o}\right)\left(\frac{P_t}{P_{to}}\right)^{\frac{1-\gamma}{\gamma}} \dot{P}_t V_{to} \tag{4.8}$$

Equation 4.8 represents the mass of air discharged from the tank. If air from the tank is discharged through the valve, $\dot{m}$ represents mass flow rate through the valve. Thus, $\dot{m}$ through the valve at different instantaneous pressures can be extracted. Combined with discharge at different lever arm angles, comprehensive flow performance/characteristics of the valve can be determined.

4.3 Experiment Setup

Equation 4.8 is implemented using a multiport air tank with a mounted electronic pressure sensor and pneumatic hoses connecting the tank to the valve. To measure angle in order to evaluate variation of flow rates with lever arm/disk rotation angles, an angle sensor is attached to the axis of rotation. In addition, an analog to USB device interface is used to collect and transfer analog voltage data from the pressure and angle sensor to the PC for data processing. Room temperature, taken from an indoor thermometer, is considered as the temperature of air in the tank since the tank, after charging, is allowed to sit for a reasonable amount of time. Lastly, a fixture to hold the valve while allowing free movement of the lever arm is required. Figure 4.2 - Figure 4.5 illustrate the experiment setup and components.

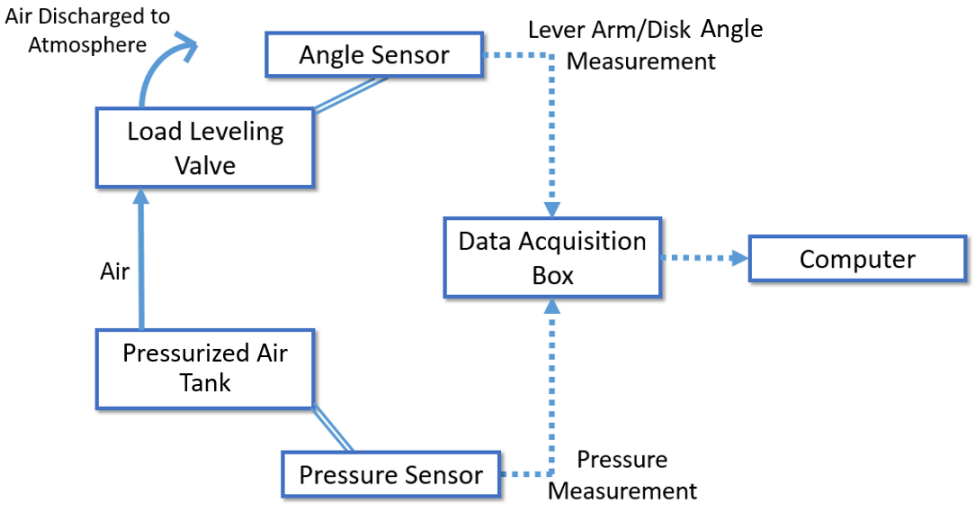

Figure 4.2: Experiment schematic

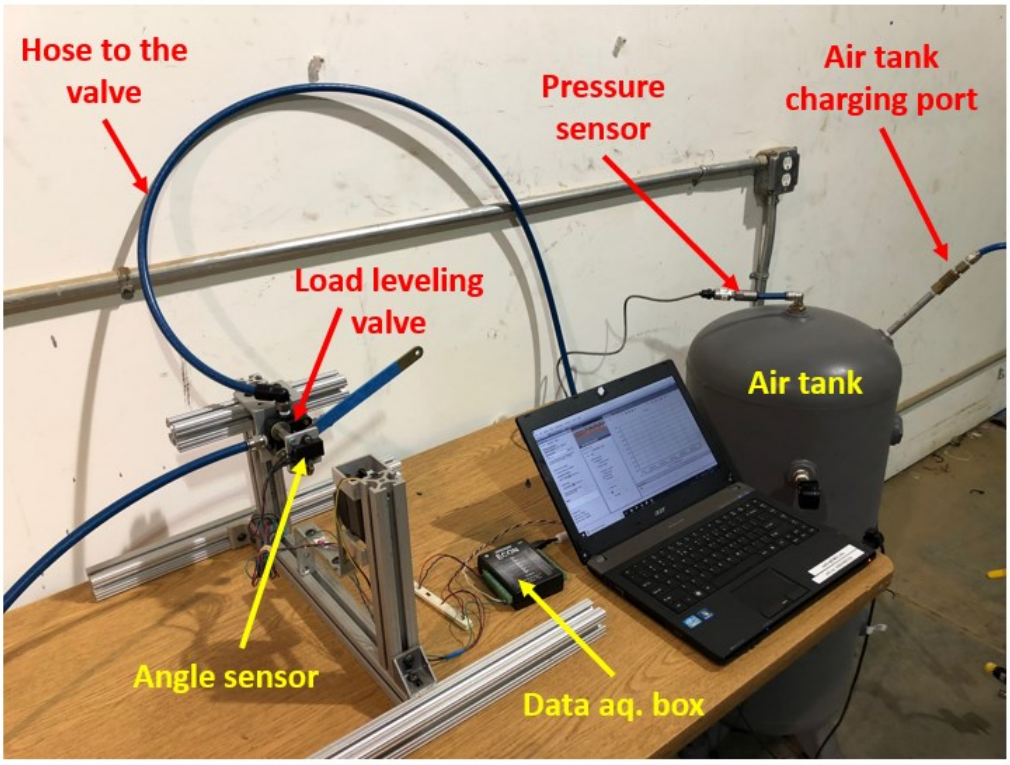

Figure 4.3: Experiment setup

Figure 4.4: Multiport air tank (left); mounted pressure sensor (right)

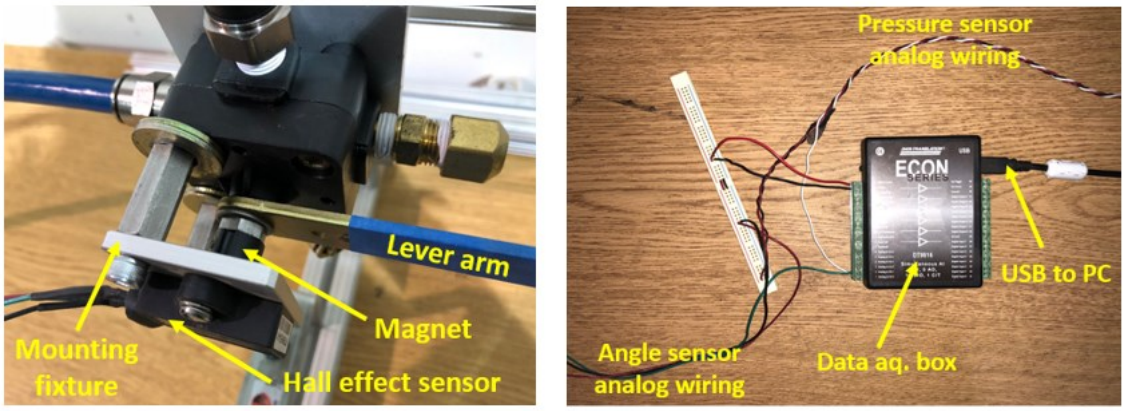

Figure 4.5: Mounted angle sensor (left); data acquisition box (right)

The pressure transducer used is the Honeywell PX2EN1XX250PSAAX [41]. It is a sealed gage 0-5VDC output sensor with a range of 0 to 250 psi and accuracy up to 10^{-3} volts with the current data acquisition box. It has a response time of less than 2ms, making it ideal for the type of application proposed (i.e. it can measure rapid discharge of air from the reservoir without much delay). Research into sensors to measure the lever arm angle led to the Honeywell RTP090HMEAA [42], which works on the principle of Hall Effect, providing an analog voltage output. Measurement ranges from -45 to +45 degrees, adequately covering the working range of load leveling valves. The magnet housing includes threads for set screws which enable it to be securely mounted and fastened on the axis of the lever arm shaft. Data Translation DT9816, a multi-channel 5V system data acquisition box, was used for analog data collection [43]. Time-stamped angle and pressure voltage measurements were directly recorded onto the computer and later converted to be processed on MATLAB.

4.4 Experiment Procedure

Calibration and appropriate placement of instruments is essential to the experiment. The pressure sensor must be calibrated, for the power source used, against a standard pressure gauge. A National Institute of Standards and Technology (NIST) certified pressure gauge was used to calibrate the pressure sensors. It must also be mounted on the tank rather than on the pipe, as is the common tendency, so that the sensor measures only the static pressure of the tank rather than the static

pressure of the airflow in the pipe. The angle sensor is pre-calibrated, but its magnetic principle makes it sensitive to very small angles. Hence, care must be taken such that the magnet is not mounted eccentric to the axis and that the distance of the magnet face from the sensing surface of the body is maintained at specified limits (2±0.5mm). Care must also be taken to ensure a good alignment between the magnet and the sensor, such that the voltage output reads a value corresponding to 0 degree when the valve lever arm is exactly horizontal. This can be achieved using a digital angle gauge to ensure null relative inclinations among the valve body, the lever arm and the sensor body. Zero error, if any, must be noted and compensated for while plotting results. Lastly, there should be no leaks in the system, which can be guaranteed using soap solution.

Data is finally collected in the following steps:

1. Charge the air tank to at least (P+10) psi pressure where P (P = 65 psi in the present case) is the highest pressure of interest for flow rate measurement, as seen in Figure 4.6.
2. Set the lever arm to the desired angle.
3. Open the ball valve completely to allow air to flow through the valve and immediately after, and start recording data.
4. Stop recording when the tank pressure has dropped past the lowest pressure of interest (here, 35psi), as seen in Figure 4.6.
5. Filter pressure and angle sensor raw data on MATLAB (Figure 4.7). Process filtered data according to derived formulations to determine mass flow rate.
6. Scope mass flow rate for the pressure of interest from the mass flow rate vs pressure plot (Figure 4.8).
7. Note results for pressure, lever arm angle, and mass flow rate.
8. Recharge air reservoir using shop air or compressor.

Uniform testing parameters are maintained between theoretical estimation, experimental testing, and CFD analysis. Hence the experiment is conducted for supply and purge/dump operations at 35psi, 50psi, and 65psi upstream pressures, and 0psi downstream pressure, at lever arm angles noted in Table 3.1 and additional positions up to ±45 degrees.

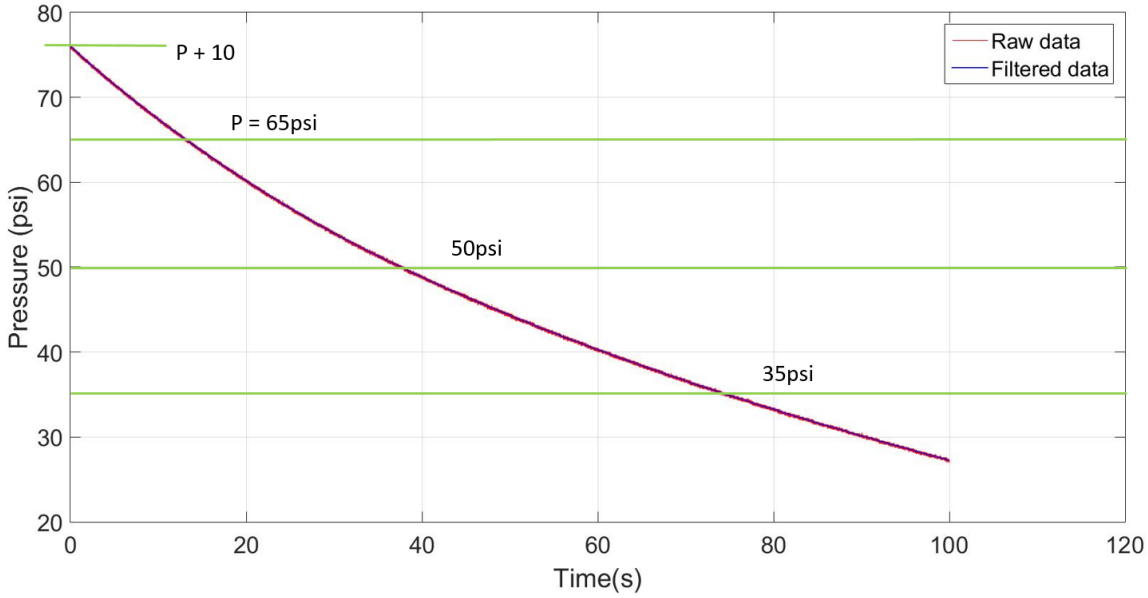

Figure 4.6: Pressure vs time at +18 deg. disk rotation

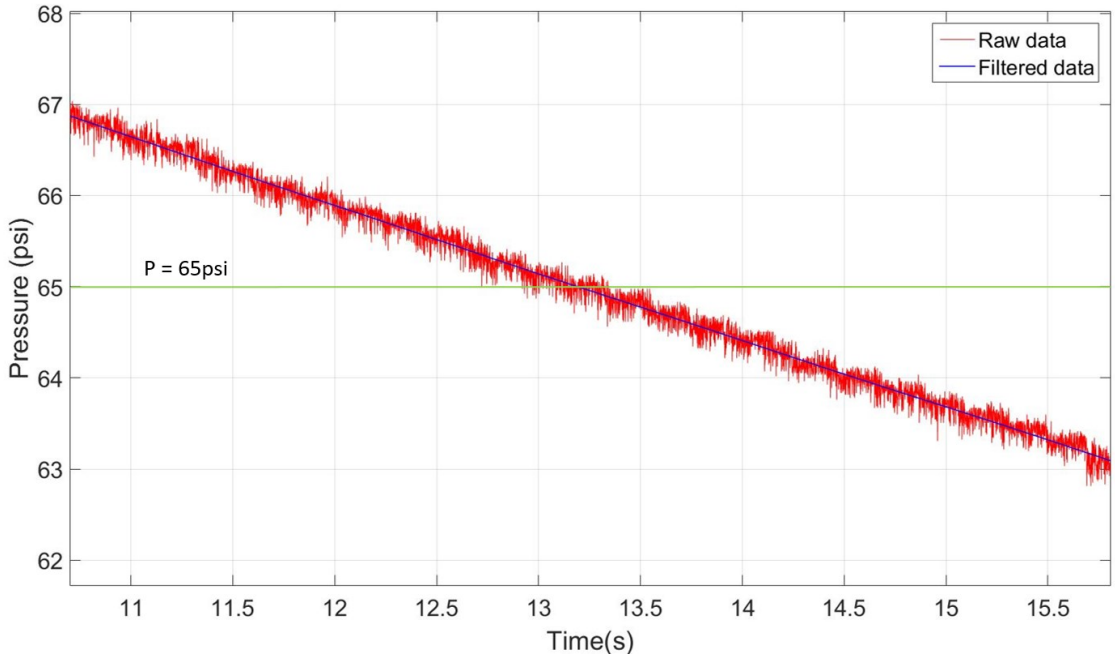

Figure 4.7: Pressure vs time at +18 deg. disk rotation (magnified)

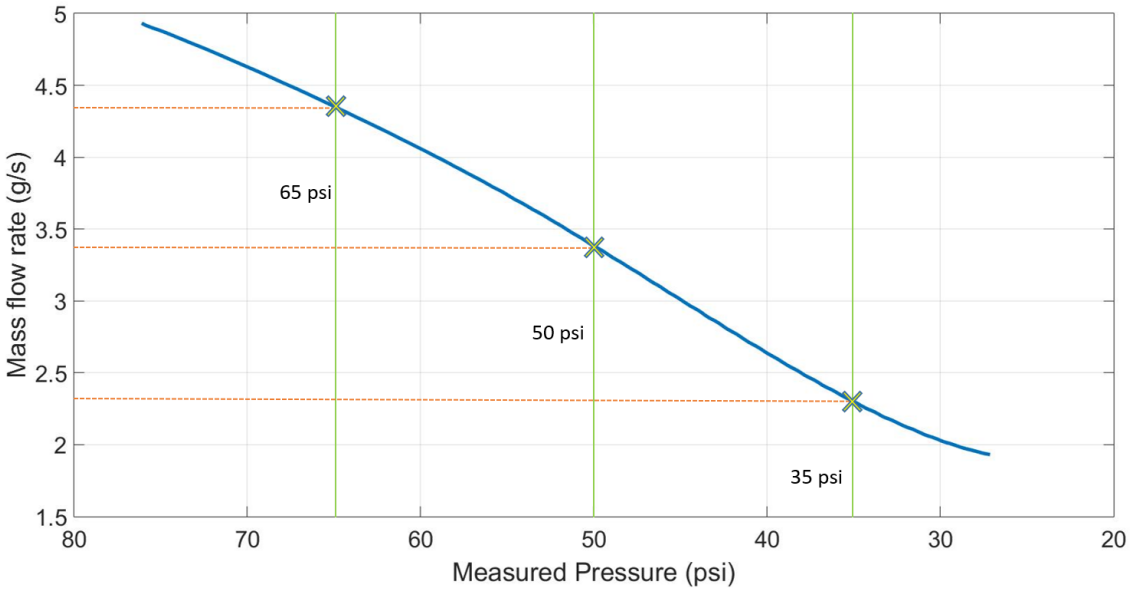

Figure 4.8: Scoping for flow rates at 65psi, 50psi, and 35psi at +18 deg. disk rotation

4.5 Flow Characteristics of the Disk-Slot Valve - Results and Discussion

Experimental testing of the disk-slot valve delivered the following results (Figure 4.9):

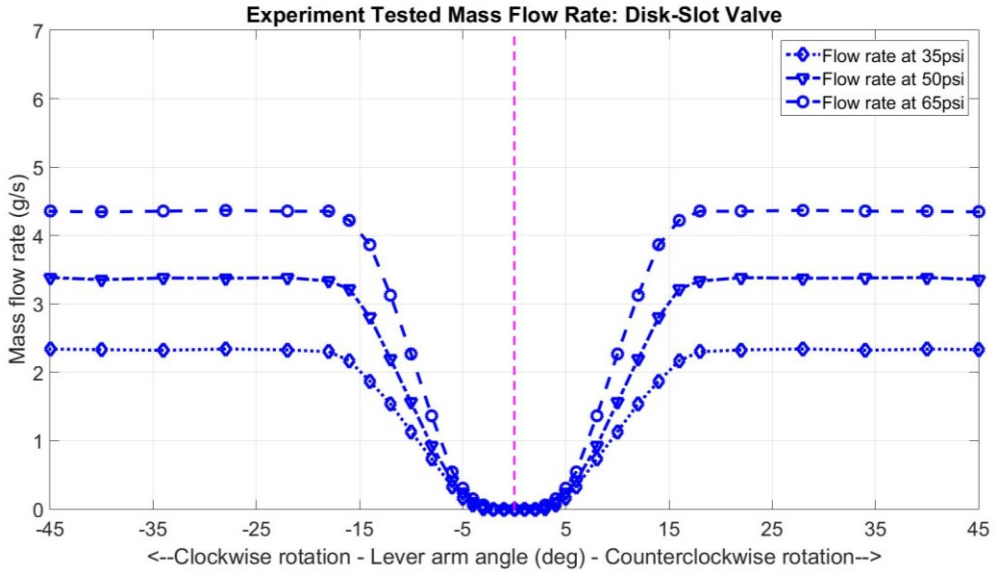

Figure 4.9: Experimentally determined flow characteristics for the disk-slot valve

Initial observation of Figure 4.9 would suggest that the dead band is slightly larger than the expected -2 to +2 degrees, but closer examination of the plot and data shows that flow rates are actually very small just after ±2 degrees, which then rise to reach their maximum at and after ±18 degrees.

Flow characteristic plots from Figure 4.9 were individually compared with those from Figure 3.7 to ascertain agreement in flow characteristics obtained through theoretical estimation, against experiment (Figure 4.10 - Figure 4.12).

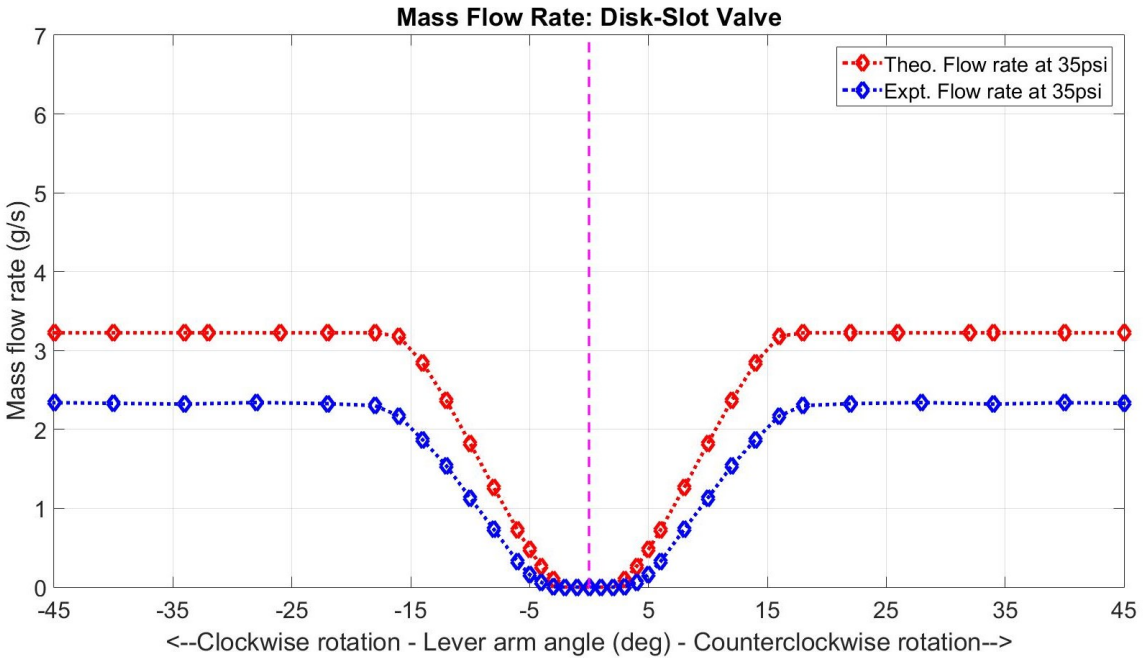

Figure 4.10: Theoretical estimation vs experiment, flow characteristics at 35psi

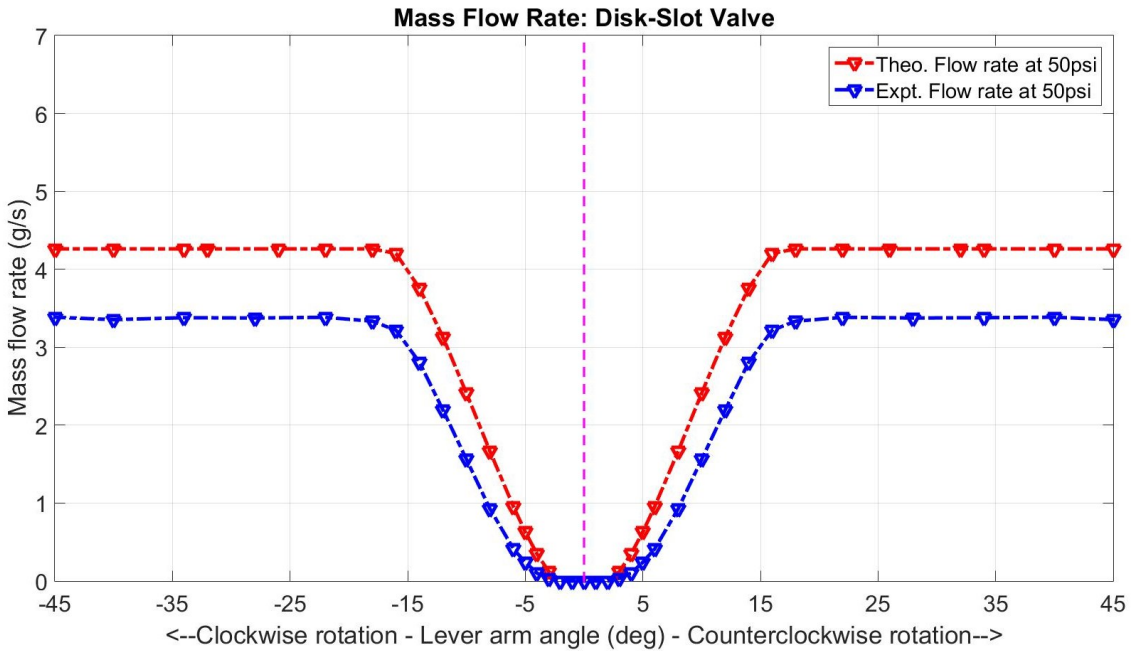

Figure 4.11: Theoretical estimation vs experiment, flow characteristics at 50psi

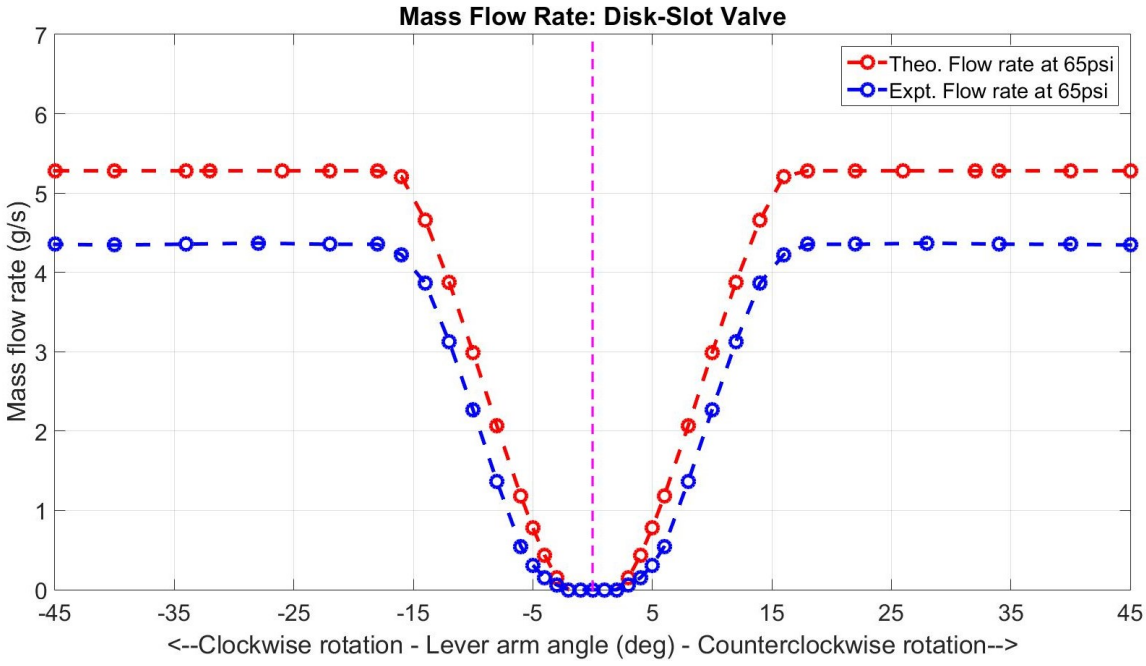

Figure 4.12: Theoretical estimation vs experiment, flow characteristics at 65psi

No agreement is observed in flow characteristics (Figure 4.10 - Figure 4.12). Closer examination reveals that there is a significant difference in flow rates (up to 1 g/s) between the theoretical and experimental results, a magnitude not acceptable for practical design purposes since its impact on air springs with a small overall volume will be quite significant. Figure 4.13 is an illustration of the magnitude of differences in flow characteristics.

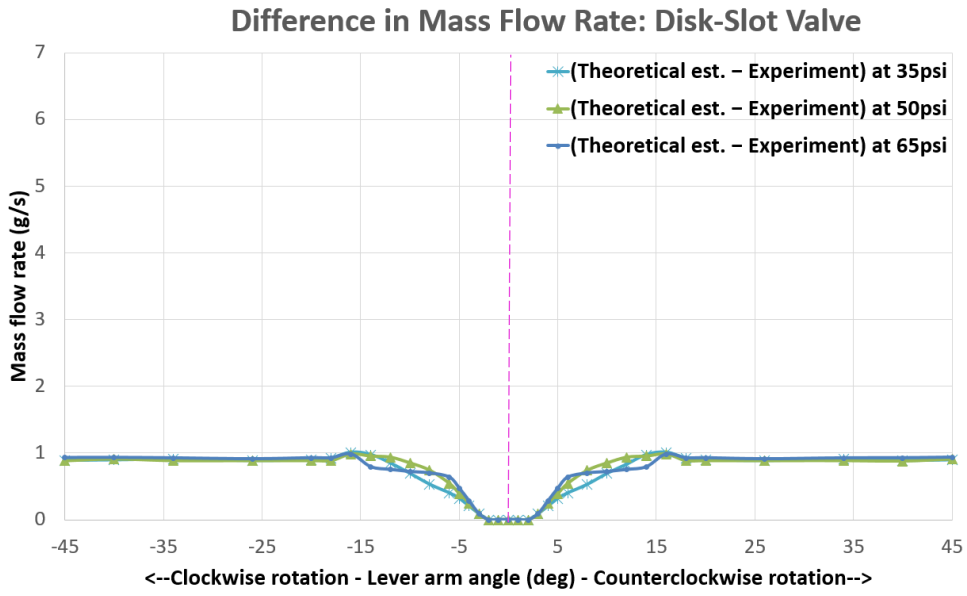

Figure 4.13: Theoretical estimation vs experiment, absolute difference in flow characteristics

It must be noted there are two key differences between theoretical estimation and experiment that contribute to this dissimilarity:

- Additional plumbing elements in the experiment such as fittings, and pipes restrict free flow.
- Inaccurate coefficient of discharge 'C_d' – The difficulty in estimating C_d was discussed in Chapter 3 while developing the theoretical formulation to calculate mass flow rates and characteristics. C_d is a crucial factor in the calculation of actual mass flow rates since it is supposed to represent head losses and losses due to eddies, geometries, etc. The formulation used to estimate C_d (Equation 3.12) was an empirically developed function of pressures only, although the literature suggested that C_d also depends on geometry. That property is elucidated by the fact that the flow characteristics determined through experiment are lower than estimated.

To ascertain if C_d is a significant cause of the difference, a factor (iteratively found to be 0.79) was multiplied to the C_d equation (Equation 3.12) to investigate if an agreement can be obtained between the estimated and experiment results. An improved agreement in flow characteristics was observed, as seen in Figure 4.14 and Figure 4.15, proving that losses are insufficiently appraised in the theoretical model.

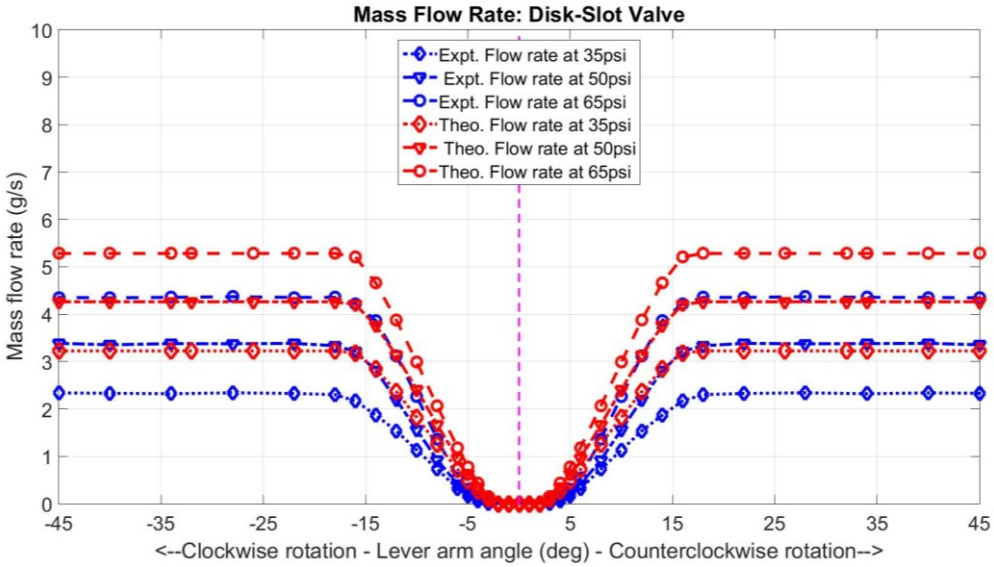

Figure 4.14: Theoretical estimation vs experiment

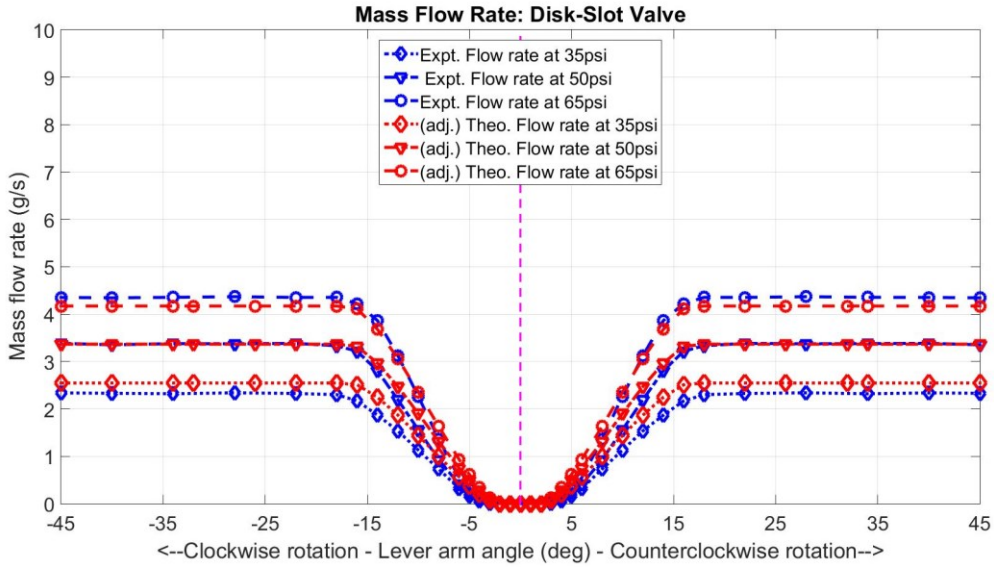

Figure 4.15: Theoretical estimation vs experiment, adjusted C_d

5. Computational Fluid Dynamics (CFD) Modeling of the Disk-Slot Valve for Flow Characterization

This chapter presents the theory underlying CFD, its application in estimating flow characteristics of load leveling valves, and results. An introduction to the governing equations of fluid dynamics and available options for CFD modeling of the valve are then discussed in detail. Thereafter, the options are scrutinized and the literature is reviewed to determine the most appropriate scheme for current application. Steps in setting up the analysis are then presented, followed by evaluation of flow characteristics of the disk slot valve, and comparison to experimental results for validation.

5.1 Introduction to Computational Fluid Dynamics

A section of fluid mechanics, CFD uses numerical investigation and data structures to work out and evaluate fluid flows on the discretized (finite volume, finite element, etc.) fluid domain. Powerful personal computers of today support CFD software in swiftly performing calculations necessary to model and visualize complex flows in interaction with its boundaries.

Governing equations of fluid dynamics, the conservation of energy, mass, and momentum, incorporated as the Navier-Stokes equations, form the basis of CFD modeling [44]:

Equation for continuity (conservation of mass):

$$\frac{\partial \rho}{\partial t} + \frac{\partial (\rho u)}{\partial x} + \frac{\partial (\rho v)}{\partial y} + \frac{\partial (\rho w)}{\partial z} = 0 \tag{5.1}$$

Conservation of X – Momentum:

$$\frac{\partial (\rho u)}{\partial t} + \frac{\partial (\rho u^2)}{\partial x} + \frac{\partial (\rho uv)}{\partial y} + \frac{\partial (\rho uw)}{\partial z} = -\frac{\partial p}{\partial x} + \frac{1}{Re}\left(\frac{\partial \tau_{xx}}{\partial x} + \frac{\partial \tau_{xy}}{\partial y} + \frac{\partial \tau_{xz}}{\partial z}\right) \tag{5.2}$$

Conservation of Y – Momentum:

$$\frac{\partial (\rho v)}{\partial t} + \frac{\partial (\rho uv)}{\partial x} + \frac{\partial (\rho v^2)}{\partial y} + \frac{\partial (\rho vw)}{\partial z} = -\frac{\partial p}{\partial y} + \frac{1}{Re}\left(\frac{\partial \tau_{xy}}{\partial x} + \frac{\partial \tau_{yy}}{\partial y} + \frac{\partial \tau_{yz}}{\partial z}\right) \tag{5.3}$$

Conservation of Z – Momentum:

$$\frac{\partial(\rho w)}{\partial t}+\frac{\partial(\rho u w)}{\partial x}+\frac{\partial(\rho v w)}{\partial y}+\frac{\partial(\rho w^2)}{\partial z}=-\frac{\partial p}{\partial z}+\frac{1}{Re}\left(\frac{\partial \tau_{xz}}{\partial x}+\frac{\partial \tau_{yz}}{\partial y}+\frac{\partial \tau_{zz}}{\partial z}\right) \quad (5.4)$$

Conservation of Energy:

$$\frac{\partial(E_T)}{\partial t}+\frac{\partial(uE_T)}{\partial x}+\frac{\partial(vE_T)}{\partial y}+\frac{\partial(wE_T)}{\partial z}=-\frac{\partial up}{\partial x}-\frac{\partial vp}{\partial y}-\frac{\partial wp}{\partial z}-\frac{1}{RePr}\left(\frac{\partial q_x}{\partial x}+\frac{\partial q_y}{\partial y}+\frac{\partial q_z}{\partial z}\right)+$$
$$\frac{1}{Re}\left(\frac{\partial(u\tau_{xx}+v\tau_{xy}+w\tau_{xz})}{\partial x}+\frac{\partial(u\tau_{xy}+v\tau_{yy}+w\tau_{yz})}{\partial y}+\frac{\partial(u\tau_{xz}+v\tau_{yz}+w\tau_{zz})}{\partial z}\right) \quad (5.5)$$

Where:

x, y, z = Spatial Coordinates
t = Time
} Independent variables

p = Pressure
ρ = Density
u, v, w = Components of velocity in the *x, y, z* directions, respectively
Temp = Temperature (contained in the Energy Equation within E_T)
} Dependent variables

E_T = Total Energy

τ = Stress

q = Heat Flux

R_e = Reynolds Number

P_r = Prandtl Number

In theory, the above coupled differential equations can be solved using calculus for any flow. But in reality, these equations are challenging to solve analytically. In many cases, simplifications and approximations, such as incompressible flow, inviscid flow, etc., are introduced for an uncomplicated solution.

5.2 Objective of CFD Analysis

The objective of CFD analysis is to determine mass flow rates of the disk-slot load leveling valve under previously selected upstream pressure conditions (35psi, 50psi, and 65psi), downstream pressure conditions (0psi), and lever arm/disk angles. The easiest way to solve for mass flow rates would have been through formulations derived in Chapter 3, but the coefficient of discharge calculated using the literature was inconsistent, leading to incorrect mass flow rates as seen from experimental testing. It is suspected that the losses occurring in the valve/orifice were not accurately captured. The literature confirms that flow domain geometry significantly affects the losses and in turn, the flow rate. Hence, inclusion of geometry effects seemed necessary, and those can be brought in through a 2-D and 3-D geometry to be analyzed using CFD.

The valve design, inlet, and outlet conditions are the known parameters and they will be used in conjunction with air as a compressible fluid and appropriate analysis settings in order to ascertain the true nature of flow through the valve. Flow characteristics thus determined must match the experimentally determined values to validate CFD modeling.

5.3 Meshing Strategies

The mesh/grid generated on the fluid domain represents the cells on which the governing equations are approximated. It is influenced by the approach taken to solve occurring flow dynamics. For instance, current test parameters (upstream and downstream pressures) produce pressure ratios lower than the critical pressure ratio according to the choked flow equations, indicating that the airflow velocity at the orifice will most likely be sonic. This necessitates consideration of air a compressible fluid, as well as the adoption of turbulence effects due to the high Reynolds number associated with such high velocities. Thus, the mesh generated must adequately cater to the physics of air flow.

Turbulence, associated eddies, and flow separation are well known causes of energy dissipation. It must be verified that turbulent quantities in complex turbulent flows are properly resolved if high efficiency is required. The presence of walls significantly affects turbulent flows since they act as a sink for energy dissipation. This turbulence (through the spatially-varying effective viscosity due to the wall no-slip condition) plays a dominant role in the transport of mean momentum and other

quantities [45]. Mean flow and turbulence have strong interactions, making the numerical results for turbulent flows more vulnerable than laminar flows when in terms of mesh dependency.

Other than the mean velocity, presence of the wall affects turbulence in superficial ways. For example, in the vicinity of the wall, viscous damping reduces tangential velocity fluctuations, while kinematic blocking reduces normal fluctuations. However, in the outer part of the near wall region, production of turbulence kinetic energy due to the large gradients in mean velocity, swiftly develops the turbulence. The numerical solution is notably affected by near wall meshing since walls are the major cause of turbulence and mean vorticity [45].

Subdivisions of the turbulent boundary layer and the law of the wall y^+ are of significance here. Wall y^+ helps ascertain the quality (coarse/fine) of mesh for a flow, such that the wall adjacent cells are not placed in the buffer layer ($5< y^+<30$). In the case of wall functions, a value of at least $y^+ > 30$ is suitable, while y^+ values < 1 are suitable for near wall modeling [46]. Gerasimov advises using calculated y^+ when dealing with turbulent flows, since this will assist in choosing the most suitable near-wall treatment (using finer mesh near the walls) vs wall functions, and the matching turbulence model based on the wall y^+ [46].

Wall Functions vs Near Wall Modeling

There are two general approaches for modeling and meshing the near wall region. One of them involves using quasi-empirical formulas called ‘wall functions’ between the wall and the fully turbulent layer in the viscosity affected (viscos sublayer and buffer layer) region, and the other involves fine meshing adjacent to the wall known as near wall meshing (Figure 5.1). Generally, wall functions necessitate that the first wall adjacent cell center lies in the log-law layer ($y^+ \approx 30 – 300$), unless they are special use. With this method, the presence of a wall is handled without the need to adjust the turbulence models, with the limitation that the numerical results degrade with grid refinement in the direction normal to the wall [45]. In fact, a suitable range of y^+ values depends on the overall Reynolds number of flow. The lower limit invariably stands at $y^+ \sim 15$, and never below $y^+ < 11$, in the case of standard wall functions.

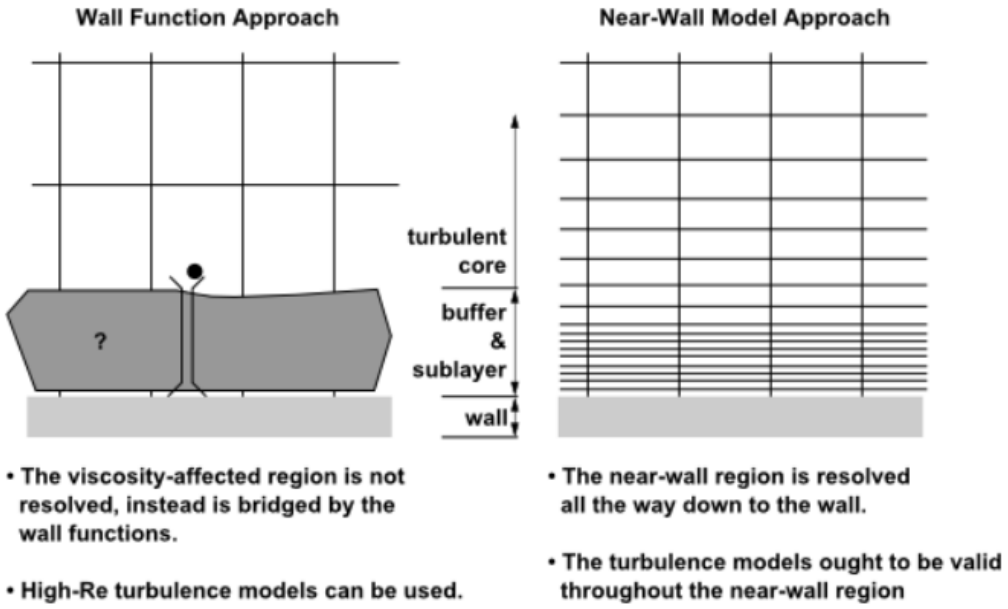

Figure 5.1: Wall functions vs near wall modeling [45]

The following wall function approaches can be considered [45]:

- Standard wall functions – Standard use (default)
- Scalable wall functions – Useful for random grid refinement to produce steady results (can scale itself according to y^+ value).
- Non-Equilibrium Wall functions – Accounts for non-equilibrium effects in the turbulent boundary layer. Improved results for complex flows.
- User Defined Wall function – Custom user-based boundary layer formulation

Wall functions have certain ideal conditions for use, although they deliver acceptable predictions for most wall-bounded high Reynolds number flows. Its reliability diminishes with the following [45]:

- Near wall effects or prevalent low Reynolds number flow
- Heavy wall transpiration
- Boundary layer separation caused by severe pressure gradients
- Powerful body forces
- Large three-dimensionality in the near wall region

Near wall modeling approach revises turbulence models so that a designed mesh up to the wall allows the viscosity affected (viscous sublayer and buffer layer) region to be resolved. Comprehensive resolution of the boundary layer guarantees good quality numerical results for the wall boundary layer, a condition that has more significance than obtaining specific y^+ values. With a y^+ value of ≤ 1, the least number of cells needed to cover the boundary layer precisely is 10, although 20 is desirable (for structured mesh) and a minimum of 15 for unstructured mesh. This implies mesh refinement only in the wall normal direction, which results in an increase in accuracy vs computational effort [45]. The above confirms the necessity of fine meshes to resolve regions of rapid changes in mean flow and large strain rates in shear layers as it occurs in the case of turbulence.

Wall effects can be avoided by defining perfect slip walls/frictionless walls (i.e. the walls do not exert a shear force on the fluid). This approximation reduces simulation time and complexity since a boundary layer will not form on any of the walls. It must be mentioned though that the purpose of the CFD simulation is not to study the boundary layer but to calculate flow rates. It is expected that net losses through the valve will reduce due to this approximation since walls damp turbulent eddies [45].

5.4 Turbulence Models and Solver Settings

In addition to models pertaining to inviscid and laminar flow, mathematical models anticipating the consequence of turbulence, called turbulence models, are available for turbulent flows. Fluctuating velocity fields are a characteristic of turbulent flows. As a result of the fluctuations, transported quantities such as energy, momentum, and species concentration are mixed and fluctuate simultaneously. These fluctuations may be small in scale but are of high frequency, which makes them computationally costly for direct simulation in practical engineering calculations. Rather, the exact/instantaneous governing equations may be time averaged, ensemble averaged, or otherwise manipulated to eliminate the resolution of small scales [45]. This results in a modified set of equations that are computationally cheaper to work out. However, these modified equations involve supplementary unknown variables. Here, turbulence models are required so as to resolve these variables in terms of known quantities and ‘close’ the system of equations.

It must be noted that turbulent flow can be completely resolved down to the smallest scales by solving the Navier-Stokes equation, with a process known as Direct Numerical Simulation (DNS). This method, however, is the costliest and is reserved for applications requiring the highest levels of accuracy.

Turbulence effects can be considered by the following models [45]:

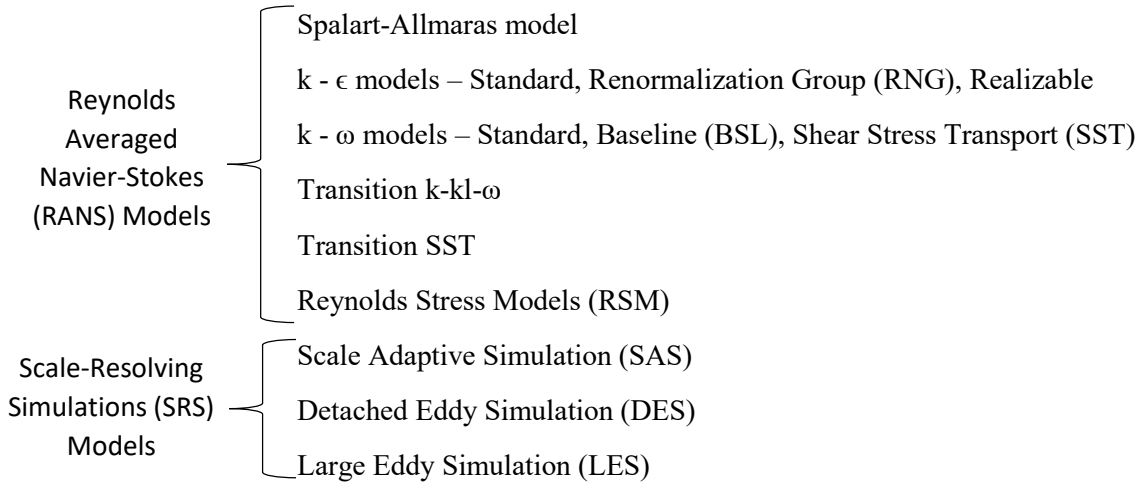

Turbulence models are useful when they are:

- Widely applicable
- Accurate
- Simple
- Economical to run

There is no one turbulence model that is best suited for all classes of flow. Flow physics, traditions in dealing with distinct flow problems, targeted accuracy, computational resources available, and simulation time all contribute in deciding the most appropriate turbulence model. Hence, the potential benefits and shortcomings of each model must be ascertained to make an informed choice.

5.4.1 RANS Turbulence Models

We know that the Navier-Stokes equations govern all aspects of fluid flow. In the case of turbulence, quantities of the equation can be broken down to represent mean and fluctuating parts

of the flow. Mean flow can be obtained by averaging the NS equations, giving rise to the Reynolds Averaged Navier-Stokes (RANS) [47].

These models employ Reynolds-Averaging to make the Navier-Stokes equations easier to solve, such that the small-scale turbulent fluctuations do not need explicit simulation. RANS models bid to provide the most prudent option in computation of complicated industrial flows [45].

The Reynolds averaging technique involves solution variables of the instantaneous Navier-Stokes equations to be broken down into the mean and fluctuating component. For example, let us consider the velocity components:

$$u_i = \overline{u_i} + \acute{u_i} \tag{5.6}$$

Where $\overline{u_i}$ is the mean component and $\acute{u_i}$ is the fluctuating component.

Similarly, for scalar quantities like pressure, energy, or species concentration:

$$\Phi = \overline{\Phi} + \acute{\Phi} \tag{5.7}$$

Now, if an ensemble or time average of the instantaneous continuity and momentum equations of the flow are taken after substituting variables of Equation 5.6 and Equation 5.7, ensemble-averaged momentum equations are obtained which can be written as a Cartesian tensor [45]:

$$\frac{\partial \rho}{\partial t} + \frac{\partial}{\partial x_i}(\rho u_i) = 0 \tag{5.8}$$

$$\frac{\partial}{\partial t}(\rho u_i) + \frac{\partial}{\partial x_j}(\rho u_i u_j) = -\frac{\partial p}{\partial x_i} + \frac{\partial}{\partial x_j}\left[\mu\left(\frac{\partial u_i}{\partial x_j} + \frac{\partial u_j}{\partial x_i} - \frac{2}{3}\delta_{ij}\frac{\partial u_l}{\partial x_l}\right)\right] + \frac{\partial}{\partial x_j}\left(-\rho\overline{\acute{u_i}\acute{u_j}}\right) \tag{5.9}$$

Equation 5.8 and Equation 5.9 are known as RANS equations. RANS and instantaneous Navier-Stokes equations share the same generic form, with the velocities and other solution variables now representing time-averaged (or ensemble-averaged) values. Effects of turbulence are thus represented by new terms that have been generated, called turbulent/Reynolds stresses ($-\rho\overline{\acute{u_i}\acute{u_j}}$) as introduced in Chapter 2. Mathematical closure of Equation 5.9 is attained by modeling these Reynolds stresses in terms of mean velocity gradients. Equation 5.8 and Equation 5.9 can also be applied to variable density flows, with velocities representing mass-averaged values (Favre-averaged Navier-Stokes equations).

Spalart-Allmaras (1 Equation) Turbulence Model:

A straightforward one equation model, Spalart-Allmaras, solves a modeled transport equation for the kinematic eddy (turbulent) viscosity ' $\frac{\mu_t}{\rho}$ '. Eddy viscosity aids in modeling momentum transfer due to turbulent eddies by relating the mean shear stress ($\tau_{turbulent} = -\rho\overline{\acute{u}\acute{v}}$) within a turbulent fluid flow to the vertical slope of velocity ($\mu_t \frac{\partial \bar{u}}{\partial y}$) [45].

Designed categorically for aerospace and aeronautics applications involving wall confined flows, the Spalart-Allmaras model has been shown to provide positive results for adverse pressure gradient affected boundary layers. It is not recommended to be used as a general use model, since its calibration for free shear flows (large errors in plane and round jet flows, as an example) is inadequate.

The original form of the Spalart-Allmaras model is effectively a low-Reynolds number model which requires the viscosity influenced domain of the boundary layer to be correctly resolved (y^+~1). Models may be implemented so as to utilize wall functions for coarse mesh resolutions (y^+ insensitive wall treatment), hence it can be used independent of the near wall y^+ resolution. However, when using y^+ insensitivity, the boundary layer must still be resolved with a minimum resolution of 10-15 cells [45].

k-ϵ (2 Equation) Turbulence Model:

The k - ϵ model is a two equation model. Two equation turbulence models ascertain turbulent length and time scale by working out two separate transport equations and Reynolds stresses using the eddy viscosity approach. They model transport equations for turbulence kinetic energy 'k' (which is derived from the exact equation), and turbulence dissipation 'ϵ' (which is attained by physical hypothesis) [45]. Phenomenon-based considerations and empirical studies helped develop and derive the model and its equations. Accuracy for a broad range of turbulent flows, in addition to economy and robustness, make it popular for industrial flows. A drawback for k-ϵ models would be their insensitivity to adverse pressure gradients and boundary layer separation. They anticipate a diminished as well as deferred flow separation compared to observations.

There are three sub-models of the k-ϵ model [45]:

- Standard k- ϵ model - Credible in the case of totally turbulent flows.
- RNG k- ϵ model - Developed using a statistical approach called 'Renormalization Group (RNG) theory' in the derivation from the instantaneous Navier-Stokes equations. Offers improved accuracy and reliability over a broader class of flows. Low Reynolds number effects are better accounted for.
- Realizable k- ϵ - Fulfils specific mathematical requirements on the Reynolds stresses in line with the science of turbulent flows. Modified transport equation for dissipation rate 'ϵ'. Overall, improved model in comparison to standard and RNG.

Generally, the Realizable k-ϵ is recommended over other k-ϵ models. For flows where adverse pressure gradients cause flow separation from smooth surfaces, using k-ϵ models in general are not recommended.

k-ω (2 Equation) Turbulence Model:

Model transport equations, the turbulence kinetic energy (k) and specific dissipation rate or ϵ to k ratio (ω), form the basis of this two equation model [45]. In comparison to the ϵ-equation, the ω-equation offers many advantages, the most outstanding one being its capability to be integrated through the viscous layer while needing no additional terms. This eases establishment of a robust insensitive treatment. ω-based models are commonly superior at anticipating boundary layer flows in adverse pressure gradients and separation. It must be noted that a near-wall modeling approach is necessary with k-ω models with $y^+ \approx 1$.

The Standard k-ω model stems from the Wilcox k-ω model [45], while including alterations for compressibility, low-Reynolds number effects, and shear flow spreading. Its weakness, however, is freestream sensitivity (outside the shear layer) of the solution.

Improvements in the standard k- ω model have led to the development of the Baseline (BSL) and Shear Stress Transport (SST) k- ω models. The BSL and SST have the k- ω equation in common with the standard model, but are different in the following ways [45]:

- BSL and SST models use the standard k-ω model in the inner part of the boundary layer, and high Reynolds number k-ϵ model in the outer region of the boundary layer, thus bypassing freestream sensitivity of the standard model.

- Turbulent viscosity formulation is altered in the SST model in the interest of transport outcomes of the principal turbulent shear stress.

The BSL k-ω model is made insensitive to freestream conditions by converting the k-ϵ model into a k-ω formulation. This transformed k-ω model and the standard model are multiplied by a blending function and added [45]. In the near wall region, the standard k-ω model is activated, while the k-ϵ model is activated distant of the surface due to the blending function. In addition to refinements of the BSL model, the SST model includes transport of the turbulent shear stress while defining turbulent viscosity. It is also calibrated for flow separation from smooth surfaces, thus becoming the best choice of k-ω model, with wider applications such as in flows with transonic shock waves.

Transition k-kl-ω (3 Equation) Turbulence Model:

This model predicts development of the boundary layer and computes the onset of transition from laminar to turbulent, hence the name 'transition' model [45]. The k-kl-ω is a three equation model of eddy-viscosity type, comprised of transport equations for k_T (turbulent kinetic energy), k_L (laminar kinetic energy), and ω (inverse turbulent time scale).

Transition SST (4 Equation) Turbulence Model:

Another model predicting transition from laminar to turbulent, the transition SST or γ-Re_θ model combines transport equations for intermittency and transition onset with the SST k-ω transport equations, the terms of this coupling being the momentum-thickness Reynolds number [45].

Reynolds Stress Models (RSM) (5 Equation) Turbulence Model:

The most intricate RANS model, RSM solves transport equations for the Reynolds Stresses jointly with a dissipation rate equation in order to close the RANS equation [45]. The eddy viscosity conjecture as used in previous models is discarded in the RSM to improve its capabilities, the most significant one being its ability to stabilize turbulence as a result of vigorous rotation and streamline curvature, as seen, for example in cyclone flows. Reduced convergence and additional equations cause the RSM to be computationally intensive, which may not always be justified with the increase in accuracy obtained. RSM can be combined with two equation models when boundary layers are of significance. Wall functions need to be used with RSM models.

5.4.2 Scale Resolving Simulation (SRS) Turbulence Models

Unlike RANS models, which adopt the closure problem, SRS models partly resolve a fraction of the turbulence for at least a segment of the flow domain. Such alternate models are known as Scale Resolving. SRS models are subdivided into the Scale-Adaptive model (SAS), Large Eddy Simulation (LES) model, and the Detached Eddy Simulation (DES) model. Since intricate details of the flow are not required in the present study, these models are not considered.

5.4.3 Solver Settings

A solver is the program/code used to work out the governing equations of a fluid flow; pressure-based and density-based solvers are the most popular. One or the other mentioned solvers may be used to solve governing integral equations for mass, momentum, and energy conservation as well as turbulence and species like scalars. Control-volume-based (finite volume) is the discretization process used in both methods, while both methods also derive velocity field from momentum equations [45].

Pressure-Based Solver:

In pressure-based solvers, momentum and pressure (or pressure correction) are taken as the primary variables, and algorithms for pressure-velocity coupling are derived by reworking the continuity equation [45]. Pressure-based solvers have two subdivisions, namely the Pressure-Based Segregated Algorithm, and the Pressure-Based Coupled Algorithm. These solvers are applicable to a wide variety of flows, from low speed incompressible to high speed compressible.

Pressure-Based Segregated Algorithm:

This solver utilizes a solution algorithm in which the governing equations are segregated so as to solve them sequentially, i.e. governing equation for u, v, w, P, T, k, ϵ and other solution variables are worked out in an ensuing manner [45]. To accomplish this, individual governing equations are segregated/decoupled from other equations. This feature (segregated storing and solution of equations) makes the algorithm memory-efficient but also slow to converge. Moreover, due to the nonlinear and coupled nature of the governing equations, iterations of the solution loop become necessary so as to arrive at a converged numerical solution.

Pressure-Based Coupled Algorithm:

As the name suggests, this algorithm solves a 'coupled' system of momentum and pressure continuity equations in a single step, followed by energy, species, turbulence, and other transport equations [45]. It differs from the multi-step segregated algorithm in which the equations are decoupled and sequentially solved. Solving equations in a closely coupled way improves solution convergence time compared to the segregated algorithm, but it also increases the memory requirement (1.5-2 times the segregated algorithm) since multiple equations need to be stored at the time of solution. It offers improved performance over the pressure-based segregated algorithm.

Density-Based Solver:

The governing equations of continuity, momentum, energy (if pertinent), and species (if pertinent) transport are solved simultaneously by density-based solvers [45]. Thereafter, governing equations for additional scalars are solved sequentially. In this solver, the density field is attained from the continuity equation, while the equation of state yields the pressure field. Again, the coupled and nonlinear nature of the governing equations necessitate multiple iterations of the solution loop for a converged solution. These solvers are applicable for flows having strong coupling/ interdependence among momentum, density, energy, and/or species.

Schemes for interpolation of cell-centered field variables to face of control volumes [45]:

- First-Order Upwind – First order accuracy, simplest to converge
- Power Law – For cell Reynolds number less than 5, they are more accurate than First Order
- Second-Order Upwind – Slower convergence but 2^{nd} order accuracy obtained
- Monotone Upstream-Centered Schemes for Conservation Laws (MUSCL) – 3rd order, higher precision in the prediction of forces, vortices, secondary flows, etc.
- Quadratic Upwind Interpolation (QUICK) – 3^{rd} order accuracy, beneficial for rotating or swirling flows

Approaches for interpolation of cell-centered gradient of solution variables [45]:

- Green-Gauss Cell-Based – Default method; solution field may smear (false diffusion)
- Green-Gauss Node-Based – Better precision; false diffusion minimized. Good for tri/tet meshes
- Least-Squares Cell-Based – Similar to Node-based Gradient, recommended for polyhedral meshes

Interpolation approaches to calculate cell-face pressure (for Pressure Based Segregated Solver) [45]:

- Standard – Default method; low accuracy for large pressure gradients perpendicular to the surface near boundaries
- PRESTO! – Useful for steep pressure gradients, swirling flows, or significant curved domains
- Linear – Alternative to other methods in the case of convergence difficulty
- Second-Order – To be used for compressible flows but not with porous media, jump, fans, or mixture multiphase models
- Body Force Weighted – Useful when body forces are large, as in the case of highly swirling flows or flows with high Rayleigh numbers

Also critical is the pressure-velocity coupling, the numerical algorithm utilizing a blend of continuity and momentum equations to extract an equation for pressure/pressure correction while employing the pressure-based solver. The following four are common [45]:

- Semi-Implicit Method for Pressure-Linked Equations (SIMPLE) – Default and robust.
- SIMPLE-Consistent (SIMPLEC) – Faster convergence with simpler problems, like laminar flows without the use of physical models.
- Pressure-Implicit with Splitting of Operator (PISO) – Advantageous for mesh cells with higher than average skewness or for unsteady flows.
- Fractional Step Method (FSM) – Similar to PISO, good with unsteady flows.

Finally, two critical parameters primarily affecting convergence are [45]:

- Courant number – Stabilizes convergence behavior. It is lowered at the time of convergence difficulties and then steadily increased.
- Under-Relaxation Factors – These are factors controlling the update of computed variables (mass, density, etc.) at each iteration in the numerical solution. They range from 0 – 1 such that factors with a value close to zero improve solution stability, and decrease convergence rate. Its effect is seen on the residuals at the time of convergence. If residuals fluctuate, under-relaxation factors need to be reduced.

5.5 CFD Analysis of the Disk-Slot Load Leveling Valve

5.5.1 Construction of the Flow Domain

The disk-slot valve was taken apart to observe and replicate the parts of the valve (Figure 2.11). Dimensions were measured for all the components (except spring and disk-lever arm shaft), and were constructed using CAD with limited simplifications and minor alterations to the flow domain (Figure 5.2). Since CFD requires fluid domains, the same was extracted using the Boolean operation (Figure 5.3).

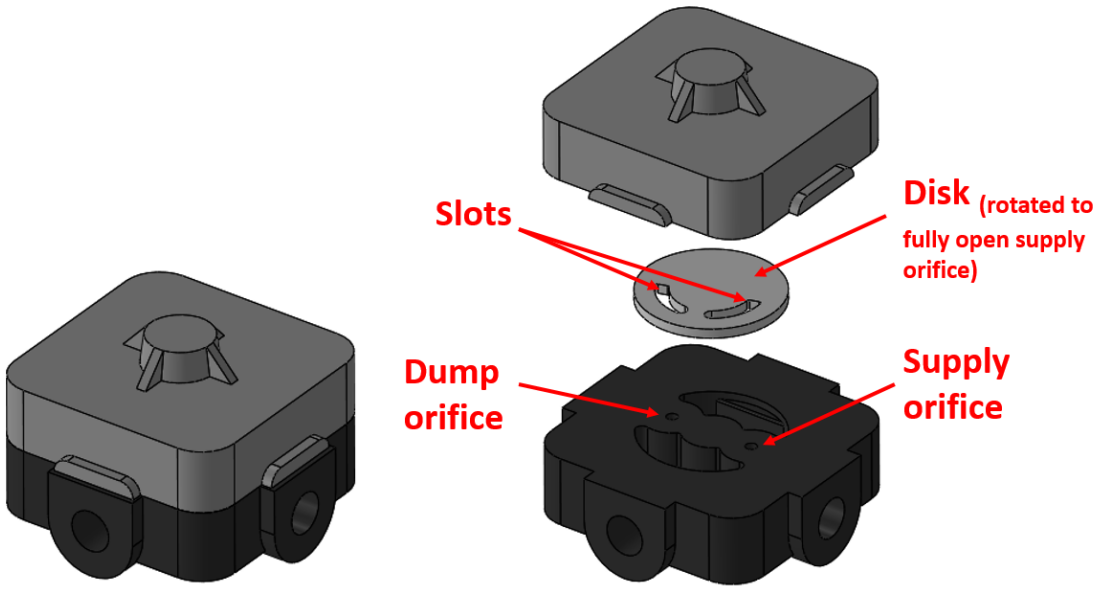

Figure 5.2: CAD model of the disk-slot valve

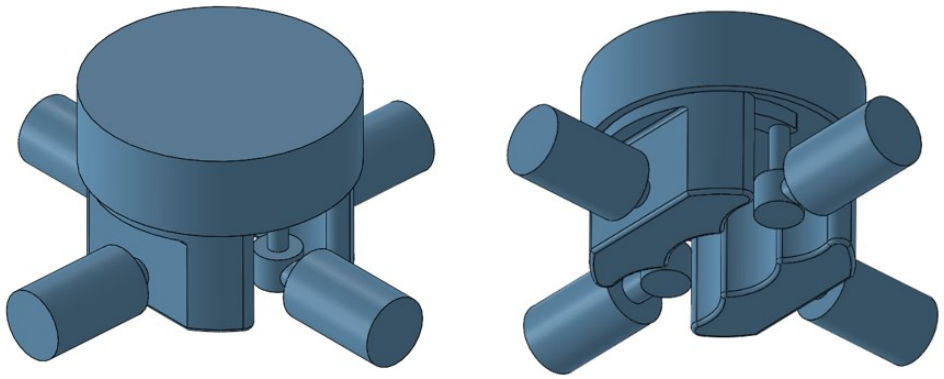

Figure 5.3: Isometric views of the entire fluid domain in the disk-slot valve

When doing computational analysis, attempts may be made to simplify the task for the software so as to improve solver speed and rate of convergence without significant loss in accuracy. In consideration, the relevant part of the actual 3-D flow domain was split into separate parts for approximation into 2-D axisymmetric sections and constructed in DESIGN MODELER. Cylindrical fluid domains were exactly represented in terms of radius and height, while irregular ones were measured for their volume and approximated to cylinders. These individual domains were then arranged into a combined axisymmetric fluid domain (Figure 5.5). An obstruction was introduced to induce a change in direction of fluid flow by a total of 360 degrees, similar to how it occurs in the 3-D geometry (Figure 5.4 and Figure 5.5). The axisymmetric domain and the 3-D domain from which it is made are representative of both the supply and purge operations due to equally sized orifice, slot, and symmetrical flow paths.

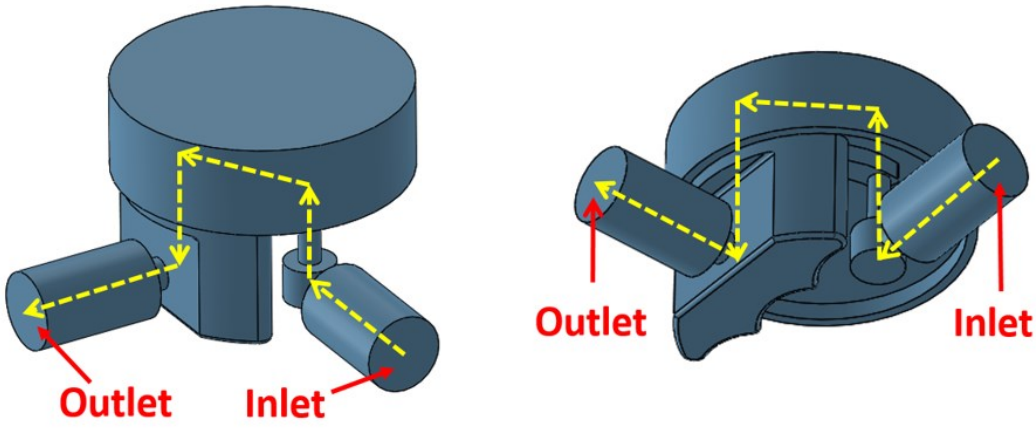

Figure 5.4: Air flow paths (yellow) in the relevant fluid domain

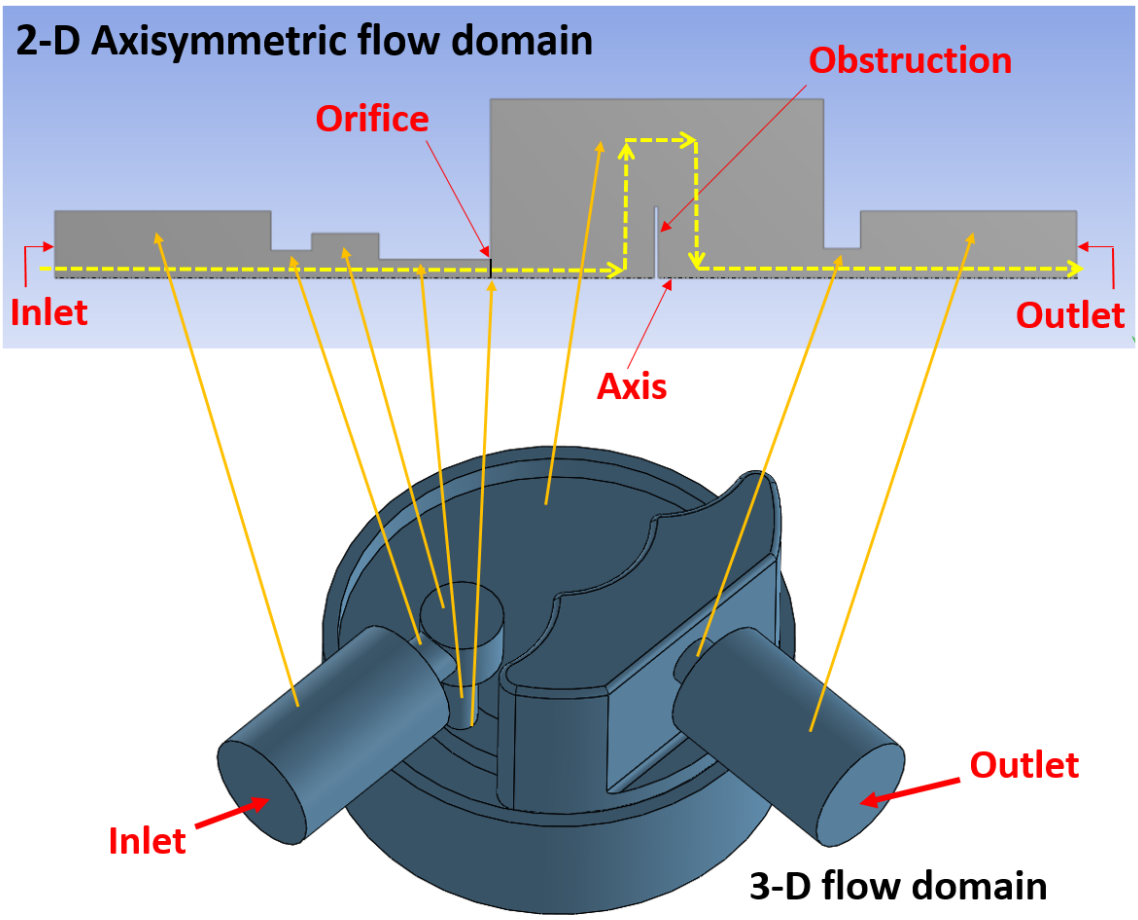

Figure 5.5: Construction of 2-D axisymmetric fluid domain (air flow path shown in yellow)

5.5.2 Preprocessor Settings – Choice of Turbulence Model and Solver

A turbulence model is required for the CFD simulation since the geometry and sonic flow of a compressible fluid, due to low pressure ratios, will cause turbulent flow, fluctuations, etc. This study requires accurate calculation of mass flow rates through the valve; hence, resolving large scale eddies and instantaneous flow field is unnecessary. Therefore, the use of SAS, LES, and DES models are ruled out. Furthermore, since transition from laminar to turbulent is of no interest, RANS transition models k-kl-ω and SST are discarded from consideration, leaving the Spalart-Allmaras, k-ϵ, k-ω, and RSM models as options. Literature review was undertaken to aid in narrowing down to a RANS turbulence model.

Prabhakar et al. probed flow rate through a filter in line with leveling valves using CFD and experimental techniques [48]. In that study, flow had been assumed to be compressible and turbulent for the CFD analysis with the use of an implicit, second order steady state and SIMPLE algorithm, but the turbulence model used was not mentioned. Moujaes et al. simulated water flow through an elbow and a T-joint with a k-ϵ turbulent model, the results of which were in agreement with experimental results [49]. Chen et al. used CFD to investigate septal deviation effects on nasal air flow, considering air to be a compressible fluid and using a k-ω SST turbulence model for its suitability of flow resolution in the complex nasal cavity [50]. Comparison of CFD results with a healthy nose showed expected differences in flow behavior. Vijiapurapu et al. compared the performance of RANS (k-ϵ, k- ω, RSM) models and LES in predicting incompressible flow through circular pipe roughened with square ribs with various spacing [51]. The study concluded that all RANS and LES models perform equally well at predicting time averaged flow stats, with RSM providing additional information on shear stress correlations, and LES enabling the study of instantaneous flows with greater insight since it accurately emulates three-dimensional flow statistics. The study recommended using k-ϵ and k-ω when studying time-averaged flow for high cost-efficiency and modest accuracy.

The literature review highlighted the reliability of RANS models for turbulence modeling. The use of k-ϵ and k-ω is quite popular for industrial flows. It is understood that although RSM is the most capable of all RANS models, its benefits versus additional solution effort may not be justified in all cases, and the one equation Spalart-Allmaras is not as capable as the two equation models. Therefore, a choice must be made between the k-ϵ and k-ω turbulence models, specifically between the advanced model of each, the Realizable k-ϵ which uses wall functions (boundary layer not resolved), and the SST k-ω model which does not use wall function (boundary layer resolved through near wall modeling). Model constants were left at their default values. *Realizable k-ϵ:* C2-Epsilon = 1.9, TKE Prandtl Number = 1, TDR Prandtl Number = 1.2, Energy Prandtl Number: 0.85, Wall Prandtl Number = 0.85. *SST k-ω:* Alpha*_inf = 1, Alpha_inf = 0.52, Beta*_inf = 0.09, Zeta* = 1.5, Mt0 = 0.25, a1 = 0.31, Beta_i(Inner) = 0.075, Beta_i(Outer) = 0.0828, TKE (inner) Prandtl # = 1.176, TKE (Outer) Prandtl # = 1, SDR (Inner) Prandtl # = 2, SDR (Outer) Prandtl # = 1.168, Energy Prandtl # = 0.85, Wall Prandtl # = 0.85, Production Limiter Clip Factor = 10;

ANSYS Fluent is used to conduct a steady state analysis using a Pressure Based Coupled algorithm on the constructed fluid domain. Based on capabilities discussed in the previous section, Green-

Gauss Node-Based gradient interpolation with second order discretization for other scalars is used for adequate accuracy. Software managed hybrid initialization is employed with numerical factors set at their default values. Convergence of mass flow rate is observed (mass flow rate at the outlet becomes steady, and the difference between inlet and outlet mass flow rates becomes zero), in addition to convergence of residuals set at $1e^{-6}$ (x-velocity, y-velocity, and energy) and $1e^{-3}$ for continuity, ω, ϵ, and k. A magnitude of zero was specified for operating pressure, as recommended for high velocity compressible flow (Mach>0.1) [45].

5.5.3 Mesh Independence Study

An initial analysis on the 2-D flow domain was carried out at six different mesh refinements, starting with a cell size of 0.4mm to 0.15mm in steps of 0.05mm, in order to study mesh sensitivity of the solution (Figure 5.6 and Figure 5.7). When mesh refinements do not alter the result, mesh convergence is said to be achieved. The Realizable k-ϵ and the SST k-ω turbulence models are analyzed with slip wall (wall shear stress = 0) initially to investigate any differences in solution. Flow rates are determined for the fully uncovered orifice, at 35psi upstream pressure and 0psi downstream pressure, noting the iterations and average values of density, pressure, and velocity. The outcome is recorded in Table 5.1.

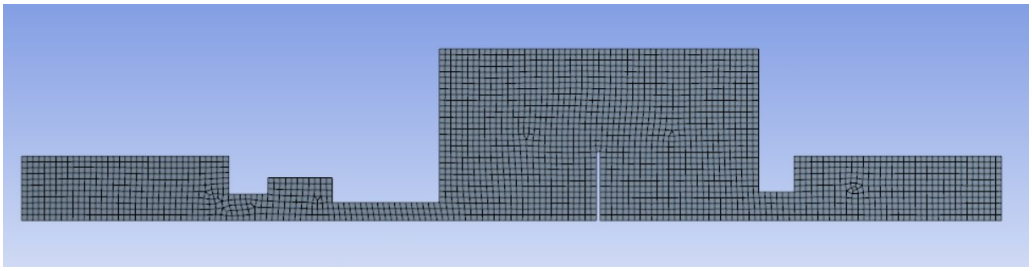

Figure 5.6: 2-D axisymmetric fluid domain with 0.4mm cell size

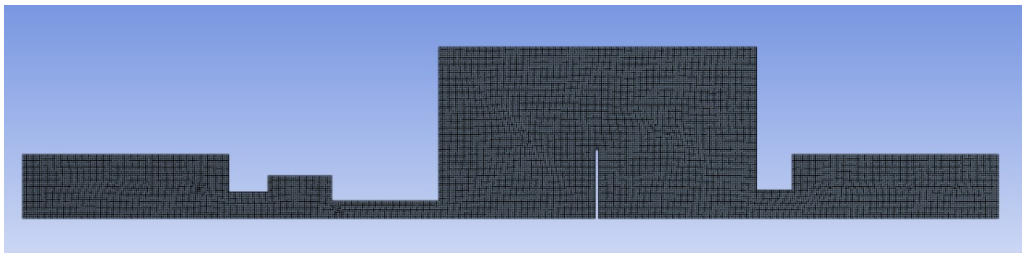

Figure 5.7: 2-D axisymmetric fluid domain with 0.15mm cell size

Table 5.1: Results of mesh sensitivity analysis

Realizable k-ϵ					
Cell size (mm)	Iterations	Mass flow rate (g/s)	avg. Pressure (psi)	avg. Density (kg/m^3)	avg. Velocity (m/s)
0.40	176	2.421	15.814	1.299	142.791
0.35	194	2.460	15.947	1.311	144.484
0.30	208	2.476	16.014	1.317	145.208
0.25	213	2.484	16.110	1.326	146.520
0.20	235	2.487	16.115	1.326	147.851
0.15	304	2.481	16.165	1.329	146.662

SST k-ω					
Cell size (mm)	Iterations	Mass flow rate (g/s)	avg. Pressure (psi)	avg. Density (kg/m^3)	avg. Velocity (m/s)
0.40	402	2.424	15.477	1.279	159.278
0.35	375	2.466	15.653	1.294	160.681
0.30	392	2.482	15.799	1.306	158.725
0.25	408	2.493	15.934	1.318	158.836
0.20	402	2.501	15.983	1.322	159.727
0.15	450	2.506	16.098	1.332	158.317

It is observed that the magnitude of critical properties (mass flow rate, average pressure, average density, average velocity, etc.) changes less than 2% of the previous iteration. The above results are also quite close to those obtained from analysis of a 0.4mm cell sized 3-D fluid domain with slip walls, which estimated a mass flow rate of 2.1 g/s (solution time = ~6 hours), and experiment which suggested a mass flow rate of ~2.3 g/s. The high solution time to simulate a single test case (pressure and lever arm/disk angle) in the 3-D domain makes it unfeasible to use for comprehensive evaluation of flow characteristics of the valve. Based on observations, the conclusion can be drawn that mass flow rates have a close correlation to, and flow properties are independent of mesh refinement.

Now the effects due to a no-slip wall have to be introduced into the 2-D axisymmetric analysis to emulate the real case for airflow through the valve. This involves modifying the mesh so as to account for a boundary layer. Wall y^+ constraints will have to be followed to ensure an appropriate grid size and layout in the near wall region. As discussed previously, the k-ϵ model employs wall functions ($y^+ > 30$) and the k-ω model requires near wall meshing ($y^+ \leq 1$) with multiple cells covering the boundary layer. Hence, by calculation, wall adjacent mesh size for each turbulence model is approximated using the following relations [52]:

First cell height = $\frac{y^+ \mu}{U_{friction} \rho}$ (5.10)

Where,

$$U_{friction} = \sqrt{\frac{\tau_{wall}}{\rho}} \quad (5.11)$$

$$\tau_{wall} = \frac{C_f \rho {U_\infty}^2}{2} \quad (5.12)$$

$$C_f(skin\ friction\ coefficient) = \frac{0.026}{{Re_x}^{1/7}} \quad (5.13)$$

$$Re_x = \frac{\rho U_\infty D_h}{\mu} \quad (5.14)$$

Values of U_∞, ρ, μ, and D_h were obtained from the analysis in Table 5.1. Analysis results for 0.15mm cell size of the k-ω model are considered to calculate a desired $y^+ = 0.6$, and analysis results for 0.15mm cell size of the k-ϵ model are considered to calculate a desired $y^+ = 105$. The following was recommended through calculation using Equations 5.10 – 5.14:

First cell height for $y^+ = 0.6$ ($y^+ \leq 1$) = ~ $1.018e^{-3}$mm

First cell height for $y^+ = 105$ ($y^+ > 30$) = ~ 0.2mm

The 2-D axisymmetric analysis is rerun using y^+ recommended cell size. Scalable wall function is specified for the Realizable k-ϵ turbulence model. Absolute roughness of 0.0015mm (stainless steel) is also specified [53]. Actual y^+ is then determined once the solution has converged and flow is established. It was found that for the Realizable k-ϵ model, using a 0.2mm cell size, average y^+ value at the walls is equal to 38.665, which is within the recommended range ($y^+ > 30$). A global 0.1mm cell size (reduced to generate a mesh blended with inflation layer) and first layer thickness of $1e^{-3}$mm with 25 inflated layers using the SST k-ω, had an average y^+ value at the walls equal to 0.463, which is within the recommended range ($y^+ < 1$). The mass flow rates for the k-ϵ model and the SST k-ω model were 2.445 g/s and 2.371 g/s respectively, bearing an insignificant difference of 0.074 g/s. It must be noted that solution with the SST k-ω required greater computational effort. Again, since only mass flow rates are of interest in this study and not the specifics of the boundary layer etc., the Realizable k-ϵ model suffices for in detail analysis of the valve.

5.5.4 Results and Discussion

The valve model was analyzed with pressures as specified in Chapter 3 and 4, (i.e. 35psi, 50psi, and 65psi upstream, and 0psi downstream) with lever arm/disk rotation angles in its working range for supply and dump operation. Orifice areas at lever arm/disk angles in Table 3.1 of Chapter 3 were used to determine the radius of a circle equivalent to the area of orifice opening for application in the 2-D axisymmetric model (Table 5.2). Figure 5.8 - Figure 5.13 illustrate valve flow analysis for the full opening (>18 degrees/<-18 degrees) condition at 35psi as a sample.

Table 5.2: Radius of circular orifice equivalent to aperture area of disk-slot valve

Disk-Slot Valve Aperture Calculation			
Action	**Angle of Disk (degrees)**	**Area of Opening (mm^2)**	**Radius of Equivalent Circle (mm)**
Supply Operation - Port S to Port A (Counterclockwise rotation of disk)	18	4.909	1.250
	16	4.842	1.241
	14	4.33	1.174
	12	3.605	1.071
	10	2.776	0.940
	8	1.918	0.781
	6	1.098	0.591
	5	0.727	0.481
	4	0.401	0.357
	3	0.14	0.211
Dead band - No flow	2	0	0.000
	1	0	0.000
	0	0	0.000
	-1	0	0.000
	-2	0	0.000
Dump Operation - Port A to Port S (Clockwise rotation of disk)	-3	0.14	0.211
	-4	0.401	0.357
	-5	0.727	0.481
	-6	1.098	0.591
	-8	1.918	0.781
	-10	2.776	0.940
	-12	3.605	1.071
	-14	4.33	1.174
	-16	4.842	1.241
	-18	4.909	1.250

Residuals are observed to have attained the specified threshold ($1e^{-6}$ for x-velocity, y-velocity, and energy, and $1e^{-3}$ for continuity, ϵ and k) indicating that the solution changes negligibly with iterations.

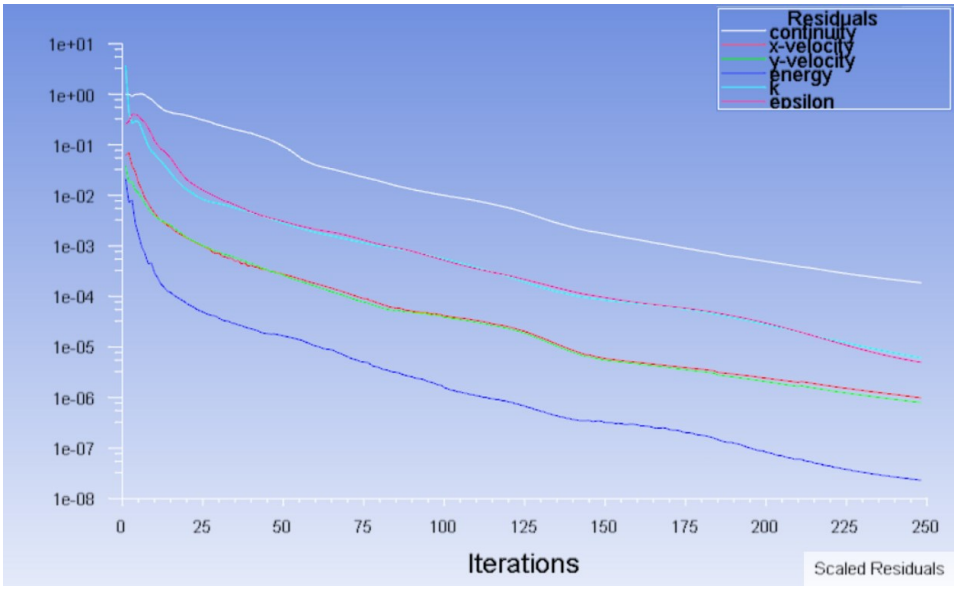

Figure 5.8: Residuals convergence plot (fully uncovered orifice $> |18deg|$) at 35psi

Continuity criterion is observed to have been obeyed since differences in mass flow rate at the inlet and outlet are observed to have reached and remain steady at a value equal to zero.

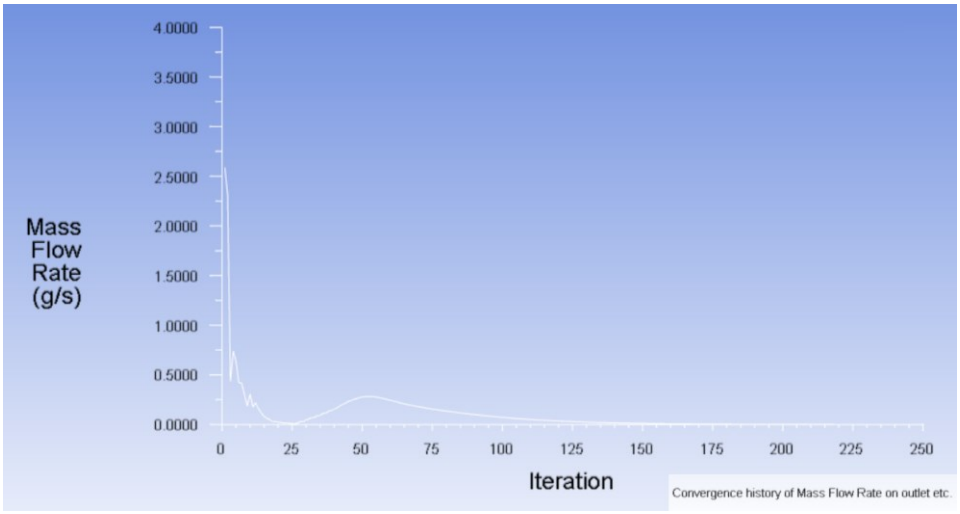

Figure 5.9: (Inlet – Outlet) mass convergence plot (fully uncovered orifice $> |18deg|$) at 35psi

Mass flow rate at the outlet is observed to have settled at a magnitude which does not change with iterations.

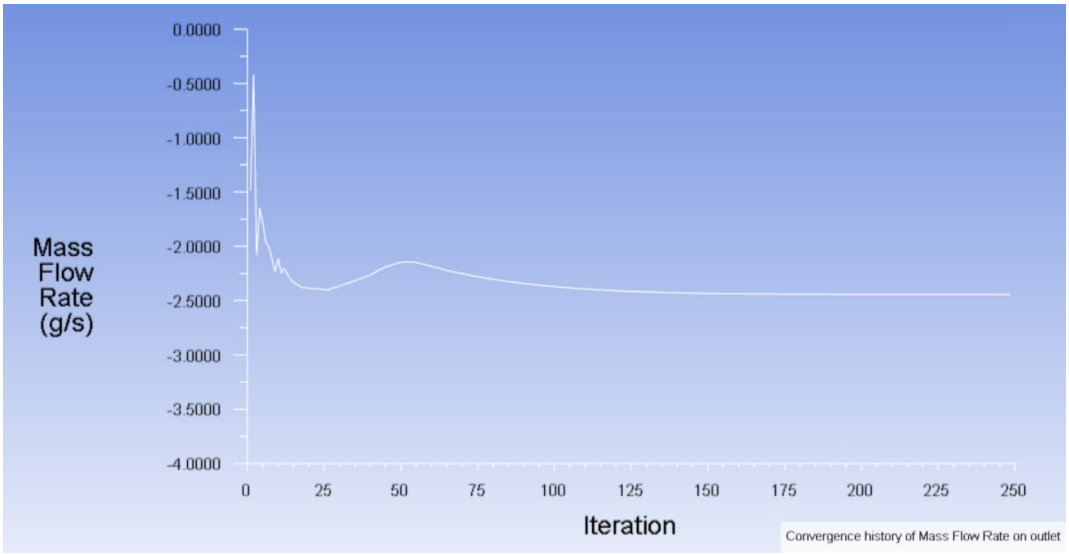

Figure 5.10: Outlet mass convergence plot (fully uncovered orifice $> |18deg|$) at 35psi

CFD analysis enables visualization of flow properties within the fluid domain, as seen in Figure 5.11 - Figure 5.13.

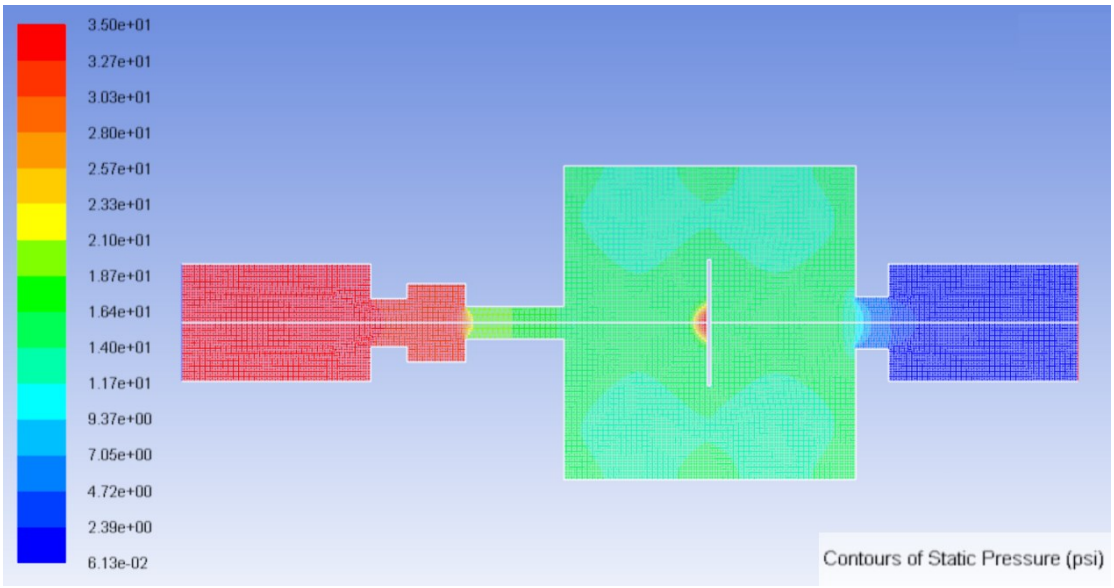

Figure 5.11: Contours of static pressure (fully uncovered orifice $> |18deg|$) at 35psi

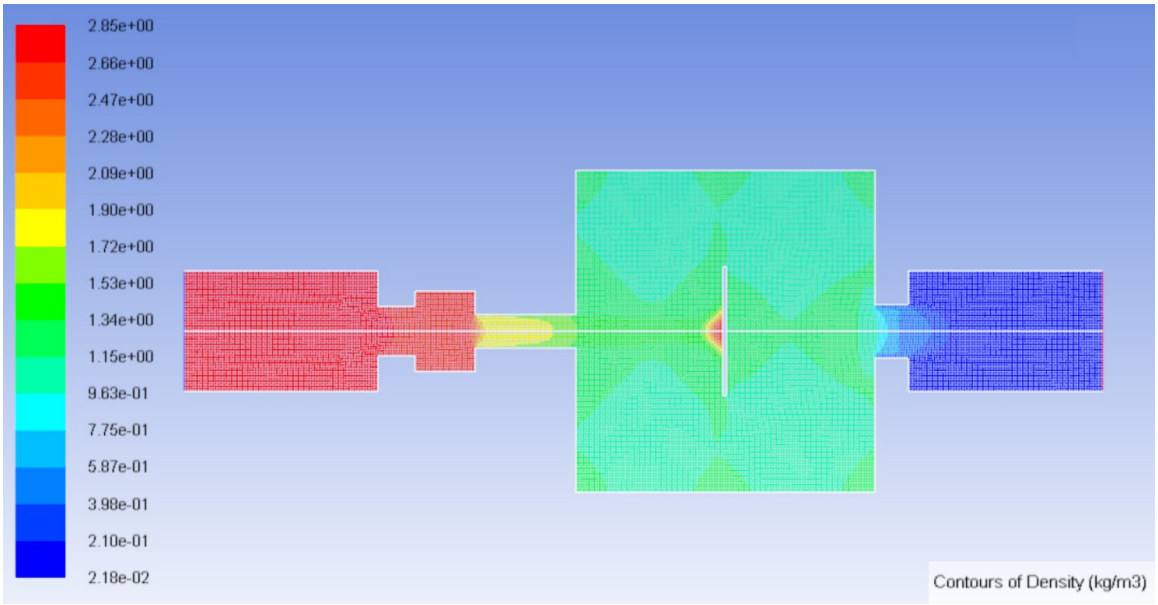

Figure 5.12: Contours of air density (fully uncovered orifice $> |18deg|$) at 35psi

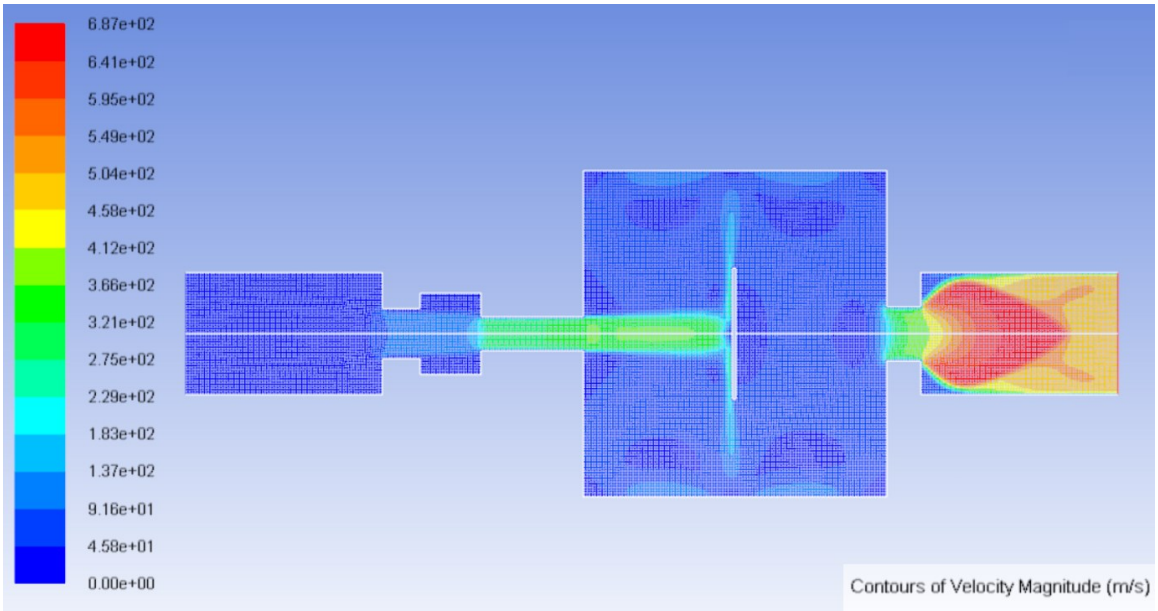

Figure 5.13: Contours of air velocity (fully uncovered orifice $> |18deg|$) at 35psi

Flow characteristics obtained through CFD are presented in Figure 5.14, followed by individual comparisons against experimental results to analyze validity (Figure 5.15 - Figure 5.17).

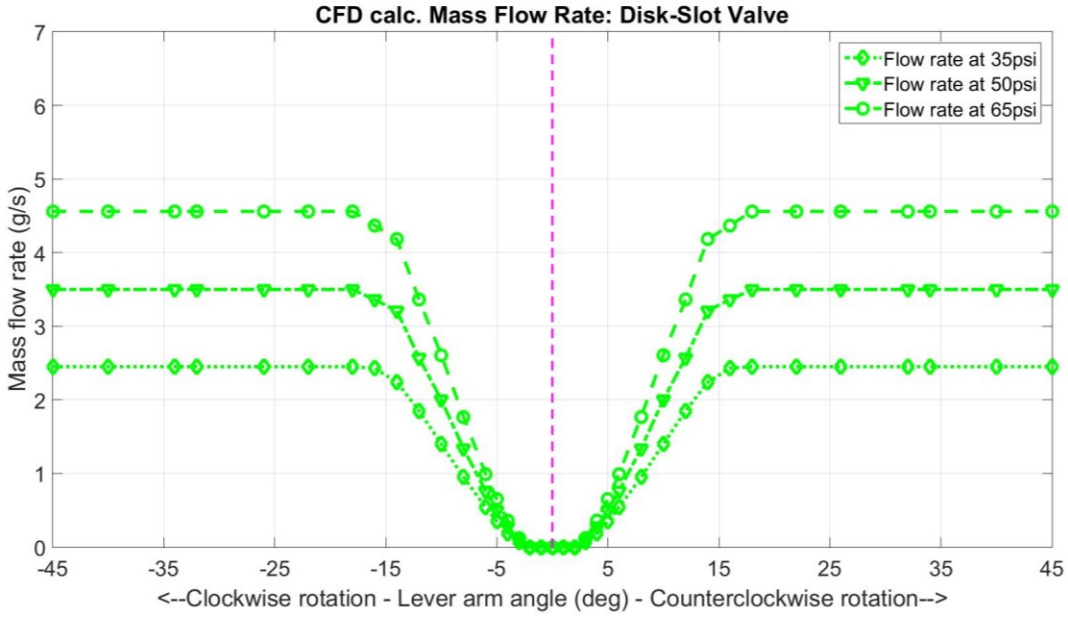

Figure 5.14: CFD determined flow characteristics of the disk-slot valve

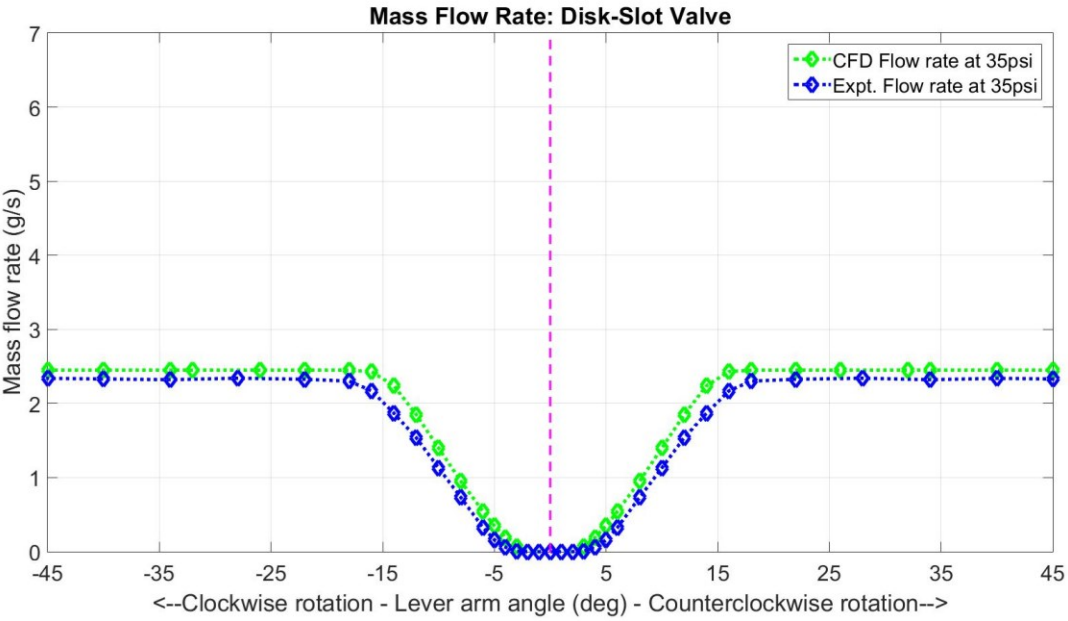

Figure 5.15: CFD vs experiment, flow characteristics at 35psi

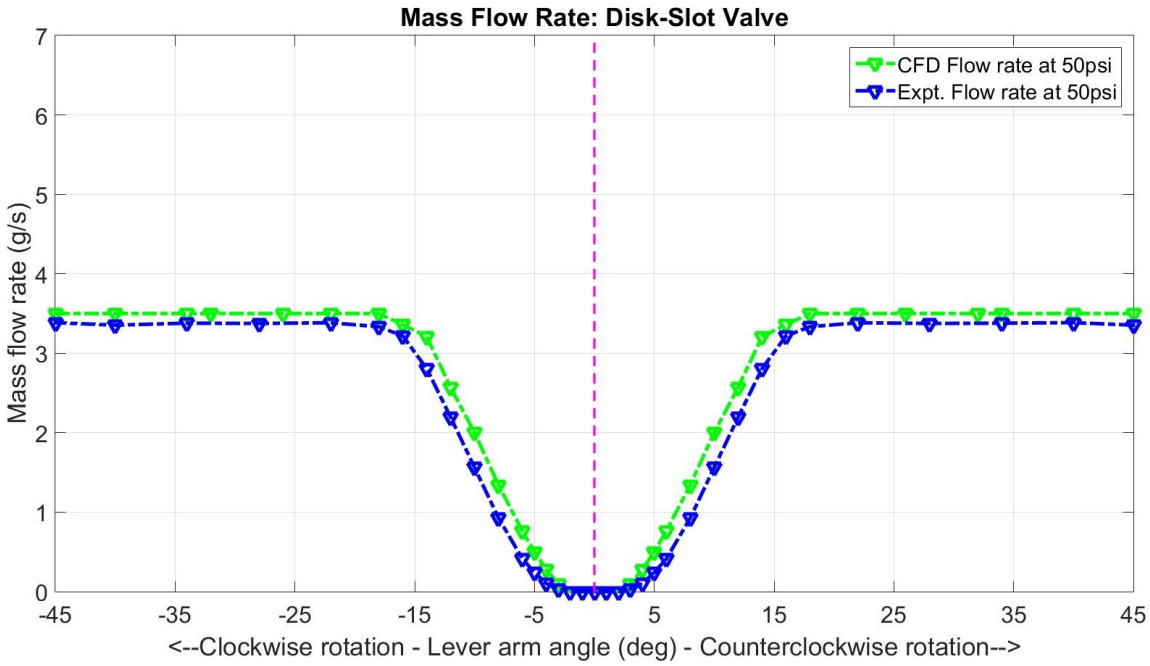

Figure 5.16: CFD vs experiment, flow characteristics at 50psi

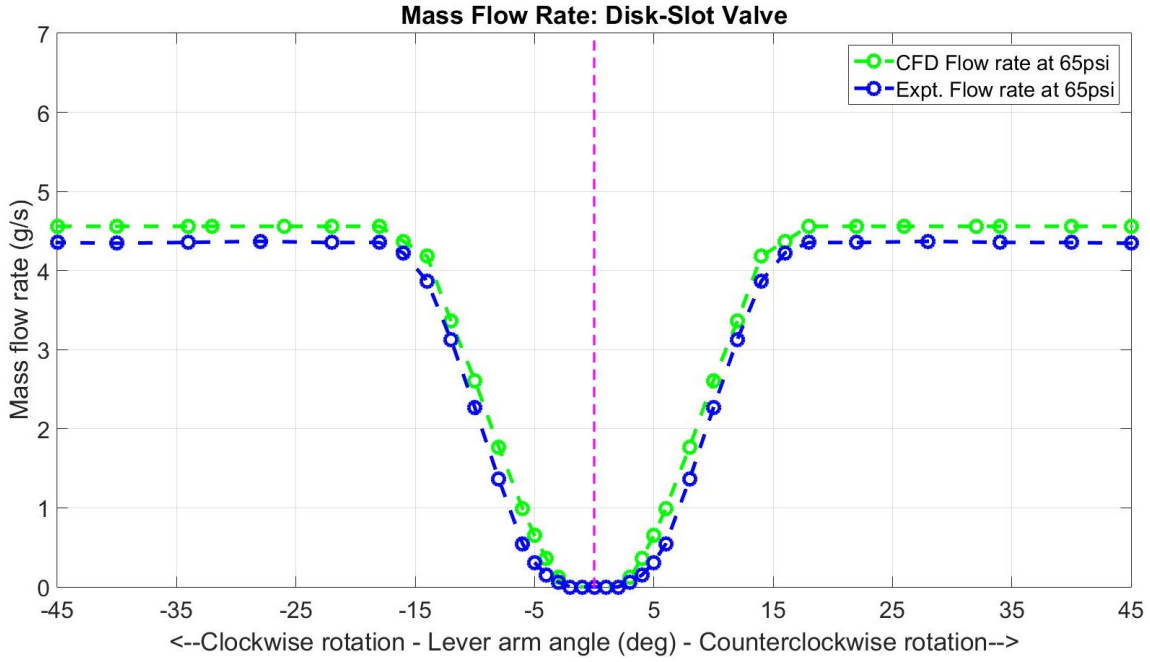

Figure 5.17: CFD vs experiment, flow characteristics at 65psi

A compelling agreement between CFD and experimental flow characteristics is observed. However, CFD-generated flow rates are marginally higher in comparison with experiment. This deviation can be attributed to two factors. First is the presence of resistive elements, such as hoses and pipe fittings in the experimental setup, since the CFD model analyzed the valve only. Second is that the 2-D axisymmetric model somewhat lacks representation of losses as in the actual and complex 3-D structure due to reduced complexities and surface areas. Differences in theoretically-estimated and CFD-generated flow characteristics against experiment were scrutinized (Figure 5.18 and Figure 5.19).

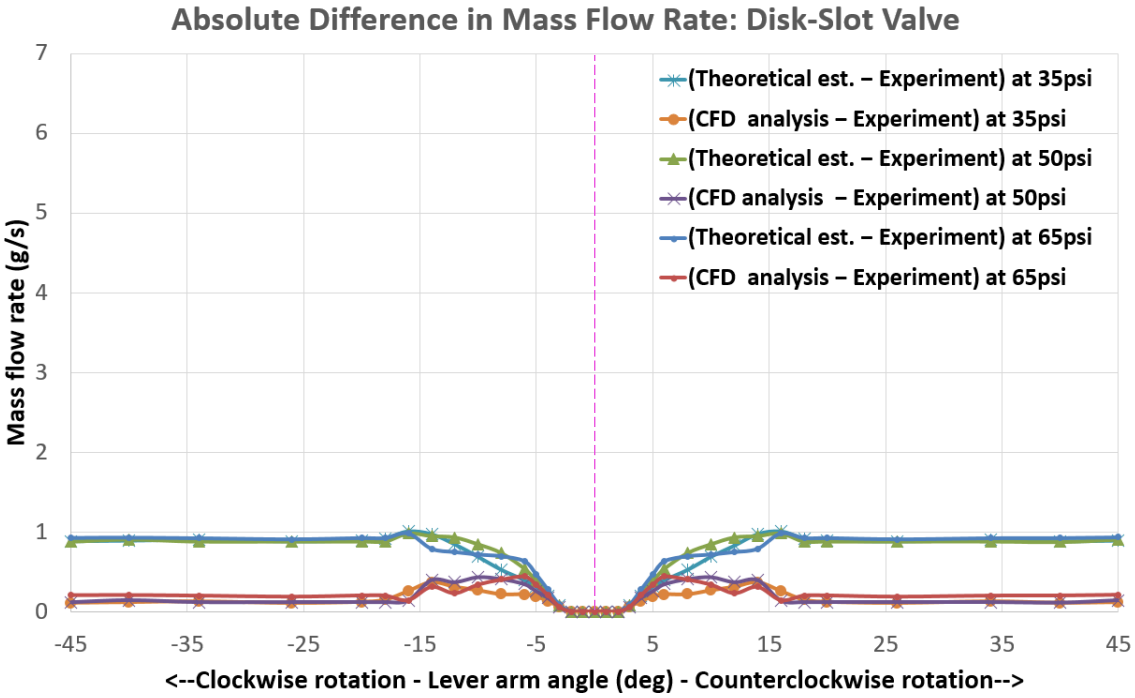

Figure 5.18: Absolute difference, CFD vs experiment, theoretical vs experiment

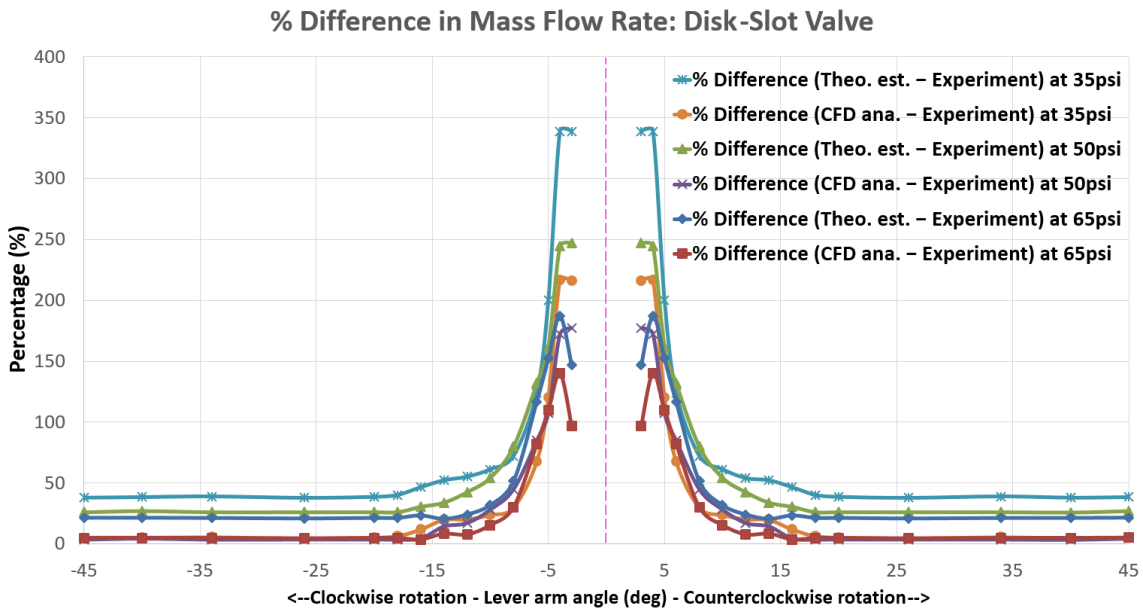

Figure 5.19: Percentage difference, CFD vs experiment, theoretical vs experiment

It is observed that:

- For the three pressures under consideration, theoretical estimation yielded a maximum difference of ~ 1g/s, while CFD modeling yielded a maximum difference of ~ 0.45g/s.
- Difference in flow rates reduced by more than 50% with CFD modeling compared to theoretical estimation, indicating that CFD analysis is significantly better at representing losses to produce results that are very close to the actual.
- The difference in both theoretical and especially CFD estimation is observed to rise as the orifice uncovers, reach a maximum when the orifice is around half uncovered, and then somewhat drop again once it is almost fully uncovered, then remain constant. A factor influencing this behavior is possibly the actual shape of the orifice, which resembles a crescent until it is fully uncovered.
- Overall, the percentage difference involved in CFD analysis is much lower than with theoretical estimation.
- Percentage difference is very large for smaller lever arm angles, and small for larger lever arm angles. This can be attributed to the small absolute magnitude of experimental flow rates.

It can be concluded that the adopted approach for flow characterization of the disk-slot load leveling valve using a 2-D axisymmetric modeling technique provides reliable information, inspiring reasonable confidence in its application for flow characterization in other valve designs. If required, precise details of fluid flow can be obtained by analysis of the 3-D fluid domain, with the only drawback being solution time, which is relatively large compared to the 2-D fluid domain. Experimental testing of prototypes in the developmental phase can thus be substituted by CFD analysis to save time and resources, and to arrive at a load leveling valve with characteristics that closely match recommendations. CFD analysis can also calculate flow rates at non-zero downstream pressures, mimicking the situation when air is being supplied from the reservoir to an already charged/pressurized airbag, as it occurs during normal operation by simply specifying its magnitude in the analysis setup. Experiments to do the same would require additional pressure tanks, control valves, etc., thus complicating the apparatus.

It has been discussed in Chapters 3 and 4 that a hitch in using theoretical formulations was accurately representing losses in the valve, i.e. the calculation of discharge coefficient. Flow characteristics estimated using theoretical formulations in Chapter 3 can be corrected/adjusted for use, as is the common practice seen in literature, but this time based on results obtained through CFD analysis instead of experiment. For example, iteratively it was found that on multiplying a factor of 0.82 to the discharge coefficient Equation 3.12, a perfect agreement in flow characteristics at one pressure (here, 50psi) and substantial agreement between others was achieved, as seen in Figure 5.20 and Figure 5.21. The adjusted theoretical formulation is now ready for use in any isolated or coupled (with vehicle dynamics model) mathematical model of a suspension system.

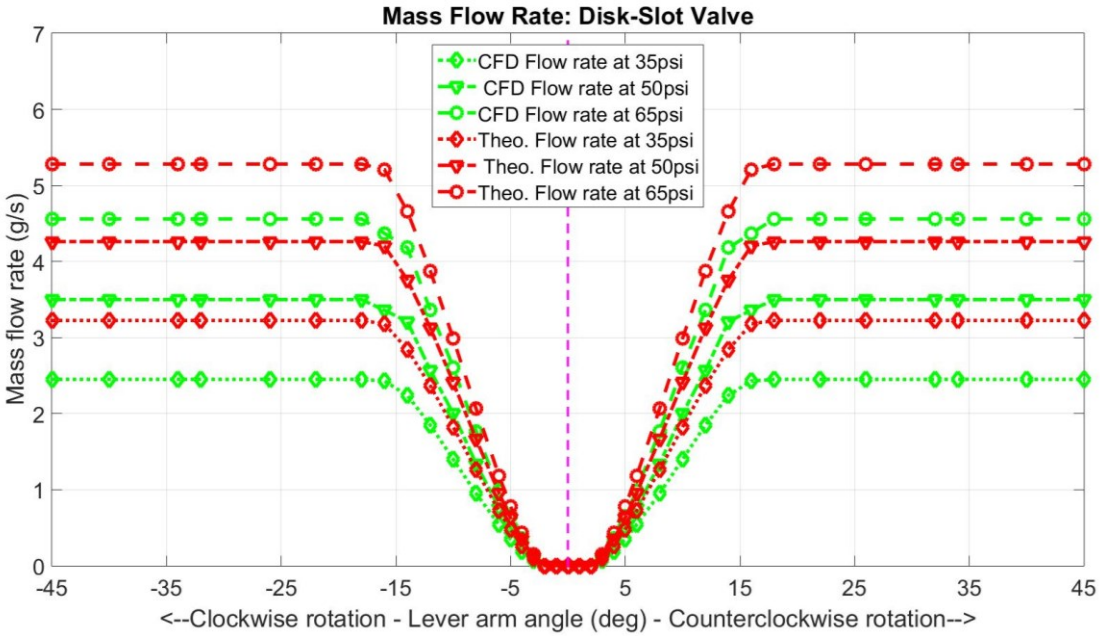

Figure 5.20: CFD vs Theoretical, flow characteristics before adjustment of C_d

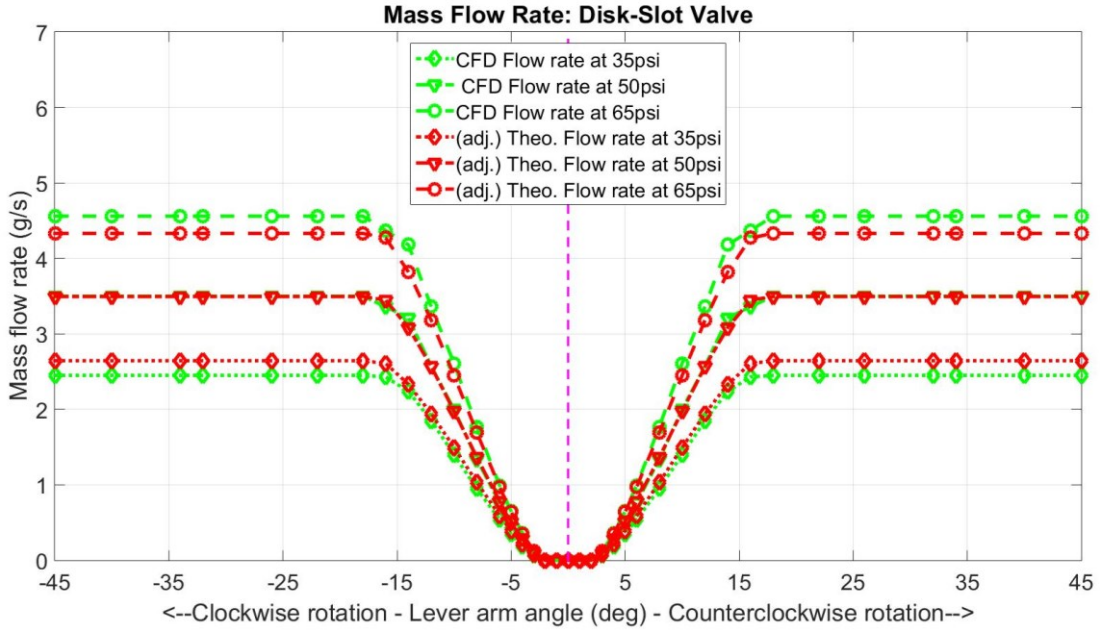

Figure 5.21: CFD vs Theoretical, flow characteristics after adjustment of C_d

6. Case Study: CFD Analysis of a Modified Disk-Slot Valve and Application

This chapter presents a sample case study of modifying flow characteristics in a disk-slot valve. CFD analysis is used to investigate the flow characteristics in a disk-slot valve with minor modifications. The original and modified flow characteristics are directly compared, followed by a discussion of the logic of implementing the valves on a heavy truck.

6.1 Approach

Flow characteristics in a disk-slot valve can be designed by altering its orifice/flow area, lever arm length, slot shape and width, and orifice shape. This section investigates the effects of modifying orifice area and lever arm length on flow characteristics.

First, the supply and dump orifice is modified to increase its area as follows, and is analyzed for flow characteristics:

- Original measurements: Counter bore (x1 = 2mm), wall thickness (x2 = 3.5mm), orifice cylinder seat diameter (x3 = 6mm). The dimensions were changed such that x1 = 1.5mm, x2 = 3mm, x3 = 7mm (Figure 6.1).

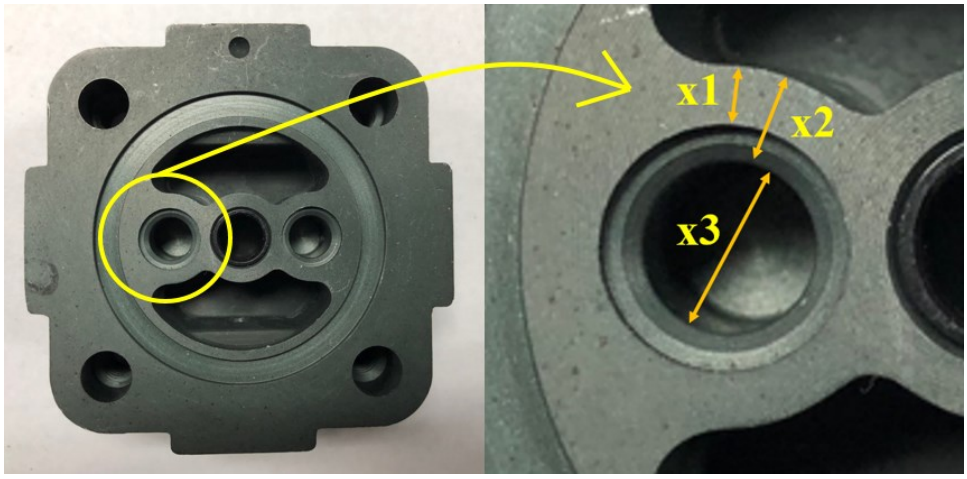

Figure 6.1: Orifice cylinder seat dimensions

- The changes translate to the orifice, increasing its diameter by 1mm. Old O_d = 2.5mm, new old O_d = 3.5mm, i.e. a 96% increase in orifice area (Figure 6.2).

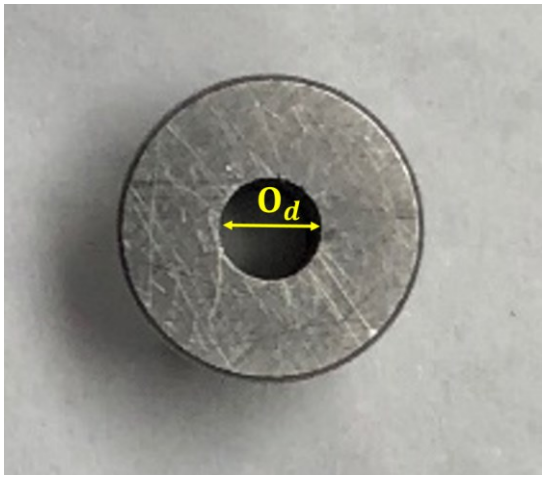

Figure 6.2: Orifice diameter dimension

- Auxiliary orifice A_d was increased in proportion to the orifice diameter, from 3.7mm to 5.2mm (Figure 6.3).

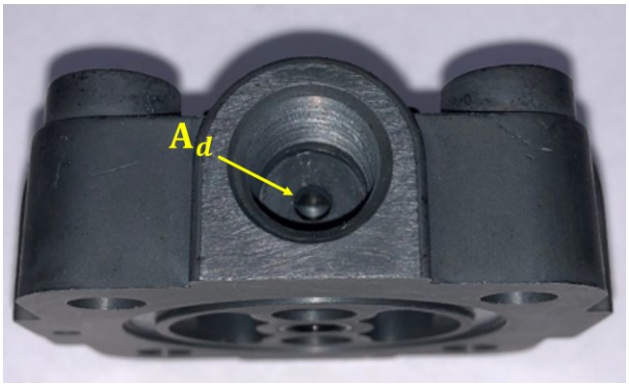

Figure 6.3: Auxiliary orifice dimension

- In addition, the slot in the disk is also widened to at least the orifice size (3.5mm wide).

These changes are simply scaled up holes and slots that can be easily implemented into the production model by a minor change in the code uploaded into the CNC machining center.

The new areas of cross-section of the uncovered part (aperture) of the orifice versus lever arm/disk angle were determined by CAD and are listed in Table 6.1.

Table 6.1: Orifice aperture areas for disk-slot valve (3.5mm dia. orifice)

Disk-Slot Valve Aperture Calculation (3.5mm dia. orifice)			
Action	**Angle of Disk (degrees)**	**Area of Opening (mm^2)**	**Radius of Equivalent Circle (mm)**
Supply Operation - Port S to Port A (Counterclockwise rotation of disk)	23	9.621	1.750
	22	9.561	1.745
	20	8.991	1.692
	18	8.14	1.610
	16	7.12	1.505
	14	5.993	1.381
	12	4.763	1.231
	10	3.573	1.066
	8	2.425	0.879
	6	1.377	0.662
	5	0.915	0.540
	4	0.511	0.403
	3	0.189	0.245
Dead band - No flow	2	0	0.00
	1	0	0.00
	0	0	0.00
	-1	0	0.00
	-2	0	0.00
Dump Operation - Port A to Port S (Clockwise rotation of disk)	-3	0.189	0.245
	-4	0.511	0.403
	-5	0.915	0.540
	-6	1.377	0.662
	-8	2.425	0.879
	-10	3.573	1.066
	-12	4.763	1.231
	-14	5.993	1.381
	-16	7.12	1.505
	-18	8.14	1.610
	-20	8.991	1.692
	-22	9.561	1.745
	-23	9.621	1.750

Next, the lever arm length was shortened from its standard 8 inches to 6.25 inches in the modified disk-slot valve with an increased orifice area.

6.2 Results and Discussion

6.2.1 Effect of Flow Area on Flow Characteristics

The modifications were incorporated into the 2-D axisymmetric model and analyzed for flow characteristics using CFD under the same conditions (pressures and lever arm angles) as in Chapters 3-5. Considering that the original and modified design use lever arms of equal length, the suspension travel for the same degree of rotation will be equal. Preprocessor and final analysis settings from Chapter 5 are reused for this analysis. The new flow characteristics are co-plotted with the original for inspection (Figure 6.4 – Figure 6.6).

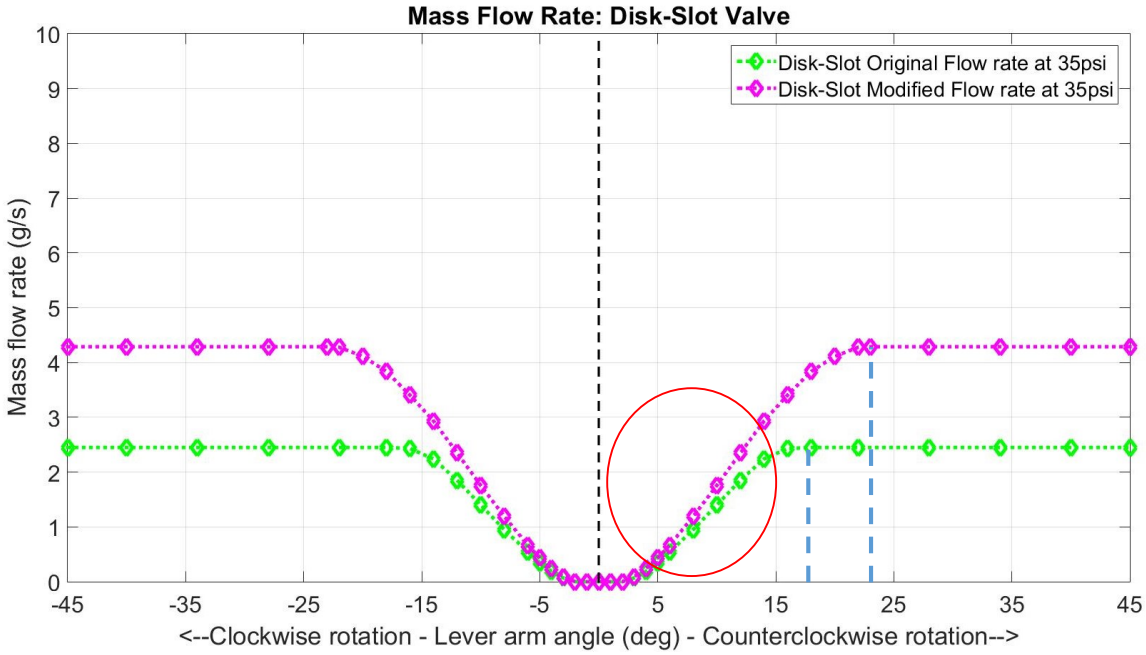

Figure 6.4: Original vs modified disk-slot valve at 35 psi

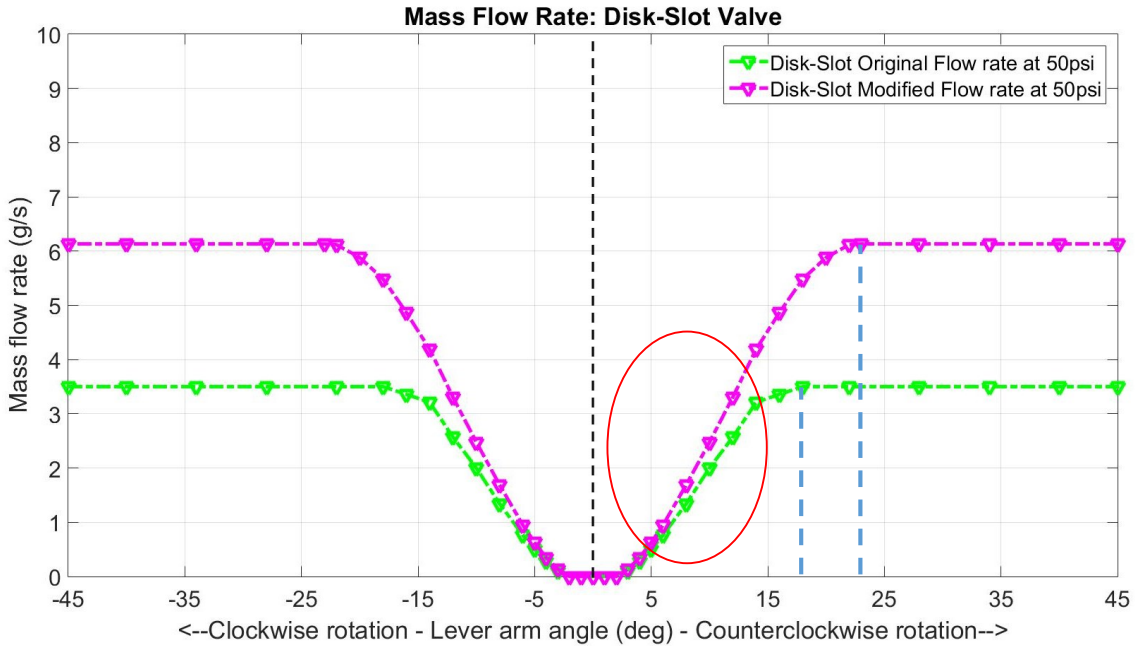

Figure 6.5: Original vs modified disk-slot valve at 50 psi

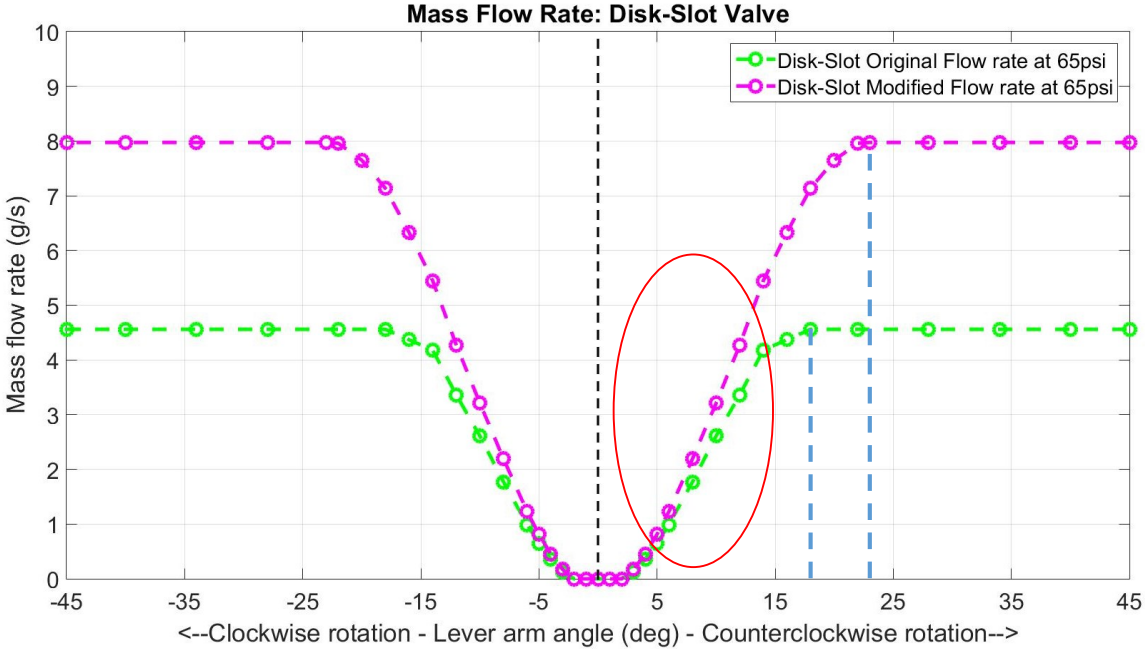

Figure 6.6: Original vs modified disk-slot valve at 65 psi

It is observed that a significant improvement in flow rates is obtained for disk rotations >±14 degrees, and not so much from 0 to ±14 degrees (circled in red, Figure 6.4 - Figure 6.6). Such behavior could be useful for improved charging (from empty air spring) or discharging (to an empty air spring) when the truck is at a standstill and suspension travel is at its maximum, but not when the truck experiences dynamic maneuvers when smaller magnitude disk/lever arm rotations occur at a higher frequency, and a larger flow rate is required. That function can be improved by taking advantage of the observation that the maximum flow rate for the original disk-slot design is arrived at and sustained post ±18 degrees, while in the modified design, maximum flow rate is arrived at and sustained post ±23 degrees (marked in Figure 6.4 - Figure 6.6). For a given suspension travel, the maxima for the modified disk-slot valve can be designed to coincide with that of the original by altering the length of its lever arm, as will be discussed next.

6.2.2 Effect of Lever Arm length and Flow Area on Flow Characteristics

From a design aspect, flow characteristics are represented in terms of lever arm rotation to remain independent of lever arm length and highlight limits of operation (maximum degree of rotation, dead band, etc.). Practically, flow characteristics are represented in terms of suspension travel when considering application on a truck. Suspension travel and lever arm rotation are related by the length of the lever arm.

For example, let us consider Figure 6.7 and Figure 6.8:

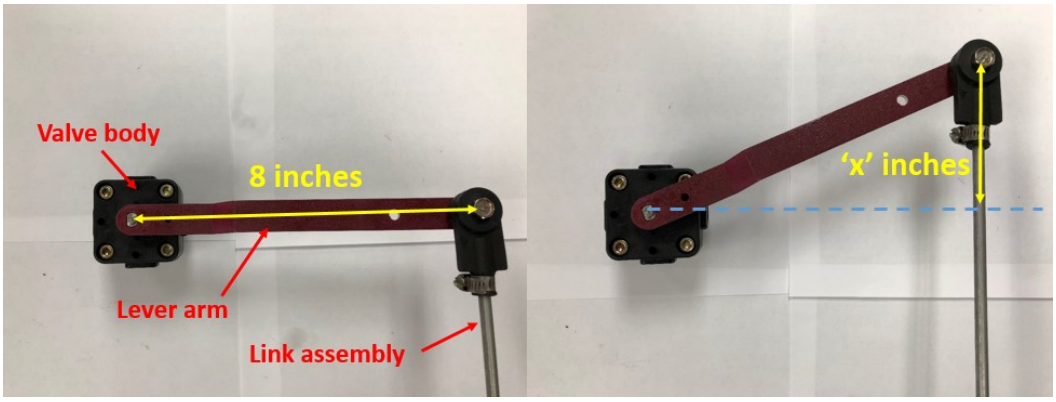

Figure 6.7: Disk-slot valve with an 8 inch lever arm and 'x' inches of suspension deflection

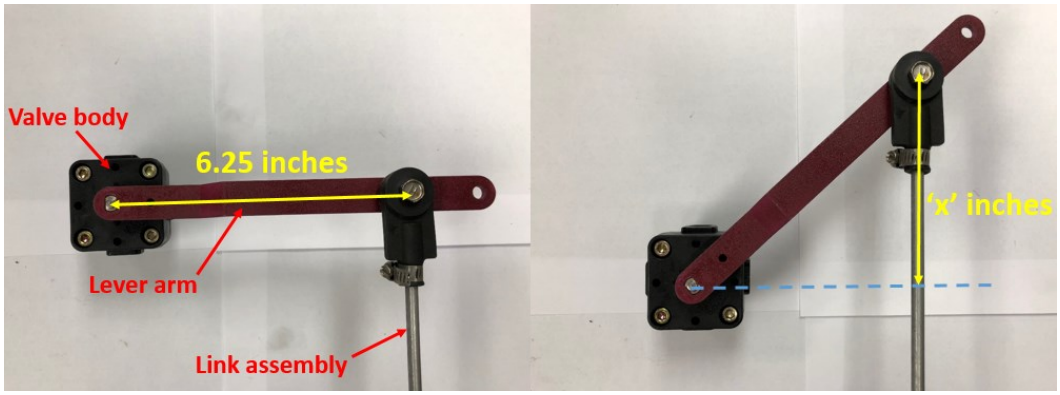

Figure 6.8: Disk-slot valve with a 6.25 inch lever arm and 'x' inches of suspension deflection

The standard length of the lever arm in the disk-slot valve is ~8inches. Hence, the suspension travel at which ±18 degrees of disk rotation is realized is equal to ~2.51 inches (arc length = angle *(in radian)**radius *(of arc)* ≡ suspension travel = disk/lever_angle *(in radian)**lever_arm_length). So for the modified design, 23 degrees is realized for a suspension travel of 2.51 inches when the lever arm length is ~6.25 inches. Figure 6.9 – Figure 6.11 compare flow characteristics of the original disk-slot design with standard lever arm length (8 inches), against the modified design with lever arm length 8 inches and 6.25 inches, as a function of suspension travel.

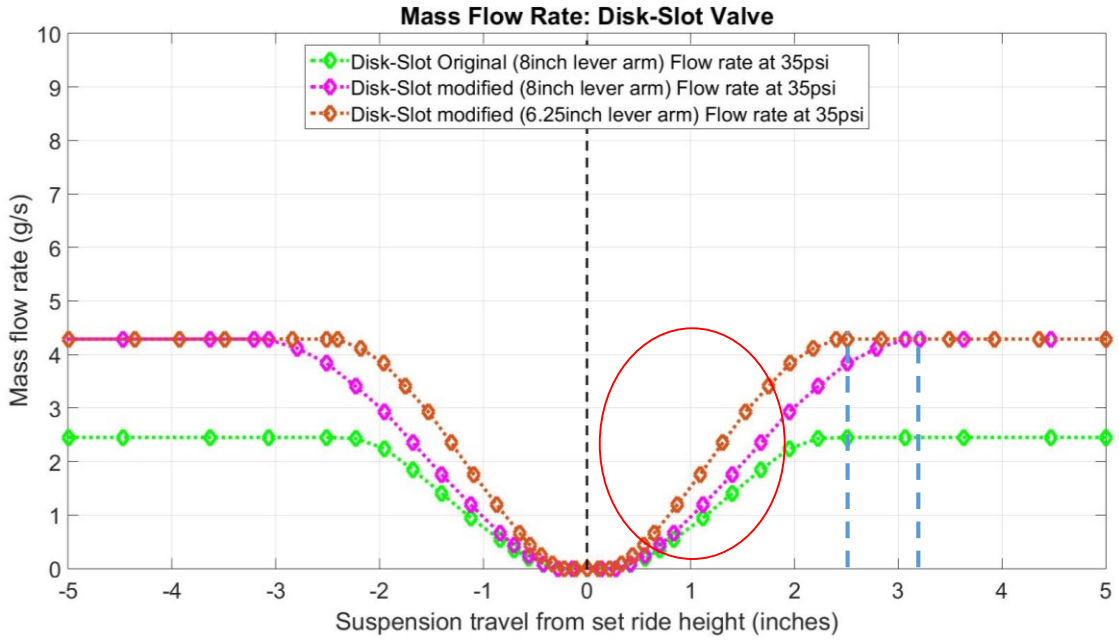

Figure 6.9: Original vs modified disk-slot valve (with and without adjusted lever arm) at 35psi

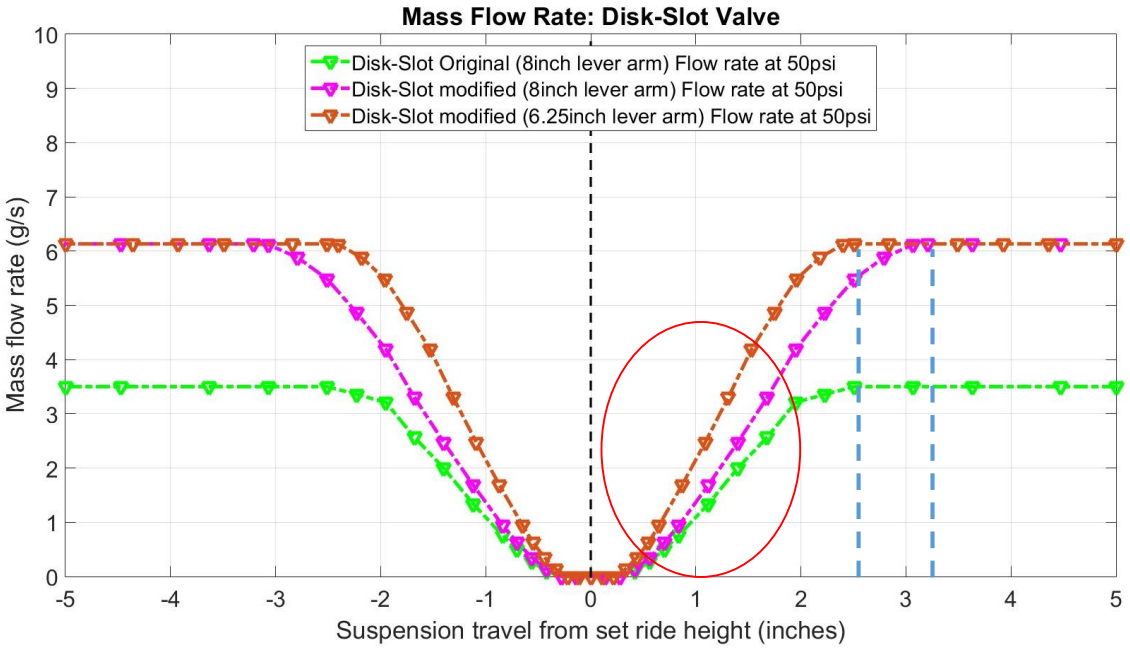

Figure 6.10:Original vs modified disk-slot valve (with and without adjusted lever arm) at 50psi

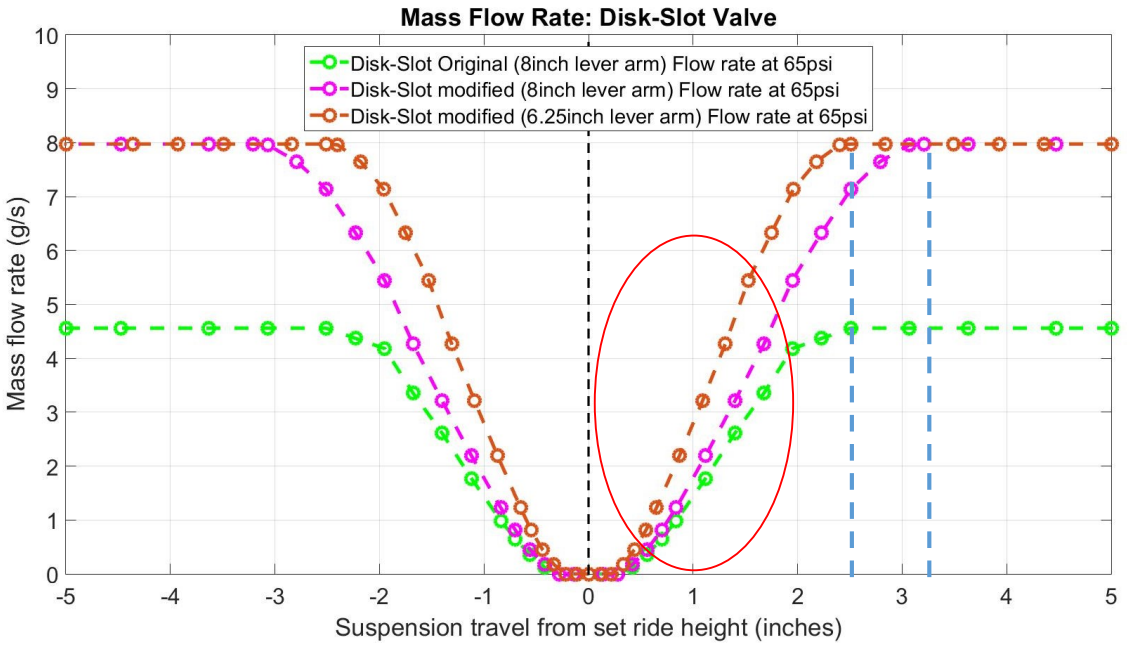

Figure 6.11:Original vs modified disk-slot valve (with and without adjusted lever arm) at 65psi

Now it is observed that flow rates at small suspension deflections (< ±2inches) are much higher for the modified design with a 6.25 inch lever arm compared to the original and modified design with 8 inch lever arms (circled in red, Figure 6.9 – Figure 6.11). Also, maximum flow rates for the original (8inch lever arm) and modified design (6.25 inch lever arm) reach a maximum (marked in Figure 6.9 – Figure 6.11) for the same suspension travel (±2.5 inches). Thus, a faster charging and discharging of the air springs will be achieved for both, static and dynamic functions of the valve.

Slot shape and width, and orifice shape were not modified in this study since their design possibilities are numerous. In comparison to the orifice and lever arm size, they would be difficult to implement from a manufacturing perspective, but it is still an option for reshaping flow characteristics.

6.3 Guidelines for Modification of Flow Characteristics in a Load Leveling Valve

Based on observations from Section 6.2, the following conclusions are drawn:

- For a given lever arm length, increasing orifice area significantly increases flow rates for large suspension travels, and marginally increases flow rates for smaller suspension travels. This modification can be introduced when dynamic response of the valve (flow rates at smaller suspension travels) is satisfactory, but charging and discharging empty/full air springs is slow. The converse is true for reduced orifice areas, where the dynamic response of the valve will be marginally affected, while the flow rates for large suspension travels would see a significant decline.
- Adjusting lever arm length stretches the flow characteristics curve in the x-axis of suspension travel. Shorter lever arm length brings the points of flow rates towards the origin, while a longer arm pushes them away from the origin, all while maintaining a constant magnitude of maximum flow rate for the valve. This modification is useful only when dynamic response needs tuning.
- Changing the slot shape and size, and orifice shape can alter the curvature and trend of the flow characteristics curve and offers the ability to specifically design features of the flow characteristics, to tune the dynamic as well as the steady state response.

7. Summary and Recommendations

This chapter summarizes the study and its findings, with recommendations for future work.

7.1 Summary

The purpose of this project was to examine different techniques and propose a Computational Fluid Dynamics (CFD) model as a tool for flow characterization of a load leveling valve, conducted on a disk-slot type load leveling valve. A portion of the objectives were accomplished by advancing knowledge of air suspension systems, load leveling valves, plumbing configurations, concepts of fluid dynamics, and relevant literature.

The first technique uses a formulation based on gas dynamics, developed to theoretically estimate mass flow rates through the orifice of the valve. As a function of upstream pressure, downstream pressure, temperature, isentropic index, discharge coefficient, and area of orifice, all parameters governing flow through the actual valve were represented. Specific test cases, in terms of upstream and downstream pressures and various levels of actuation within the working range of the valve, were selected for flow characterization. Fidelity of the results, however, were in doubt since magnitudes for the discharge coefficient were uncertain. Hence, flow characteristics had to be determined by experiment for verification, constituting the second technique.

Shortcomings of commercially available flowmeters led to the development of an alternate apparatus comprised of an air tank, pneumatic fittings, pressure angle sensors to determine mass flow rates through the load leveling valve, and an angle sensor for lever arm angles. Pressure drop in the tank due to discharge of air through the valve was used to calculate mass flow rates using gas law formulations. Flow characteristics of the valve determined through experiment for the set test cases were compared with those estimated theoretically. A disagreement was observed between the results, found to be rectifiable to a large extent by altering the magnitude of discharge coefficient in the theoretical formulations.

CFD analysis was then conducted on the valve as the third technique of flow characterization for two reasons. First, to address the inability of theoretical estimation to accurately capture the reality of fluid flow through the valve, and second, to investigate the deviation of its results from

experimental evaluation. After a thorough review of the analysis schemes involved in modeling, the most appropriate for the desired level of flow detail was selected. Flow characteristics for the set test cases were determined using CFD and were found to be in agreement with experimental results, thus validating CFD analysis as a means to determine flow characteristics, rectify theoretical formulations, and possibly substitute experimental testing. A prospect to save time and resources opened up since design iterations based on desired flow characteristics can be analyzed using CFD instead of manufacturing prototypes for experimental testing. This study is thus able to benefit suspension engineers involved in the development and testing of load leveling valves.

A sample case study investigating the effects of modifying orifice area and lever arm length on flow characteristics using CFD concludes the study, to demonstrate its practical application on a heavy truck.

7.2 Recommendations

This study has evaluated flow characteristics of the original disk-slot valve using theoretical formulations, experiment, and CFD modeling. Fabrication and experimental testing of the modified disk-slot valve previously analyzed using CFD should be undertaken. A similar evaluation of other load leveling valve types in the market should be conducted for comparison against the original disk-slot valve. Armed with CFD as an analysis tool, new valve designs corresponding to recommended flow characteristics for various truck-suspension configurations should be evaluated. Examples of a new design could include a non-circular orifice, tapering slots, etc. Ultimately, there should be a load leveling valve with unique flow characteristics for trucks employing air suspensions that differ in structure, load capacity, and air spring size, at the least.

REFERENCES

[1] 'Logistics and transportation industry in the United States', accessed at https://www.selectusa.gov/logistics-and-transportation-industry-united-states.

[2] White D. L., 'Parametric Study of Leveling System Characteristics on Roll Stability of Trailing Arm Air Suspension for Heavy Trucks', SAE Technical Paper Series 2000-01-3840.

[3] Chen Y., 'Modeling, Control and Design Study of Balanced Pneumatic Suspension for Improved Roll Stability in Heavy Trucks', PhD Dissertation, Virginia Polytechnic Institute and State University, Blacksburg, Virginia, USA, 2017.

[4] SirAlec, 'A day with LPT1613 TC, a TATA 1210E and Semi Forward 1613TC', accessed at http://www.team-bhp.com/forum/commercial-vehicles/67389-day-lpt1613-tc-tata-1210e-semi-forward-1613tc.html.

[5] Sheldon Axle Company, 'Leaf Springs: Their Characteristics and Methods of Specification', Wilkesbarre, PA: 1912. p. 1.

[6] Gieck J., 'Riding on Air', SAE International 1999, ISBN: 0768004543

[7] Richardson, S., Sandvik, A., Jones, C., Josevski, N., Pok, P. W., Orton, T., 'The Comparative Testing of a Single and Double Ride Height Control Valve Suspension Control Systems', 23rd International Technical Conference on the Enhanced Safety of Vehicles (ESV), no. 13-0292, 2013.

[8] Hendrickson, 'Understand Trailer Air Suspensions', accessed at http://www.hendrickson-intl.com/getattachment/9e8b5109-84b9-4e17-a026-50094ff96370/L761-Understanding-Air-Ride.aspx,.pdf.

[9] Werminghausen M., 'Mercedes Air Suspension', Mercedes Air Suspension from the 1960s.

[10] Bennett S., Norman I. A., 'Heavy Duty Truck Systems', Fifth Edition, Delmar Cengage Learning.

[11] HWH® Online Technical School, 'Introduction to Air Suspensions', accessed at https://www.hwhcorp.com/ml57000-000.html.

[12] Haldex, 'Type CR Controlled Response Height Control Valve', L31177 Rev.2/10, accessed at https://www.haldex.com/globalassets/north-america/documents/suspension-controls/l31183.

[13] Haldex, ‘Air Control Kit for Suspensions with Two Height Control Valves’, L31177 Rev.2/10, accessed at https:// www.haldex.com / globalassets / north-america / documents / suspension-controls / l31177.

[14] Trudeau C. A., Pierce M. W., ‘Leveling valve for air springs’, US Patent 5560591A, accessed from Google Patents.

[15] Reitz V., ‘Valves Keep Trucks on the Level’, Machine Design, 2002 July 11, p. 39.

[16] Barksdale, ‘Air Suspension Valves 52321 – brochure#2017’, accessed at http://www.barksdale.com/en/products/datasheet/310/air-suspension-valve---52321-series/.

[17] Hendrickson, ‘Height Control Valve Brochure - L1024’, accessed at http://www.hendrickson-intl.com/Trailer/On-Highway/Height-Control-Valve.

[18] Nakajima, T., Shimokawa Y., Mizuno M., Sugiyama H., ‘Air suspension system model coupled with leveling and differential pressure valves for railroad vehicle dynamics simulation’, Journal of Computational and Nonlinear Dynamics, 9(3): p. 031006.

[19] Robinson, W.D., Kelkar A.G., and Vogel J.M., ‘Modeling and Identification of a Pneumatic Air Spring-Valve-Accumulator System for Semi-Active Suspension Control’, ASME 2012 DSCC2012-MOVIC2012-8835.

[20] Lee, S. J., ‘Development and analysis of an air spring model’, International Journal of Automotive Technology ‘, 11(4): 471-479.

[21] Hao L., Jaecheon L., ‘Model Development of Automotive Air Spring Based on Experimental Research,’ Third International Conference on Measuring Technology and Mechatronics Automation, pp. 585-590. doi: 10.1109/ICMTMA.2011.433.

[22] Nieto A.J., Morales A.L., González A., Chicharro J.M., Pintado P., ‘An analytical model of pneumatic suspensions based on an experimental characterization’, Journal of Sound and Vibration, Volume 313, Issues 1–2, 2008, Pages 290-307, ISSN 0022-460X.

[23] Kim H., Lee H., ‘Height and Leveling Control of Automotive Air Suspension System Using Sliding Mode Approach’, IEEE Transactions on Vehicular Technology, vol. 60, no. 5, pp. 2027-2041, Jun 2011.

[24] Sreedhar B., Deshmukh C., ‘A Simplified Model of Air Suspension for Multi Body Simulation of the Commercial Passenger Vehicle," SAE Technical Paper 2013-26-0157, 2013.

[25] Engineering Archives®, ‘Viscous and Inviscid Flow’, accessed at http://www.engineeringarchives.com/les_fm_viscousinviscidflow.html.

[26] Cengel Y. A., Cimbala J. M., 'Fluid Mechanics – fundamentals and applications', 1st ed. McGraw-Hill series in mechanical engineering, ISBN 0–07–247236–7.

[27] NASA Glenn Research Center, 'Boundary Layer', accessed at https://www.grc.nasa.gov/www/k-12/airplane/boundlay.html.

[28] DeGroff C. G., Shandas R., Valdes-Cruz L., 'Analysis of the Effect of Flow Rate on the Doppler Continuity Equation for Stenotic Orifice Area Calculations', Clinical Investigation and Reports Circulation. 1998; 97:1597-1605.

[29] SMC Company, 'Modern Practical Pneumatic Technologies, Third Edition', ISBN: 978-7-111-23810-2.

[30] Stanton T. E., 'The Flow of Gases at High Speeds', 1926 Proc. Roy. Soc. A. vol. 111, p. 306.

[31] Driskell L. R., 'Ideal Gas Flow through Nozzles, Restrictions and Enlargements', accessed at https://www.isa.org/books/Mulley_Papers/Nozzles.html.

[32] Crane®, 'Flow of Fluids', Crane Technical Paper No. 410, © 1988 Crane Co. (Twent-fifth printing - 1991).

[33] Jobson D. A., 'On the Flow of a Compressible Fluid Through Orifices', 1955 Proc. Instn Mech. Engrs, Lond., vol. 169, p. 767.

[34] Bragg, S. L., 'Effect of Compressibility on the Discharge Coefficient of Orifices and Convergent Nozzles', Journal of Mechanical Engineering Science 1960 2(1): 35-44.

[35] Kayser J. C., Shambaugh R. L., 'Discharge coefficients for compressible flow through small-diameter orifices and convergent nozzles', Chemical Engineering Science, Volume 46, Issue 7, 1991, Pages 1697-1711, ISSN 0009-2509.

[36] Ward-Smith A.J., 'Critical flowmetering: The characteristics of cylindrical nozzles with sharp upstream edges', Int. J. Heat and Fluid Flow, vol 1, No 3, 1979.

[37] SA, LMS IMAGINE AMESim Library Manual, 'PNOR002 – pneumatic orifice (Perry's Cq)'.

[38] Omega, 'FMA1700A/1800A Series electronic gas mass flow meters', accessed at https://www.omega.com/pptst/FMA1700A_1800A.html.

[39] Omega, 'Electronic Mass Flowmeters – flow reference section', accessed at https://www.omega.com/toc_asp/frameset.html?book=Green&file=MASS_FLOW_REF.

[40] Zhu Z., 'Flow Characterization and Redesign of Load Leveling Valves for Improving Transient Dynamics of Heavy Truck Air Suspension', Master's Thesis, Virginia tech 2016.

[41] Honeywell, 'PX2 Series Heavy Duty Pressure Transducer', accessed from https://sensing.honeywell.com/PX2EN1XX250PSAAX-heavy-duty-pressure-transducers.

[42] Honeywell, 'Hall-effect Rotary Position Sensors: RTP Series with External Actuator', accessed at http: // sensing.honeywell.com / honeywell- sensing- rty- series- rtp- series- datasheet- 32307665-b-en.pdf.

[43] Measurement Computing DT9816 Series, accessed at https:// www.mccdaq.com/ Products/ Multifunction-DAQ/D T9816.

[44] NASA Glenn Research Center, 'Navier-Stokes Equations', accessed at https://www.grc.nasa.gov/www/k-12/airplane/nseqs.html.

[45] ANSYS FLUENT Help – User and Theory Guide.

[46] Gerasimov A., 'Modeling Turbulent Flows with FLUENT', Europe, ANSYS lnc. 2006.

[47] Andersson B., Andersson R., Hakansson L., Mortensen M., Sudiyo R., Wachem B., 'Computational fluid dynamics for engineers', Cambridge: Cambridge University Press, ISBN 978-1-107-01895-2.

[48] Prabhakar, N., Sripathy, P., Bharathiraja, S., Ayyappan, K., 'Theoretical and Experimental Investigation of Flow Rate of Leveling Valve with Filters for Different Operating Angles,' SAE Technical Paper 2013-26-0042, 2013.

[49] Moujaes, S. F., Deshmukh S., 'Three-Dimensional CFD Predications and Experimental Comparison of Pressure Drop of Some Common Pipe Fittings in Turbulent Flow', Journal of Energy Engineering 132(2): 61-66.

[50] Chen X. B., Lee H. P., Hin Chong V. F., Wang, D. Y, 'Assessment of septal deviation effects on nasal air flow: A computational fluid dynamics model', The Laryngoscope, 119: 1730-1736.

[51] Vijiapurapu S., Cui J., 'Performance of turbulence models for flows through rough pipes', Applied Mathematical Modeling, Volume 34, Issue 6, 2010, ISSN 0307-904X.

[52] White F. M., 'Fluid Mechanics', 5th Edition Mc-Graw-Hill Series in Mechanical Engineering.

[53] Engineering Toolbox, 'Ventilation Ducts - Roughness and Surface Coefficients', accessed at: https://www.engineeringtoolbox.com/surface-roughness-ventilation-ducts-d_209.html.